



SATHYABAMA

INSTITUTE OF SCIENCE AND TECHNOLOGY
(DEEMED TO BE UNIVERSITY)

Accredited "A" Grade by NAAC | 12B Status by UGC | Approved by AICTE

www.sathyabama.ac.in

**SCHOOL OF MECHANICAL ENGINEERING
DEPARTMENT OF AERONAUTICAL ENGINEERING**

HIGH SPEED AERODYNAMICS

SAEA1505

UNIT – I CONCEPT OF COMPRESSIBLE FLOW – SAEA1505

1.1. ALTERNATIVE FORMS OF THE ONE-DIMENSIONAL ENERGY EQUATION

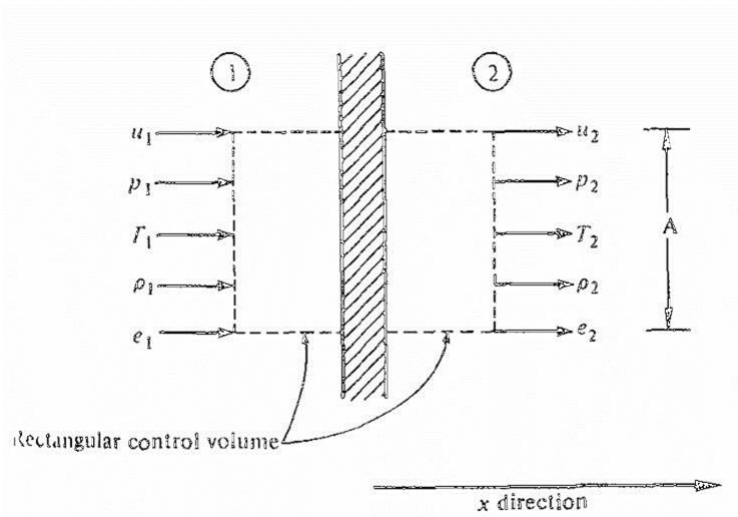


Fig. 1.1 Rectangular Control Volume

We have the energy equation for steady one-dimensional flow

$$h_1 + \frac{u_1^2}{2} + q = h_2 + \frac{u_2^2}{2} \quad (1)$$

Assuming no heat addition, this becomes

$$h_1 + \frac{u_1^2}{2} = h_2 + \frac{u_2^2}{2} \quad (2)$$

where points 1 and 2 correspond to the regions 1 and 2 identified in the above figure (Fig. 1.1). Specializing further to a calorically perfect gas, where $h = C_p T$, the above equation becomes,

$$c_p T_1 + \frac{u_1^2}{2} = c_p T_2 + \frac{u_2^2}{2} \quad (3)$$

$$c_p = \frac{\gamma R}{\gamma - 1} \quad (4)$$

Combining the above we get,

$$\frac{\gamma R T_1}{\gamma - 1} + \frac{u_1^2}{2} = \frac{\gamma R T_2}{\gamma - 1} + \frac{u_2^2}{2} \quad \text{Since } a = \sqrt{\gamma R T}$$

The above equation becomes,

$$\frac{a_1^2}{\gamma - 1} + \frac{u_1^2}{2} = \frac{a_2^2}{\gamma - 1} + \frac{u_2^2}{2} \quad (5)$$

When $a = \sqrt{\frac{\gamma P}{\rho}}$

The above equation can be written as,

$$\frac{\gamma}{\gamma - 1} \left(\frac{P_1}{\rho_1} \right) + \frac{u_1^2}{2} = \frac{\gamma}{\gamma - 1} \left(\frac{P_2}{\rho_2} \right) + \frac{u_2^2}{2} \quad (6)$$

The actual speed of sound and velocity at point A are a and u , respectively. At the imagined condition of Mach 1 (point 2 in the above equations), the speed of sound is a^* and the flow velocity is sonic, hence $u_2 = a^*$. Thus, the above equation yields,

$$\frac{a^2}{\gamma - 1} + \frac{u^2}{2} = \frac{a^{*2}}{\gamma - 1} + \frac{a^{*2}}{2} \quad (7)$$

$$\frac{a^2}{\gamma - 1} + \frac{u^2}{2} = \frac{\gamma + 1}{2(\gamma - 1)} a^{*2} \quad (8)$$

If the actual flowfield is nonadiabatic from A to B, $a^*_A \neq a^*_B$.

On the other hand, if the general flowfield is adiabatic throughout, then a^* is a constant value at every point in the flow. Since many practical aerodynamic flows are reasonably adiabatic, this is an important point to remember.

Let point 1 in correspond to point A and let point 2 correspond to our imagined conditions where the fluid element is brought to rest isentropically at point A. If T and u are the actual values of static temperature and velocity, respectively, at point A, then $T_1 = T$ and $u_1 = u$. Also, by definition of total conditions, $u_2 = 0$ and $T_2 = T_o$ Hence, equation

$$c_p T_1 + \frac{u_1^2}{2} = c_p T_2 + \frac{u_2^2}{2} \quad (9)$$

becomes

$$c_p T + \frac{u^2}{2} = c_p T_o \quad (10)$$

The above equation provides a formula from which the defined total temperature, T_o , can be calculated for the given actual conditions of T and u at any point in a general flow field. Remember that total conditions are defined earlier as those where the fluid element is isentropically brought to rest. However, in the derivation of the above equation, only the energy equation for an adiabatic flow is used. Isentropic conditions have not been imposed so far. Hence, the definition of T_o such as expressed in the above Eq is less restrictive than the definition of total conditions. Isentropic flow implies reversible and adiabatic conditions; Eq. tells us that, for the definition of T_o , only the "adiabatic" portion of the isentropic definition is required. That is, we can now redefine T_o as that temperature that would exist if the fluid element were brought to rest adiabatically. However, for the definition of total pressure, p_o , and total density, ρ_o , the imagined isentropic process is still necessary.

We have,

$$c_p T + \frac{u^2}{2} = c_p T_o \quad (11)$$

Several very useful equations for total conditions are obtained as follows from the above two equations.

$$\frac{T_o}{T} = 1 + \frac{u^2}{2c_p T} = 1 + \frac{u^2}{2\gamma RT/(\gamma - 1)} = 1 + \frac{u^2}{2a^2/(\gamma - 1)} = 1 + \frac{\gamma - 1}{2} \left(\frac{u}{a}\right)^2$$

Hence

$$\frac{T_o}{T} = 1 + \frac{\gamma - 1}{2} M^2 \quad (12)$$

The above equation gives the ratio of total to static temperature at a point in a flow as a function of the Mach number M at that point. Furthermore, for an isentropic process, the below equation

$$\frac{p_2}{p_1} = \left(\frac{\rho_2}{\rho_1}\right)^\gamma = \left(\frac{T_2}{T_1}\right)^{\gamma/(\gamma-1)} \quad (13)$$

holds, such that

$$\frac{p_o}{p} = \left(\frac{\rho_o}{\rho}\right)^\gamma = \left(\frac{T_o}{T}\right)^{\gamma/(\gamma-1)} \quad (14)$$

Combining the above two equations, we find

$$\frac{p_o}{p} = \left(1 + \frac{\gamma - 1}{2} M^2\right)^{\gamma/(\gamma-1)} \quad (15)$$

$$\frac{\rho_o}{\rho} = \left(1 + \frac{\gamma - 1}{2} M^2\right)^{1/(\gamma-1)}$$

The above two equations give the ratios of total to static pressure and density, respectively, at a point in the flow as a function of Mach number M at that point. Along with the following Eq.,

$$\frac{p_2}{p_1} = \left(\frac{\rho_2}{\rho_1}\right)^\gamma = \left(\frac{T_2}{T_1}\right)^{\gamma/(\gamma-1)} \quad (16)$$

they represent important relations for total properties—so important that their values are tabulated in Table (see Gas table) as a function of M for $\gamma = 1.4$ (which corresponds to air at standard conditions).

Example 3.1.

At a point in the flow over an F-15 high-performance fighter airplane, the pressure, temperature, and Mach number are 1890 lb/ft², 450°R, and 1.5, respectively. At this point, calculate T_0 , p_0 , T^* , p^* , and the flow velocity.

Table 1.3 Rankine temperature conversion formulae

	from Rankine	to Rankine
Celsius	$[^\circ\text{C}] = ([\text{R}] - 491.67) \times \frac{5}{9}$	$[\text{R}] = ([^\circ\text{C}] + 273.15) \times \frac{9}{5}$
Fahrenheit	$[^\circ\text{F}] = [\text{R}] - 459.67$	$[\text{R}] = [^\circ\text{F}] + 459.67$
Kelvin	$[\text{K}] = [\text{R}] \times \frac{5}{9}$	$[\text{R}] = [\text{K}] \times \frac{9}{5}$

Example 2:

Consider the flow through a rocket engine nozzle. Assume that the gas flow through the nozzle is an isentropic expansion of a calorically perfect gas. In the combustion chamber, the gas which results from the combustion of the rocket fuel and oxidizer is at a pressure and temperature of 15 atm and 2500 K, respectively, the molecular weight and specific heat at constant pressure of the combustion gas are 12 and 4157 J/kg K, respectively. The gas expands to supersonic speed through the nozzle, with a temperature of 1350 K at the nozzle exit. Calculate the pressure at the exit.

Solution. From our earlier discussion on the equation of state,

$$R = \frac{\mathcal{R}}{\mathcal{M}} = \frac{8314}{12} = 692.8 \text{ J/kg} \cdot \text{K}$$

From Eq. (1.20)

$$c_v = c_p - R = 4157 - 692.8 = 3464 \text{ J/kg} \cdot \text{K}$$

Thus

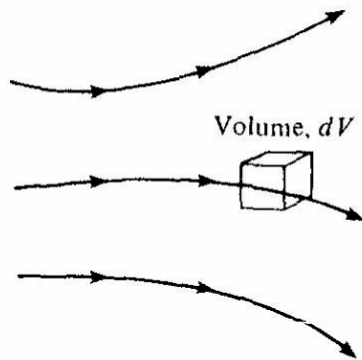
$$\gamma = \frac{c_p}{c_v} = \frac{4157}{3464} = 1.2$$

From Eq. (1.43), we have

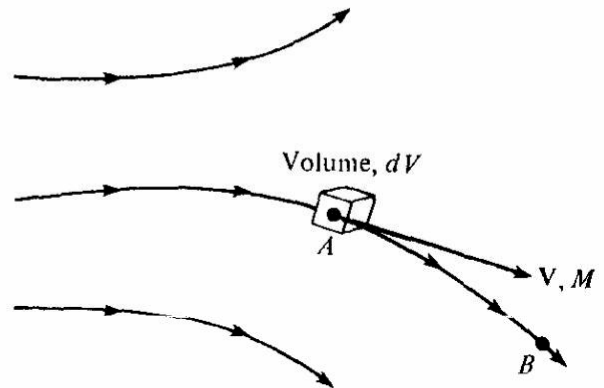
$$\frac{p_2}{p_1} = \left(\frac{T_2}{T_1} \right)^{\gamma/(\gamma-1)} = \left(\frac{1350}{2500} \right)^{1.2/(1.2-1)} = 0.0248$$

$$p_2 = 0.025 p_1 = (0.0248)(15 \text{ atm}) = \boxed{0.372 \text{ atm}}$$

1.2. Control Volume Approach:



Infinitesimal fluid element fixed in space with the fluid moving through it



Infinitesimal fluid element moving along a streamline with the velocity V equal to the flow velocity at each point

Fig. 1.2 Infinitesimal small control volume.

It should be emphasized again that the below four equations provide formulas from which the defined quantities T_o , p_o , and ρ_o can be calculated from the actual conditions of M , u , T , p , and ρ at a given point in a general flowfield, as sketched in Fig 1.2 (see above).

Again, the actual flowfield itself does not have to be adiabatic or isentropic from one point to the next. In these equations, the isentropic process is just in our minds as part of the definition of total conditions at a point.

$$c_p T + \frac{u^2}{2} = c_p T_o$$

$$\frac{T_o}{T} = 1 + \frac{\gamma - 1}{2} M^2$$

$$\frac{p_o}{p} = \left(1 + \frac{\gamma - 1}{2} M^2 \right)^{\gamma/(\gamma-1)}$$

$$\frac{\rho_o}{\rho} = \left(1 + \frac{\gamma - 1}{2} M^2 \right)^{1/(\gamma-1)}$$

Applied at point A in the above Fig 2.2, the above equations give us the values of T_o , p_o , and ρ_o associated with point A.

Similarly, applied at point B, the above equations give us the values of T_o , p_o , and ρ_o associated with point B. If the actual flow between A and B is nonadiabatic and irreversible, then

$$T_{o_A} \neq T_{o_B}, \quad p_{o_A} \neq p_{o_B}, \quad \text{and} \quad \rho_{o_A} \neq \rho_{o_B}.$$

On the other hand, if the general flow field is isentropic throughout, then T_o , p_o , and ρ_o are constant values at every point in the flow. The idea of constant total (stagnation) conditions in an isentropic flow will be very useful in our later discussions of various practical applications in compressible flow — keep it in mind!

We have

$$\frac{a_1^2}{\gamma - 1} + \frac{u_1^2}{2} = \frac{a_2^2}{\gamma - 1} + \frac{u_2^2}{2} \quad (1)$$

A few additional equations will be useful in subsequent sections. For example, from the above equation,

$$\frac{a^2}{\gamma - 1} + \frac{u^2}{2} = \frac{a_o^2}{\gamma - 1} \quad (2)$$

where a_o is the stagnation speed of sound.

$$\text{Stagnation speed of sound } a_o = \sqrt{\gamma RT_o}.$$

We have,

$$\frac{a^2}{\gamma - 1} + \frac{u^2}{2} = \frac{\gamma + 1}{2(\gamma - 1)} a^{*2} \quad (3)$$

$$\frac{a^2}{\gamma - 1} + \frac{u^2}{2} = \frac{a_o^2}{\gamma - 1} \quad (4)$$

Equating the R.H.S of the above two equations,

$$\frac{\gamma + 1}{2(\gamma - 1)} a^{*2} = \frac{a_o^2}{\gamma - 1} \quad (5)$$

Solving the above equation for a^*/a_o , and invoking

$$a = \sqrt{\gamma RT}$$

We get,

$$\left(\frac{a^*}{a_o}\right)^2 = \frac{T^*}{T_o} = \frac{2}{\gamma + 1} \quad (6)$$

$$\frac{p_o}{p} = \left(1 + \frac{\gamma - 1}{2} M^2\right)^{\gamma/(\gamma-1)} \quad (7)$$

$$\frac{\rho_o}{\rho} = \left(1 + \frac{\gamma - 1}{2} M^2\right)^{1/(\gamma-1)} \quad (8)$$

Recall that p^* and ρ^* are defined for conditions at Mach 1; hence, the above two equations with $M = 1$ lead to

$$\frac{p^*}{p_o} = \left(\frac{2}{\gamma + 1}\right)^{\gamma/(\gamma-1)} \quad (9)$$

$$\frac{\rho^*}{\rho_o} = \left(\frac{2}{\gamma + 1}\right)^{1/(\gamma-1)} \quad (10)$$

For air at standard conditions, where $\gamma = 1.4$, these ratios are

$$\frac{T^*}{T_o} = 0.833$$

$$\frac{p^*}{p_o} = 0.528$$

$$\frac{\rho^*}{\rho_o} = 0.634$$

which will be useful numbers to keep in mind for subsequent discussions.

$$\frac{a^2}{\gamma - 1} + \frac{u^2}{2} = \frac{\gamma + 1}{2(\gamma - 1)} a^{*2}$$

Dividing the above equation by u^2 , we have

$$\frac{(a/u)^2}{\gamma - 1} + \frac{1}{2} = \frac{\gamma + 1}{2(\gamma - 1)} \left(\frac{a^*}{u} \right)^2$$

$$\frac{(1/M)^2}{\gamma - 1} = \frac{\gamma + 1}{2(\gamma - 1)} \left(\frac{1}{M^*} \right)^2 - \frac{1}{2}$$

$$M^2 = \frac{2}{\left[(\gamma + 1)/M^{*2} \right] - (\gamma - 1)}$$

The above equation provides a direct relation between the actual Mach number M and the characteristic Mach number M^* .

Characteristic Mach number $M^* = V/a^*$. (Note that the real Mach number is $M = V/a$.)

$$M^2 = \frac{2}{\left[(\gamma + 1)/M^{*2} \right] - (\gamma - 1)} \quad (11)$$

Using the above relation find the value of M when,

$$M^* = 1$$

$$M^* < 1$$

$$M^* > 1$$

$$M^* \rightarrow \sqrt{\frac{\gamma + 1}{\gamma - 1}} \quad (12)$$

$$M^* = 1 \quad \text{if } M = 1$$

$$M^* < 1 \quad \text{if } M < 1$$

$$M^* > 1 \quad \text{if } M > 1$$

$$M^* \rightarrow \sqrt{\frac{\gamma + 1}{\gamma - 1}} \quad \text{if } M \rightarrow \infty$$

Hence, qualitatively, M^* acts in the same fashion as M , except when M goes to infinity.

In future discussions involving shock and expansion waves, M^* will be a useful parameter because it approaches a finite number as M approaches infinity.

All the equations in this section, either directly or indirectly, are alternative forms of the original, fundamental energy equation for one-dimensional, adiabatic flow (see below Eq.11).

$$\boxed{h_1 + \frac{u_1^2}{2} = h_2 + \frac{u_2^2}{2}} \quad (13)$$

Make certain that you examine these equations and their derivations closely. It is important at this stage that you feel comfortable with these equations, especially those with a box around them for emphasis.

Problem 1:

An aircraft flies at 800km/hr at an altitude of 10,000 meters ($T=223.15$ K, $p = 0.264$ bar). The air is reversibly compressed in an inlet diffuser ($\gamma = 1.4$, $R = 287$ J/kg K). The Mach number at the exit of the diffuser is 0.36 determine (a) entry Mach number and (b) velocity, pressure and temperature of air at the diffuser exit. (Hint: Use gas table)

Solution:

Let subscripts i and e refer to conditions at entry and exit of the diffuser respectively.

- (a) $P_i = 0.264$ bar, $T_i = 223.15$ K
 $u_i = 800 \times 1000 / 3600 = 222.22$ m/s
 We have

$$\boxed{c_p T + \frac{u^2}{2} = c_p T_o}$$

Using the above equation, we will get $T_o = 247.84$ K

= 0.74 Ans.

(b) From isentropic flow table for $\gamma = 1.4$ at

$M_i = 0.74$ (calculated) find P_i/P_0

$M_e = 0.36$ (given) find P_e/P_0 and T_e/T_0

From the isentropic flow table we have,

$$P_i/P_0 = 0.695$$

$$P_0 = P_i / 0.695 = 0.264 / 0.695$$

$$= 0.379$$

$$P_e/P_0 = 0.914$$

$$P_e = P_0 \times 0.914$$

$$= 0.379 \times 0.914$$

$$= \underline{\underline{0.346 \text{ Ans.}}}$$

Again from table: $T_e/T_0 = 0.975$

$$T_e = T_0 \text{ (calculated)} \times 0.975$$

$$= 247.84 \times 0.975$$

$$= \underline{\underline{241.6 \text{ K Ans.}}}$$

$$a_e = \sqrt{\gamma R T_e} = \sqrt{1.4 \times 287 \times 241.6}$$

$$= 311.57 \text{ m/s}$$

$$u_e = M_e a_e = 0.36 \times 311.57$$

$$= \underline{\underline{112.17 \text{ m/s Ans}}}$$

Table 1.2: Physical Properties of Standard Atmosphere in SI Units

Altitude (meters)	Temperature (K)	Pressure (Pa)	Density (kg/m ³)	Viscosity (N-s/m ²)
-5,000	320.7	1.778E+5	1.931	1.942E-5
-4,000	314.2	1.596E+5	1.770	1.912E-5
-3,000	307.7	1.430E+5	1.619	1.882E-5
-2,000	301.2	1.278E+5	1.478	1.852E-5
-1,000	294.7	1.139E+5	1.347	1.821E-5

0	288.2	1.013E+5	1.225	1.789E-5
1,000	281.7	8.988E+4	1.112	1.758E-5
2,000	275.2	7.950E+4	1.007	1.726E-5
3,000	268.7	7.012E+4	9.093E-1	1.694E-5
4,000	262.2	6.166E+4	8.194E-1	1.661E-5
5,000	255.7	5.405E+4	7.364E-1	1.628E-5
6,000	249.2	4.722E+4	6.601E-1	1.595E-5
7,000	242.7	4.111E+4	5.900E-1	1.561E-5
8,000	236.2	3.565E+4	5.258E-1	1.527E-5
9,000	229.7	3.080E+4	4.671E-1	1.493E-5
10,000	223.3	2.650E+4	4.135E-1	1.458E-5
15,000	216.7	1.211E+4	1.948E-1	1.422E-5
20,000	216.7	5.529E+3	8.891E-2	1.422E-5
30,000	226.5	1.197E+3	1.841E-2	1.475E-5
40,000	250.4	2.871E+2	3.996E-3	1.601E-5
50,000	270.7	7.978E+1	1.027E-3	1.704E-5
60,000	255.8	2.246E+1	3.059E-4	1.629E-5
70,000	219.7	5.520	8.754E-5	1.438E-5
80,000	180.7	1.037	1.999E-5	1.216E-5
90,000	180.7	1.644E-1	3.170E-6	1.216E-5

Problem-2

Air ($C_p = 1.03 \text{ kJ/kg K}$, $\gamma = 1.38$) at $P_1 = 3 \times 10^5 \text{ N/m}^2$ and $T_1 = 500 \text{ K}$ flows with a velocity of 200 m/s in a 30 cm diameter duct. Calculate:

- (a) Mass flow rate
- (b) Stagnation temperature © Mach number, and
- (c) Stagnation pressure values assuming the flow as compressible and incompressible.

Solution:

$$R = C_p - C_v = 0.289 \text{ kJ/kg K}$$

$$\rho_1 = P_1/RT_1 = 2.076 \text{ kg/m}^3$$

- (a) Mass flow rate = 29.348 kg/s
- (b) Stagnation temperature, $T_0 = 519.047 \text{ K}$
- (c) Mach number = 0.4478

- (d) Stagnation pressure

For compressible flow

$$\frac{P_0}{P_1} = \left(\frac{T_0}{T_1} \right)^{\gamma/(\gamma-1)}$$

$$1.145 (T_0 = 519.047 \text{ (calculated) and } T_1 = 500 \text{ K (given)}) P_0 = 1.145 \times 3 \times 10^5 \text{ N/m}^2 \\ = 3.435 \times 10^5 \text{ N/m}^2$$

For incompressible flow

$$P_0 = P_1 + \frac{1}{2} \rho_1 u_1^2 \\ = 3 \times 10^5 + \frac{1}{2} \times 2.076 \times 200^2 = 3.415 \times 10^5 \text{ N/m}^2$$



SATHYABAMA

INSTITUTE OF SCIENCE AND TECHNOLOGY
(DEEMED TO BE UNIVERSITY)

Accredited "A" Grade by NAAC | 12B Status by UGC | Approved by AICTE
www.sathyabama.ac.in

**SCHOOL OF MECHANICAL ENGINEERING
DEPARTMENT OF AERONAUTICAL ENGINEERING**

HIGH SPEED AERODYNAMICS

SAEA1505

UNIT – II – COMPRESSION AND EXPANSION WAVE – SAEA1505

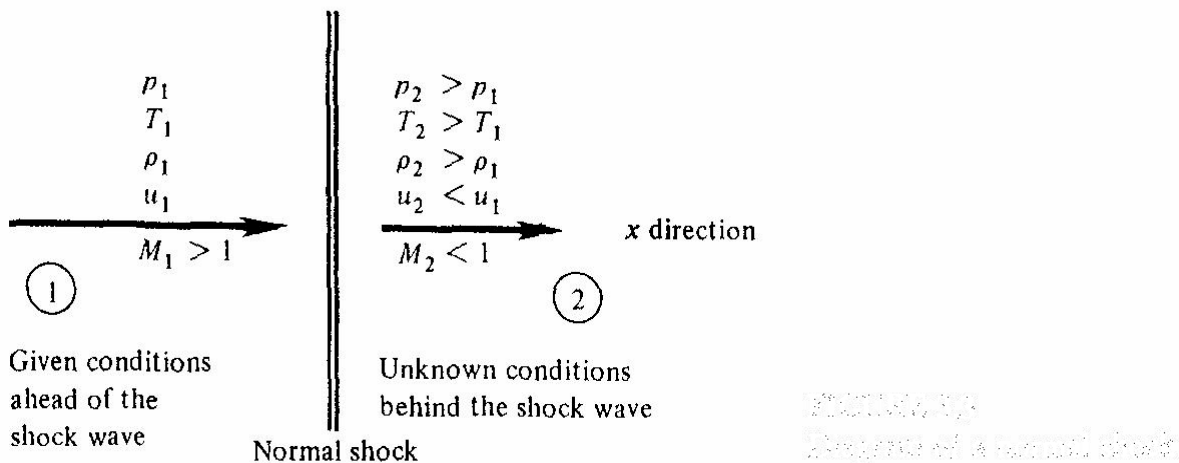


Fig. 2.1. Illustration of Normal shock relations

2.1 NORMAL SHOCK RELATIONS

Let us now apply the previous information to the practical problem of a normal shock wave. As discussed earlier normal shocks occur frequently as part of many supersonic flow fields. By definition, a normal shock wave is perpendicular to the flow, as sketched in Fig. 2.1 (see above). The shock is a very thin region (the shock thickness is usually on the order of a few molecular mean free paths, typically 10^{-5} cm for air at standard conditions). The flow is supersonic ahead of the wave, and subsonic behind it, as noted in Fig 2.1. Furthermore, the static pressure, temperature, and density increase across the shock, whereas the velocity decreases, all of which we will demonstrate shortly. Nature establishes shock waves in a supersonic flow as a solution to a perplexing problem having to do with the propagation of disturbances in the flow.

To obtain some preliminary physical feel for the creation of such shock waves, consider a flat-faced cylinder mounted in a flow, as sketched in Fig. 2.2 (see below).

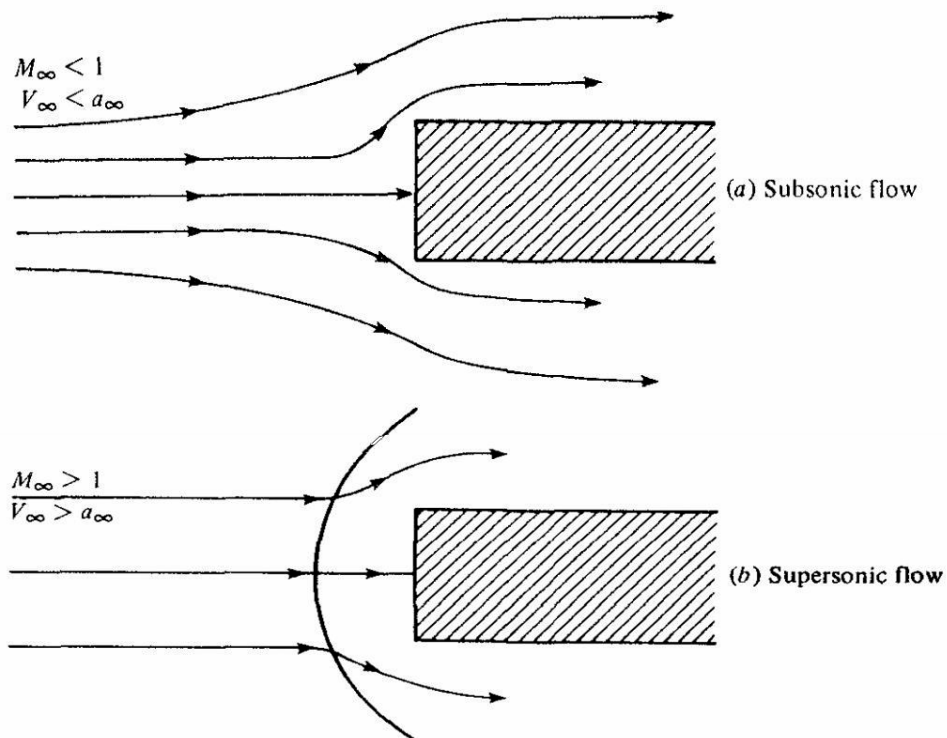


Fig. 2.2. Comparison between subsonic and supersonic streamlines for flow over a flat-faced cylinder or slab.

Recall that the flow consists of individual molecules, some of which impact on the face of the cylinder. There is in general a change in molecular energy and momentum due to impact with the cylinder, which is seen as an obstruction by the molecules. Therefore, just as in our example of the creation of a sound wave, as discussed earlier, the random motion of the molecules communicates this change in energy and momentum to other regions of the flow. The presence of the body tries to be propagated everywhere, including directly upstream, by sound waves.

In Fig. 2.2 a, the incoming stream is subsonic, $V_\infty < a_\infty$, and the sound waves can work their way upstream and forewarn the flow about the presence of the body. In this fashion, as shown in Fig. 2.2 a, the flow streamlines begin to change and the flow properties begin to compensate for the body far upstream (theoretically, an infinite distance upstream). In contrast, if the flow is supersonic, then $V_\infty > a_\infty$, and the sound waves can no longer propagate upstream. Instead, they tend to coalesce a short distance ahead of the body. In so doing, their coalescence forms a thin shock wave, as shown in Fig. 3.1b. Ahead of the shock wave, the flow has no idea of the presence of the body. Immediately behind the normal shock, however, the flow is subsonic, and hence the streamlines quickly compensate for the obstruction. Although the picture shown in Fig. 2.2 b is only one of many situations in which nature creates shock waves, the physical mechanism discussed above is quite general.

To begin a quantitative analysis of changes across a normal shock wave, consider again Fig. 2.2. Here, the normal shock is assumed to be a discontinuity across which the flow properties suddenly change. For purposes of discussion,

Assume that all conditions are known ahead of the shock (region 1), and that we want to solve for all conditions behind the shock (region 2). There is no heat added or taken away from the flow as it traverses the shock wave (for example, we are not putting the shock in a refrigerator, nor are we irradiating it with a laser); hence the flow across the shock wave is adiabatic. Therefore, the basic normal shock equations are obtained directly from the below equations (formulated earlier with $q = 0$) as,

$$\begin{aligned}\rho_1 u_1 &= \rho_2 u_2 && \text{(continuity)} \\ p_1 + \rho_1 u_1^2 &= p_2 + \rho_2 u_2^2 && \text{(momentum)} \\ h_1 + \frac{u_1^2}{2} &= h_2 + \frac{u_2^2}{2} && \text{(energy)}\end{aligned}$$

The above equations are general—they apply no matter what type of gas is being considered. Also, in general they must be solved numerically for the properties behind the shock wave, as will be discussed later for the cases of thermally perfect and chemically reacting gases. However, for a calorically perfect gas, we can immediately add the thermodynamic relations

$$\rho_1 u_1 = \rho_2 u_2 \quad (\text{continuity})$$

$$p_1 + \rho_1 u_1^2 = p_2 + \rho_2 u_2^2 \quad (\text{momentum})$$

$$h_1 + \frac{u_1^2}{2} = h_2 + \frac{u_2^2}{2} \quad (\text{energy})$$

$$p = \rho RT$$

and

$$h = c_p T$$

The above five equations with five unknowns, ρ_2 , u_2 , p_2 , h_2 , and T_2 can be solved algebraically, as follows.

First divide the momentum equation by the continuity equation,

$$\frac{p_1}{\rho_1 u_1} - \frac{p_2}{\rho_2 u_2} = u_2 - u_1$$

Recalling that $a = \sqrt{\gamma p / \rho}$

the above equation becomes,

$$\frac{a_1^2}{\gamma u_1} - \frac{a_2^2}{\gamma u_2} = u_2 - u_1 \quad (1)$$

The above equation is a combination of the continuity and momentum equations. The energy equation can be utilized in one of its alternative forms,

$$\frac{a^2}{\gamma - 1} + \frac{u^2}{2} = \frac{\gamma + 1}{2(\gamma - 1)} a^{*2}$$

which yields,

$$a_1^2 = \frac{\gamma + 1}{2} a^{*2} - \frac{\gamma - 1}{2} u_1^2 \quad (2)$$

and

$$a_2^2 = \frac{\gamma + 1}{2} a^{*2} - \frac{\gamma - 1}{2} u_2^2 \quad (3)$$

Since the flow is adiabatic across the shock wave, a^* in Eqs (2) and (3) is the same constant value.

Substituting Eqs. (2) and (3) into (1), we obtain

$$\frac{\gamma + 1}{2} \frac{a^{*2}}{\gamma u_1} - \frac{\gamma - 1}{2\gamma} u_1 - \frac{\gamma + 1}{2} \frac{a^{*2}}{\gamma u_2} + \frac{\gamma - 1}{2\gamma} u_2 = u_2 - u_1$$

or

$$\frac{\gamma + 1}{2\gamma u_1 u_2} (u_2 - u_1) a^{*2} + \frac{\gamma - 1}{2\gamma} (u_2 - u_1) = u_2 - u_1$$

Dividing by $(u_2 - u_1)$,

$$\frac{\gamma + 1}{2\gamma u_1 u_2} a^{*2} + \frac{\gamma - 1}{2\gamma} = 1$$

Solving for a^* , this gives

$$\boxed{a^{*2} = u_1 u_2}$$

(4)

The above equation is called the **Prandtl relation**, and is a useful intermediate relation for normal shocks.

For example, from this simple equation we obtain directly

$$1 = \frac{u_1}{a^*} \frac{u_2}{a^*} = M_1^* M_2^*$$

or

$$\boxed{M_2^* = \frac{1}{M_1^*}}$$

(5)

Based on our previous physical discussion, the flow ahead of a shock wave must be supersonic, i.e, $M_1 > 1$. It implies $M_1^* > 1$. Thus, from the above Eq. $M_2^* < 1$ and thus $M_2 < 1$. Hence, the Mach number behind the normal shock is always subsonic. This is a general result, not just limited to a calorically perfect gas.

We have

$$M^2 = \frac{2}{[(\gamma + 1)/M^{*2}] - (\gamma - 1)} \quad (6)$$

Which solved for M^* , gives

$$M^{*2} = \frac{(\gamma + 1)M^2}{2 + (\gamma - 1)M^2} \quad (7)$$

Substitute the above equation into

$$M_2^* = \frac{1}{M_1^*}$$

We get,

$$\frac{(\gamma + 1)M_2^2}{2 + (\gamma - 1)M_2^2} = \left[\frac{(\gamma + 1)M_1^2}{2 + (\gamma - 1)M_1^2} \right]^{-1}$$

Solving the above Eq. for M_2^2

$$M_2^2 = \frac{1 + [(\gamma - 1)/2] M_1^2}{\gamma M_1^2 - (\gamma - 1)/2} \quad (8)$$

The above equation demonstrates that, for a calorically perfect gas with a constant value of γ , the Mach number behind the shock is a function of only the Mach number ahead of the shock. It also shows that when $M_1=1$, then $M_2=1$. This is the case of an infinitely weak normal shock, which is defined as a Mach wave. In contrast, as M_1 increases above 1, the normal shock becomes stronger and M_2

becomes progressively less than 1. However, in the limit, as $M_1 \rightarrow \infty$, M_2 approaches a finite minimum value, $M_2 \rightarrow \sqrt{(\gamma - 1)/2\gamma}$, which for air is 0.378

The upstream Mach number M_1 is a powerful parameter which dictates shock wave properties. This is already seen in the above Eq. Ratios of other properties across the shock can also be found in terms of M_1 . For example, from Eq.

$$\rho_1 u_1 = \rho_2 u_2 \quad (\text{continuity})$$

combined with

$$a^{*2} = u_1 u_2$$

$$\frac{\rho_2}{\rho_1} = \frac{u_1}{u_2} = \frac{u_1^2}{u_2 u_1} = \frac{u_1^2}{a^{*2}} = M_1^{*2}$$

Substituting (we have)

$$M^{*2} = \frac{(\gamma + 1) M^2}{2 + (\gamma - 1) M^2}$$

into the above equation,

$$\boxed{\frac{\rho_2}{\rho_1} = \frac{u_1}{u_2} = \frac{(\gamma + 1) M_1^2}{2 + (\gamma - 1) M_1^2}} \quad (9)$$

To obtain the pressure ratio, return to the momentum equation

$$p_2 - p_1 = \rho_1 u_1^2 - \rho_2 u_2^2$$

which, combined with the continuity equation, yields

$$p_2 - p_1 = \rho_1 u_1 (u_1 - u_2) = \rho_1 u_1^2 \left(1 - \frac{u_2}{u_1}\right)$$

Dividing the above Eq. by p_1 ,
and recalling that $a_1^2 = \gamma p_1 / \rho_1$, we obtain

$$\frac{p_2 - p_1}{p_1} = \gamma M_1^2 \left(1 - \frac{u_2}{u_1}\right)$$

We have

$$\frac{u_1}{u_2} = \frac{(\gamma + 1) M_1^2}{2 + (\gamma - 1) M_1^2} \quad (10)$$

Substitute it in the above Eq., we get,

$$\frac{p_2 - p_1}{p_1} = \gamma M_1^2 \left[1 - \frac{2 + (\gamma - 1) M_1^2}{(\gamma + 1) M_1^2}\right] \quad (11)$$

It simplifies to,

$$\boxed{\frac{p_2}{p_1} = 1 + \frac{2\gamma}{\gamma + 1}(M_1^2 - 1)} \quad (12)$$

To obtain the temperature ratio, recall the equation of state, $p = \rho RT$. Hence

$$\frac{T_2}{T_1} = \left(\frac{p_2}{p_1}\right)\left(\frac{\rho_1}{\rho_2}\right)$$

We have

$$\boxed{\frac{\rho_2}{\rho_1} = \frac{u_1}{u_2} = \frac{(\gamma + 1)M_1^2}{2 + (\gamma - 1)M_1^2}} \quad (13)$$

Combining the above three equations,

$$\boxed{\frac{T_2}{T_1} = \frac{h_2}{h_1} = \left[1 + \frac{2\gamma}{\gamma + 1}(M_1^2 - 1)\right] \left[\frac{2 + (\gamma - 1)M_1^2}{(\gamma + 1)M_1^2}\right]} \quad (14)$$

Examine the following equations.

$$M_2^2 = \frac{1 + [(\gamma - 1)/2] M_1^2}{\gamma M_1^2 - (\gamma - 1)/2} \quad (15)$$

$$\frac{\rho_2}{\rho_1} = \frac{u_1}{u_2} = \frac{(\gamma + 1) M_1^2}{2 + (\gamma - 1) M_1^2} \quad (16)$$

$$\frac{T_2}{T_1} = \frac{h_2}{h_1} = \left[1 + \frac{2\gamma}{\gamma + 1} (M_1^2 - 1) \right] \left[\frac{2 + (\gamma - 1) M_1^2}{(\gamma + 1) M_1^2} \right] \quad (17)$$

For a calorically perfect gas with a given γ , they give M_2 , ρ_2/ρ_1 , P_2/P_1 , and T_2/T_1 as functions of M_1 only. This is our first major demonstration of the importance of Mach number in the quantitative

$$M_2^2 = \frac{1 + [(\gamma - 1)/2] M_1^2}{\gamma M_1^2 - (\gamma - 1)/2} \quad (18)$$

governance of compressible flowfields.

In contrast, as will be shown later for an equilibrium thermally perfect gas, the changes across a normal shock depend on both M_1 and T_1 , whereas for an equilibrium chemically reacting gas they depend on M_1 , T_1 and p_1 . Moreover, for such high-temperature cases, closed-form expressions such as the above derived equations are generally not possible, and the normal shock properties must be calculated numerically. Hence, the simplicity brought about by the calorically perfect gas assumption in this section is clearly evident. Fortunately, the results of this section hold reasonably accurately up to approximately $M_1 = 5$ in air at standard conditions. Beyond Mach 5, the temperature behind the normal shock becomes high enough that γ is no longer constant. However, the flow regime $M_1 < 5$ contains a large number of everyday practical problems, and therefore the results of this section are extremely useful.

Problem-3

A normal shock wave is standing in the test section of a supersonic wind tunnel. Upstream of the wave, $M_1 = 3$, $p_1 = 0.5$ atm, and $T_1 = 200$ K. Find M_2 , p_2 , T_2 , and u_2 downstream of the wave.

Solution. From Table A 2, for $M_1 = 3$, $p_2/p_1 = 10.33$, $T_2/T_1 = 2.679$, and $M_2 = 0.4752$. Hence

$$p_2 = \frac{p_2}{p_1} p_1 = 10.33(0.5) = 5.165 \text{ atm}$$

$$T_2 = \frac{T_2}{T_1} T_1 = 2.679(200) = 535.8 \text{ K}$$

$$a_2 = \sqrt{\gamma R T_2} = \sqrt{(1.4)(287)(535.8)} = 464 \text{ m/s}$$

$$u_2 = M_2 a_2 = (0.4752)(464) = 220 \text{ m/s}$$

$$\frac{\rho_2}{\rho_1} = \frac{u_1}{u_2} = \frac{(\gamma + 1)M_1^2}{2 + (\gamma - 1)M_1^2}$$

$$\frac{p_2}{p_1} = 1 + \frac{2\gamma}{\gamma + 1}(M_1^2 - 1)$$

$$\frac{T_2}{T_1} = \frac{h_2}{h_1} = \left[1 + \frac{2\gamma}{\gamma + 1}(M_1^2 - 1) \right] \left[\frac{2 + (\gamma - 1)M_1^2}{(\gamma + 1)M_1^2} \right]$$

The limiting case of $M_1 \rightarrow \infty$ can be visualized as $u_1 \rightarrow \infty$, where the calorically perfect gas assumption is invalidated by high temperatures, or as $a_1 \rightarrow \infty$, where the perfect gas equation of state is invalidated by extremely low temperatures. Nevertheless, it is interesting to examine the variation of properties across the normal shock as $M_1 \rightarrow \infty$ in the following equations (derived earlier).

We find, when $M_1 \rightarrow \infty$ for $\gamma = 1.4$

$$\lim_{M_1 \rightarrow \infty} M_2 = \sqrt{\frac{\gamma - 1}{2\gamma}} = 0.378 \quad (\text{as discussed previously})$$

$$\lim_{M_1 \rightarrow \infty} \frac{\rho_2}{\rho_1} = \frac{\gamma + 1}{\gamma - 1} = 6$$

$$\lim_{M_1 \rightarrow \infty} \frac{p_2}{p_1} = \infty$$

$$\lim_{M_1 \rightarrow \infty} \frac{T_2}{T_1} = \infty$$

At the other extreme, we also find when $M_1 = 1$ for $\gamma = 1.4$

$M_2 = 1$

$$\rho_2/\rho_1 = p_2/p_1 = T_2/T_1 = 1.$$

This is the case of an infinitely weak normal shock degenerating into a Mach wave, where no finite changes occur across the wave. This is the same as the sound wave discussed earlier.

$$M_2^2 = \frac{1 + [(\gamma - 1)/2] M_1^2}{\gamma M_1^2 - (\gamma - 1)/2}$$

$$\frac{\rho_2}{\rho_1} = \frac{u_1}{u_2} = \frac{(\gamma + 1) M_1^2}{2 + (\gamma - 1) M_1^2}$$

$$\frac{p_2}{p_1} = 1 + \frac{2\gamma}{\gamma + 1} (M_1^2 - 1)$$

$$\frac{T_2}{T_1} = \frac{h_2}{h_1} = \left[1 + \frac{2\gamma}{\gamma + 1} (M_1^2 - 1) \right] \left[\frac{2 + (\gamma - 1) M_1^2}{(\gamma + 1) M_1^2} \right]$$

To prove that the above equations have physical meaning only when $M_1 > 1$, we must invoke the second law of thermodynamics.

We have,

$$s_2 - s_1 = c_p \ln \frac{T_2}{T_1} - R \ln \frac{p_2}{p_1}$$

Substitute for T_2/T_1 and p_2/p_1 , we get

$$s_2 - s_1 = c_p \ln \left\{ \left[1 + \frac{2\gamma}{\gamma + 1} (M_1^2 - 1) \right] \left[\frac{2 + (\gamma - 1)M_1^2}{(\gamma + 1)M_1^2} \right] \right\} - R \ln \left[1 + \frac{2\gamma}{\gamma + 1} (M_1^2 - 1) \right]$$

The above equation demonstrates that the entropy change across the normal shock is also a function of upstream mach number, M_1 only.

Moreover, it shows that,

$$\begin{aligned} &\text{if } M_1 = 1 \text{ then } s_2 - s_1 = 0, \\ &\text{if } M_1 < 1 \text{ then } s_2 - s_1 < 0, \\ &\text{and if } M_1 > 1 \text{ then } s_2 - s_1 > 0. \end{aligned}$$

Therefore, since it is necessary that $s_2 - s_1 \geq 0$ from the second law of thermodynamics, the upstream Mach number M_1 must be greater than or equal to 1.

Here is another example of how the second law tells us the direction in which a physical process will proceed. If M_1 is subsonic, then the above equation says that the entropy decreases across the normal shock — an impossible situation. The only physically possible case is $M_1 > 1$, which in turn dictates from the above four equations that

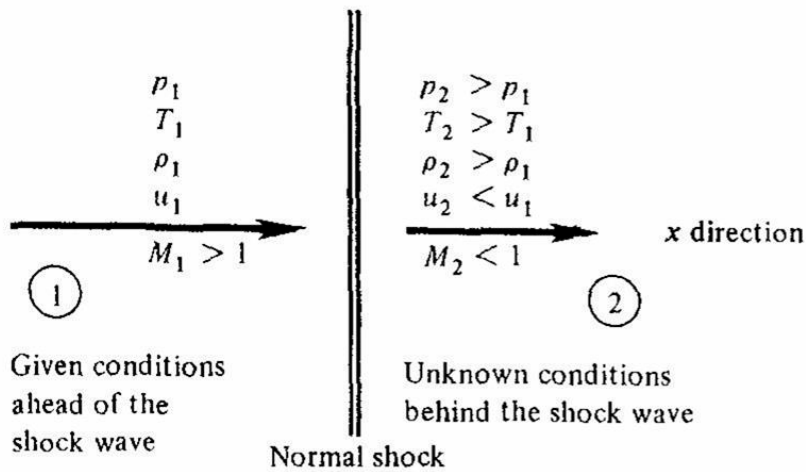


Fig. 2.3. Flow properties variations across a normal shock.

Thus, we have now established the phenomena sketched in Fig. 2.3, namely, that across a normal shock wave the pressure, density, and temperature increase, whereas the velocity decreases and the Mach number decreases to a subsonic value.

What really causes the entropy increase across a shock wave?

To answer this, recall that the changes across the shock occur over a very short distance, on the order of 10^{-5} cm. Hence, the velocity and temperature gradients inside the shock structure itself are very large. In regions of large gradients, the viscous effects of viscosity and thermal conduction become important. In turn, these are dissipative, irreversible phenomena which generate entropy. Therefore, the net entropy increase predicted by the normal shock relations in conjunction with the second law of thermodynamics is appropriately provided by nature in the form of friction and thermal conduction inside the shock wave structure itself.

stagnating of the fluid element has been done isentropically. In region 2 behind the shock, a fluid element is moving with actual conditions of M_2 , p_2 , T_2 , and s_2 . Consider in this region the imaginary state $2a$ where the fluid element has been brought to rest isentropically. Here, by definition, the pressure and temperature in state $2a$ are the total values of p_{02} and T_{02} , respectively. The entropy at state $2a$ is still s_2 , by definition. The question is now raised how p_{02} and T_{02} behind the shock compare with p_{01} and T_{01} , respectively, ahead of the shock. To answer this question, we use the following equation for calorically perfect gas,

$$c_p T_1 + \frac{u_1^2}{2} = c_p T_2 + \frac{u_2^2}{2}$$

The total temperature is given by

$$c_p T_o = c_p T + \frac{u^2}{2}$$

Hence

$$c_p T_{o1} = c_p T_{o2}$$

and thus

$$T_{o_1} = T_{o_2}$$

From the above equation, we see that the total temperature is constant across a stationary normal shock wave, which holds for a calorically perfect gas, is a special case of the more general result that the total enthalpy is constant across the shock, as demonstrated earlier using the following equation,

$$h_1 + \frac{u_1^2}{2} = h_2 + \frac{u_2^2}{2} \quad (\text{energy})$$

For a stationary normal shock, the total enthalpy is always constant across the shock wave, which for calorically or thermally perfect gases translates into a constant total temperature across the shock. However, for a chemically reacting gas, the total temperature is not constant across the shock (will be discussed later). Also, if the shock wave is not stationary — if it is moving through space — neither the total enthalpy nor total temperature are constant across the wave. This becomes a matter of reference systems (will discuss later).

$$s_{2a} - s_{1a} = c_p \ln \frac{T_{2a}}{T_{1a}} - R \ln \frac{p_{2a}}{p_{1a}}$$

However, $s_{2a} = s_2$, $s_{1a} = s_1$, $T_{2a} = T_o = T_{1a}$, $p_{2a} = p_{o_2}$, and $p_{1a} = p_{o_1}$

Hence the above equation becomes,

$$\boxed{s_2 - s_1 = -R \ln \frac{p_{o_2}}{p_{o_1}}} \quad (2)$$

OR

$$\frac{p_{o_2}}{p_{o_1}} = e^{-(s_2 - s_1)/R}$$

Where,

$$s_2 - s_1 = c_p \ln \left\{ \left[1 + \frac{2\gamma}{\gamma + 1} (M_1^2 - 1) \right] \left[\frac{2 + (\gamma - 1)M_1^2}{(\gamma + 1)M_1^2} \right] \right\} - R \ln \left[1 + \frac{2\gamma}{\gamma + 1} (M_1^2 - 1) \right]$$

From the above two equations we see that the ratio of total pressures across the normal shock depends on M_1 only. Also, because $s_2 > s_1$, the following equations (derived above) show that $p_{o2} < p_{o1}$. The total pressure decreases across a shock wave.

$$\boxed{s_2 - s_1 = -R \ln \frac{p_{o2}}{p_{o1}}} \quad (3)$$

$$\frac{p_{o2}}{p_{o1}} = e^{-(s_2 - s_1)/R}$$

The variations of p_2/p_1 , ρ_2/ρ_1 , T_2/T_1 , p_{o2}/p_{o1} , and M_2 with M_1 as obtained from the above equations are tabulated in the gas table for various values of γ .

To provide more physical feel, these variations are plotted in the below figure for $\gamma = 1.4$. Note that (as stated earlier) these curves show how, as M_1 becomes very large, T_2/T_1 and p_2/p_1 also become very large, whereas ρ_2/ρ_1 and M_2 approach finite limits.

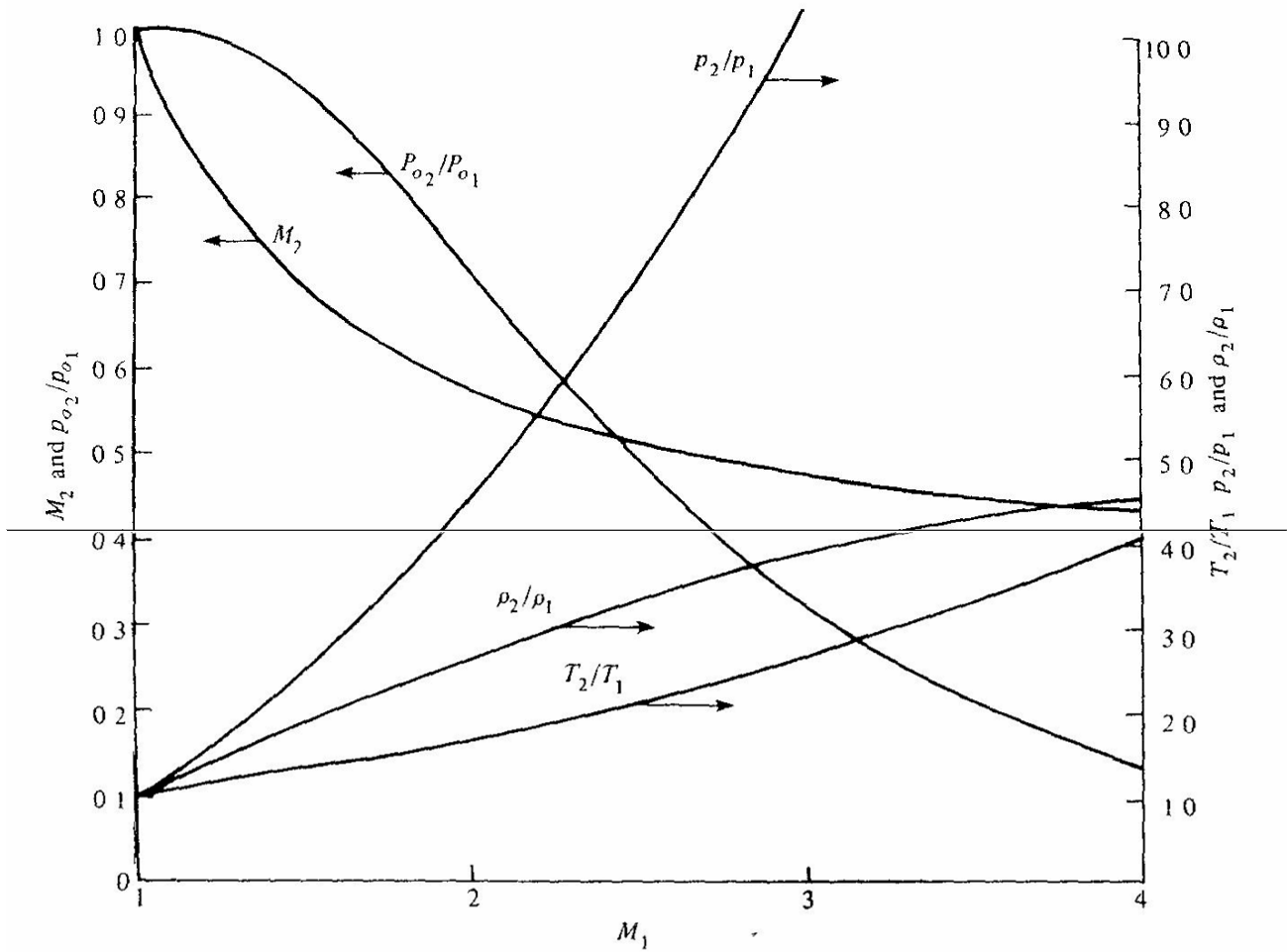


Fig. 2.6. Flow properties around a normal shock wave

Example-4

A blunt-nosed missile is flying at Mach 2 at standard sea level. Calculate the temperature and pressure at the nose of the missile.

Solution. The nose of the missile is a stagnation point, and the streamline through the stagnation point has also passed through the normal portion of the bow shock wave. Hence, the temperature and pressure at the nose are equal to the total temperature and pressure behind a normal shock. Also, at standard sea level, $T_1 = 519^\circ\text{R}$ and $p_1 = 2116 \text{ lb/ft}^2$.

From Table A 1, for $M_1 = 2$: $T_{o_1}/T_1 = 1.8$ and $p_{o_1}/p_1 = 7.824$. Also, for adiabatic flow through a normal shock, $T_{o_2} = T_{o_1}$. Hence

$$T_{o_2} = T_{o_1} = \frac{T_{o_1}}{T_1} T_1 = 1.8(519) = \boxed{934.2^\circ\text{R}}$$

From Table A 2, for $M_1 = 2$: $p_{o_2}/p_{o_1} = 0.7209$. Hence

$$p_{o_2} = \frac{p_{o_2}}{p_{o_1}} \frac{p_{o_1}}{p_1} p_1 = (0.7209)(7.824)(2116) = \boxed{11,935 \text{ lb/ft}^2}$$

2.2 Analytical Exercises

Prove that the change in internal energy equals the mean pressure across the shock times the change in specific volume. i.e.,

$$e_2 - e_1 = \frac{p_1 + p_2}{2} (v_1 - v_2)$$

Hint:

Eliminate the velocity term from the following energy equation.

$$h_1 + \frac{u_1^2}{2} = h_2 + \frac{u_2^2}{2}$$

Where,

$$h = e + p/\rho$$

Use the following continuity and momentum equation for getting the desired solution.

$$\rho_1 u_1 = \rho_2 u_2 \quad (\text{continuity})$$

$$p_1 + \rho_1 u_1^2 = p_2 + \rho_2 u_2^2 \quad (\text{momentum})$$

2.3 HUGONIOT EQUATION

The results obtained in the previous section for the normal shock wave were couched in terms of velocities and Mach numbers—quantities which quite properly emphasize the fluid dynamic nature of shock waves. However, because the static pressure always increases across a shock wave, the wave itself can also be visualized as a thermodynamic device which compresses the gas. Indeed, the changes across a normal shock wave can be expressed in terms of purely thermodynamic variables without explicit reference to a velocity or Mach number, as follows From the continuity equation

$$u_2 = u_1 \left(\frac{\rho_1}{\rho_2} \right) \quad (1)$$

Substitute the above equation into the momentum equation,

$$p_1 + \rho_1 u_1^2 = p_2 + \rho_2 \left(\frac{\rho_1}{\rho_2} u_1 \right)^2 \quad (2)$$

Solve the above equation for u_1^2

$$u_1^2 = \frac{p_2 - p_1}{\rho_2 - \rho_1} \left(\frac{\rho_2}{\rho_1} \right) \quad (3)$$

Alternatively, writing the continuity equation as

$$u_1 = u_2 \left(\frac{\rho_2}{\rho_1} \right) \quad (4)$$

and again substituting into the momentum equation, this time solving for u_2 , we obtain

$$u_2^2 = \frac{p_2 - p_1}{\rho_2 - \rho_1} \left(\frac{\rho_1}{\rho_2} \right) \quad (5)$$

From the energy equation, we have

$$h_1 + \frac{u_1^2}{2} = h_2 + \frac{u_2^2}{2} \quad (6)$$

and recalling that by definition $h = e + p/\rho$, we have

$$e_1 + \frac{p_1}{\rho_1} + \frac{u_1^2}{2} = e_2 + \frac{p_2}{\rho_2} + \frac{u_2^2}{2} \quad (7)$$

Substituting the values of u_1^2 and u_2^2 into the above equation, the velocities are eliminated, yielding

$$e_1 + \frac{p_1}{\rho_1} + \frac{1}{2} \left[\frac{p_2 - p_1}{\rho_2 - \rho_1} \left(\frac{\rho_2}{\rho_1} \right) \right] = e_2 + \frac{p_2}{\rho_2} + \frac{1}{2} \left[\frac{p_2 - p_1}{\rho_2 - \rho_1} \left(\frac{\rho_1}{\rho_2} \right) \right]$$

This simplifies to

$$e_2 - e_1 = \frac{(p_1 + p_2)}{2} \left(\frac{1}{\rho_1} - \frac{1}{\rho_2} \right)$$

$$\boxed{e_2 - e_1 = \frac{p_1 + p_2}{2} (v_1 - v_2)} \quad (8)$$

The above equation is called the Hugoniot equation. It has certain advantages because it relates only thermodynamic quantities across the shock. Also, we have made no assumption about the type of gas; the above is a general relation that holds for a perfect gas, chemically reacting gas, real gas, etc.

In addition, note that the above Hugoniot equation has the form of

$$\underline{\Delta e = -p_{\text{ave}} \Delta v} \quad (9)$$

i.e., the change in internal energy equals the mean pressure across the shock times the change in specific volume. This strongly reminds us of the first law of thermodynamics in the form of

$$\delta q - p dv = de ,$$

with

$$\delta q = 0 \quad (10)$$

for the adiabatic process across the shock

In general, in equilibrium thermodynamics any state variable can be expressed as a function of any other two state variables, for example $e = e(p, v)$. This relation could be substituted into Eq (3.72), resulting in a functional relation

$$p_2 = f(p_1, v_1, v_2) \quad (3.73)$$

For given conditions of p_1 and v_1 upstream of the normal shock, Eq (3.73) represents p_2 as a function of v_2 . A plot of this relation on a pv graph is called the *Hugoniot curve*, which is sketched in Fig 3.10. This curve is the locus of all possible pressure-volume conditions behind normal shocks of various strengths for one specific set of upstream values for p_1 and v_1 (point 1 in Fig 3.10). Each point on the Hugoniot curve in Fig. 3.10 therefore represents a different shock with a different upstream velocity u_1 .

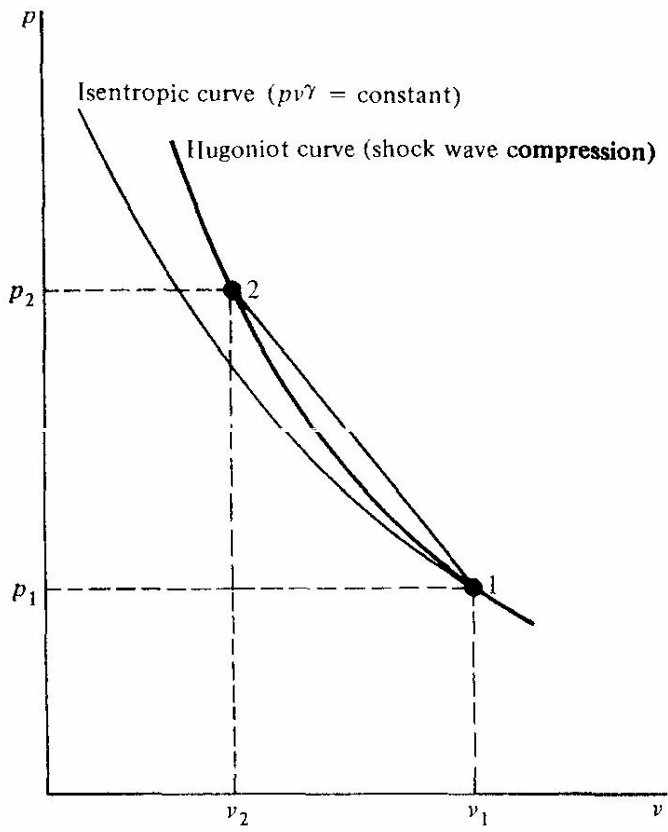


Fig. 2.6. Rankine Hugoniot Relation.

2.4 OBLIQUE SHOCK WAVES







Fig. 2. 7 A Boeing F/A-18 with afterburners on. Note shock/expansion patterns in the supersonic nozzle exhaust.

http://images.google.co.in/imgres?imgurl=http://www.ae.gatech.edu/labs/windtunl/classes/Propulsion/mig25mm.jpg&imgrefurl=http://www.ae.gatech.edu/labs/windtunl/classes/Propulsion/ae42512.html&usg=__2oZgbPgFEoyr-GAsJ3FDrziF9w=&h=391&w=638&sz=27&hl=en&start=8&um=1&tbnid=u37vEw2l3lOESM:&tbnh=84&tbnw=137&prev=/images%3Fq%3Doblique%2Bshock%26hl%3Den%26sa%3DX%26um%3D1

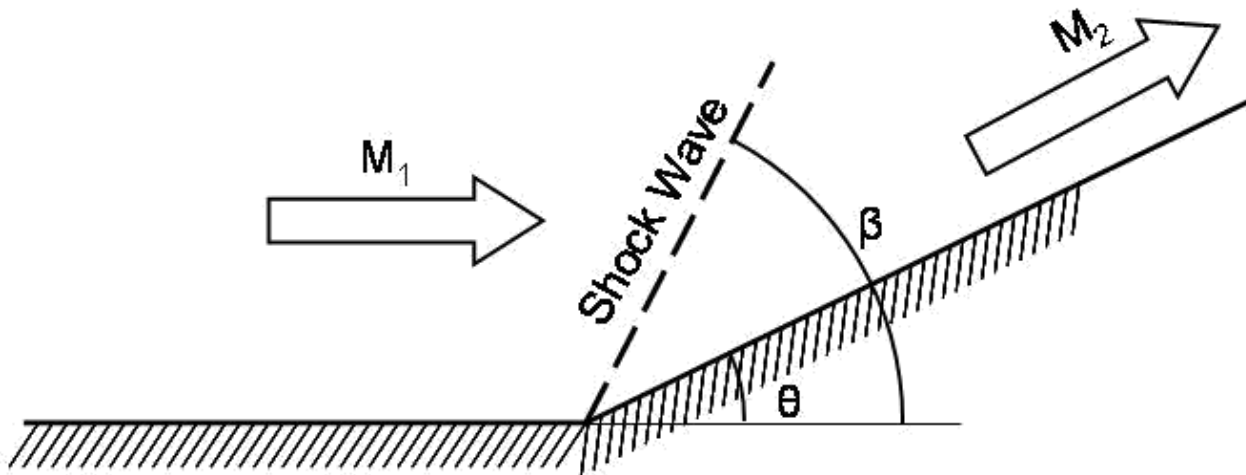


Fig. 2.8. Convex corner supersonic flow

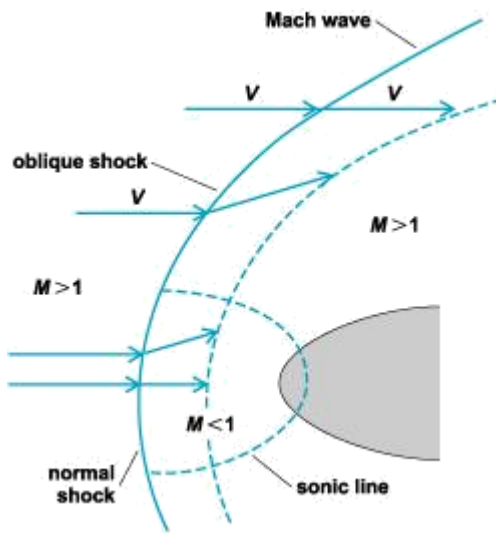


Fig. 2.9 Supersonic flow over a blunt body.

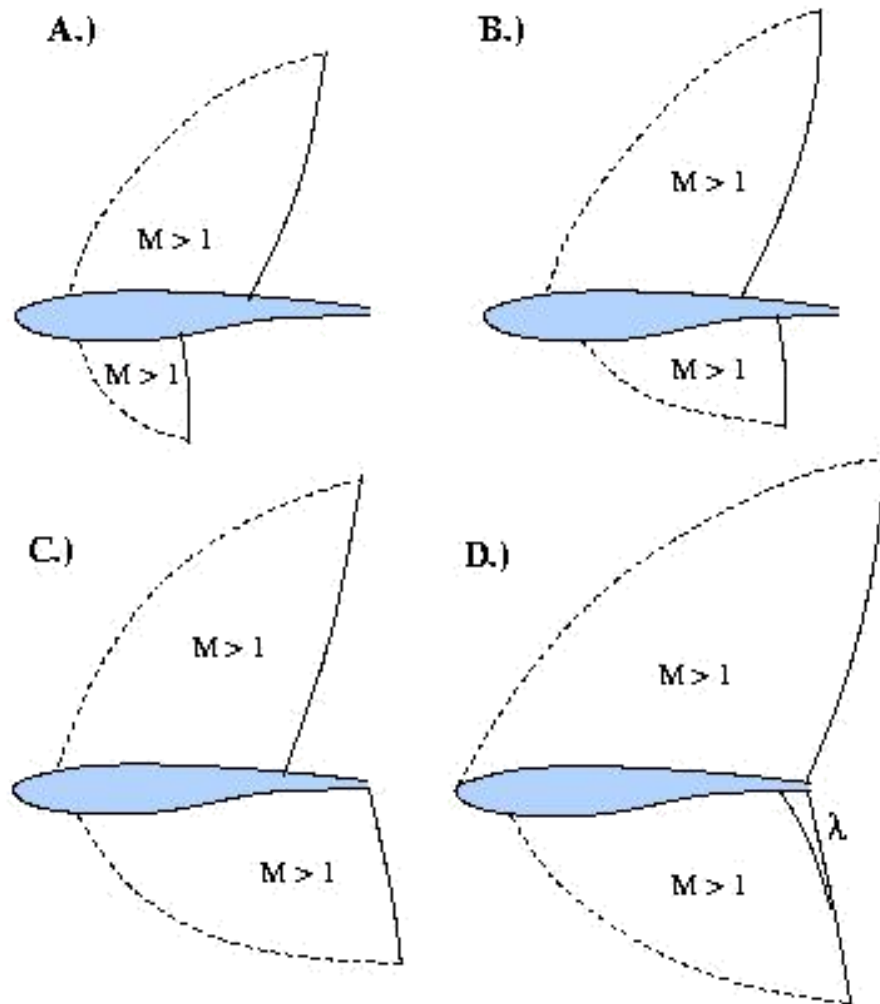


Fig. 2.10 Shock Progression on Airfoil

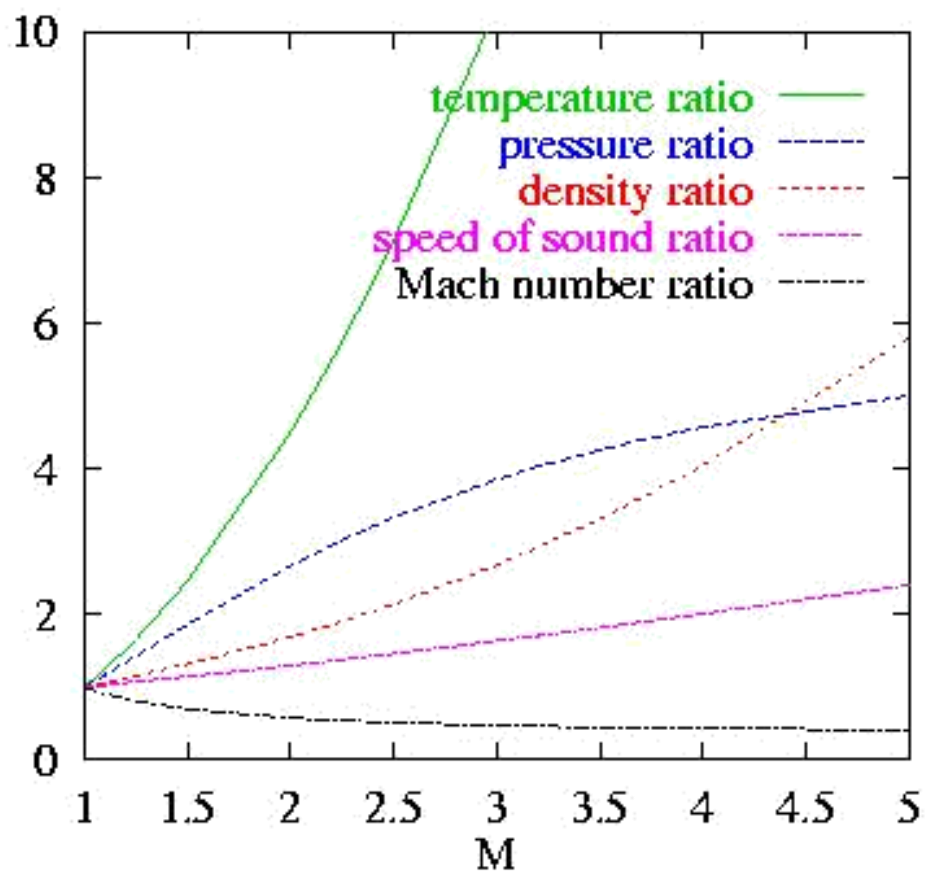


Fig. 2.11 Normal shock ratios at supersonic speeds

2.5. EXTERNAL FLOW APPLIED TO AIRCRAFT / SPACECRAFT

Viscosity.- There are basically three states of matter - solid, liquid, and gas. H₂O is commonly called "ice" in the solid state, "water" in the liquid state, and "water vapor" in the gaseous state. Assume one has a piece of ice and side forces are applied to it (called shearing forces). Very large forces are needed to deform or break it. The solid has a very high internal friction or resistance to shearing. The word for internal friction is viscosity and for a solid its value is generally very large.

Liquids and gases are considered to be fluids since they behave differently from a solid. Imagine two layers of water or air. If shear forces are applied to these layers, one discovers a substantial and sustained relative motion of the layers with the air layers sliding faster over one another than the water layers. However, the fact that a shear force must be applied to deform the fluids indicates that they also possess internal friction.

Water, under normal temperatures, is about fifty times more viscous than air. Ice is 5×10^{16} times more viscous than air. One concludes that, in general, solids have extremely high viscosities whereas fluids have low viscosities. Under the category of fluids, liquids generally possess higher viscosities than gases. Air, of primary interest in aerodynamics, has a relatively small viscosity, and in some theories, it is described as a perfect fluid-one that has zero viscosity or is "inviscid." But it will be shown that even this small viscosity of air (or internal friction) has important effects on an airplane in terms of lift and drag.

2.6. Oblique Shock

- The discontinuities in supersonic flows do not always exist as normal to the flow direction. There are oblique shocks which are inclined with respect to the flow direction. Refer to the shock structure on an obstacle, as depicted qualitatively in the below Fig.
- The segment of the shock immediately in front of the body behaves like a normal shock.
- Oblique shock can be observed in following cases-
 1. **Oblique shock formed as a consequence of the bending of the shock in the free-stream direction**
(shown in the below Fig.2.7)
 2. **In a supersonic flow through a duct, viscous effects cause the shock to be oblique near the walls, the shock being normal only in the core region.**
 3. **The shock is also oblique when a supersonic flow is made to change direction near a sharp corner**

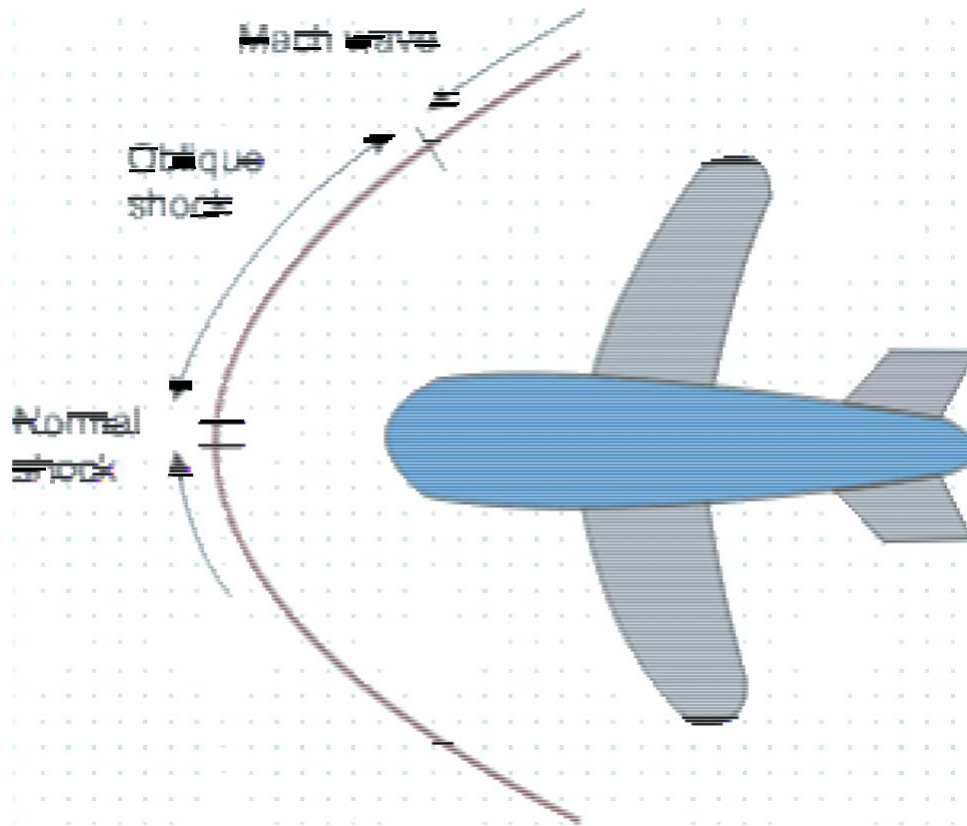


Fig. 2.12 Normal and oblique Shock in front of an Obstacle

- The relationships derived earlier for the normal shock are valid for the velocity components normal to the oblique shock. The oblique shock continues to bend in the downstream direction until the Mach number of the velocity component normal to the wave is unity. At that instant, the oblique shock degenerates into a so called

Mach wave across which changes in flow properties are infinitesimal.

2.7 Tutorial:

A pitot tube mounted on the nose of a supersonic aircraft shows that the ratio of stagnation to static pressure is 27. Find out the aircraft speed in terms of Mach number.

$$\frac{P_{\text{stagnation}}}{P_{\text{static}}} = \frac{\left[\frac{\gamma+1}{2} M^2 \right]^{\left(\frac{\gamma}{\gamma-1} \right)}}{\left[\frac{2\gamma}{\gamma+1} M^2 - \frac{\gamma-1}{\gamma+1} \right]^{\left(\frac{1}{\gamma-1} \right)}}$$

$$= \frac{\gamma+1}{2} M^2 \left[\frac{(\gamma+1)^2 M^2}{4\gamma M^2 - 2(\gamma-1)} \right]^{\left(\frac{1}{\gamma-1} \right)}$$

Therefore, the Mach angle is simply determined by the local Mach number as

$$\mu = \sin^{-1} \frac{1}{M} \tag{4.1}$$

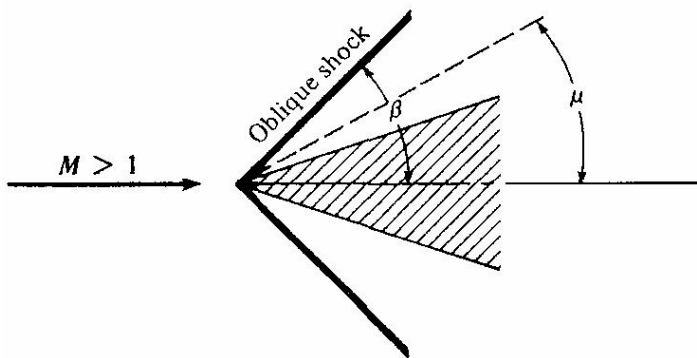


Fig. 2.13 Comparison between Oblique shock angle and Mach angle.

2.8. SUMMARY

Whenever a supersonic flow is turned into itself, shock waves can occur; when the flow is turned away from itself, expansion waves can occur. In either case, if the wave is infinitely weak, it becomes a Mach wave, which makes an angle μ with respect to the upstream flow direction; μ is called the Mach angle, defined as

$$\mu = \sin^{-1} \frac{1}{M} \quad (4.1)$$

Across an oblique shock wave, the tangential components of velocity in front of and behind the wave are equal (However, the tangential components of Mach number are *not* the same.) The thermodynamic properties across the oblique shock are dictated by the normal component of the upstream Mach number M_{n_1} . The values of p_2/p_1 , ρ_2/ρ_1 , T_2/T_1 , $s_2 - s_1$, and p_{o_2}/p_{o_1} across the oblique shock are the same as for a normal shock wave with an upstream Mach number of M_{n_1} . In this fashion, the normal shock tables in Appendix A.2 can be used for oblique shocks. The value of M_{n_1} depends on both M_1 and the wave angle, β , via

$$M_{n_1} = M_1 \sin \beta \quad (4.7)$$

In turn, β is related to M_1 and the flow deflection angle θ through the θ - β - M relation

$$\tan \theta = 2 \cot \beta \left[\frac{M_1^2 \sin^2 \beta - 1}{M_1^2 (\gamma + \cos 2\beta) + 2} \right] \quad (4.17)$$

In light of the above, we can make the following comparison (1) In Chapter 3, we noted that the changes across a normal shock depended *only* on one flow parameter, namely the upstream Mach number M_1 (2) In the present chapter, we note that *two* flow parameters are needed to uniquely define the changes across an oblique shock. Any combination of two parameters will do. For example, an

oblique shock is uniquely defined by any one of the following pairs of parameters: M_1 and β , M_1 and θ , θ and β , M_1 and p_2/p_1 , β and p_2/p_1 etc.

For the solution of shock wave problems, especially cases involving shock intersections and reflections, the graphical constructions associated with the shock polar and the pressure-deflection diagrams are instructional.

For the curved, detached bow shock wave in front of a supersonic blunt body, the properties at any point immediately behind the shock are given by the oblique shock relations studied in this chapter, for the values of M_1 and the local β . Indeed, the oblique shock relations studied here apply in general to points immediately behind *any* curved, three-dimensional shock wave, so long as the component of the upstream Mach number *normal* to the shock at a given point is used to obtain the shock properties.

The properties through and behind a Prandtl-Meyer expansion fan are dictated by the differential relation

$$d\theta = \sqrt{M^2 - 1} \frac{dV}{V} \quad (4.31)$$

When integrated across the wave, this equation becomes

$$\theta_2 = \nu(M_2) - \nu(M_1) \quad (4.41)$$

where θ_1 is assumed to be zero and ν is the Prandtl-Meyer function given by

$$\nu(M) = \sqrt{\frac{\gamma + 1}{\gamma - 1}} \tan^{-1} \sqrt{\frac{\gamma - 1}{\gamma + 1} (M^2 - 1)} - \tan^{-1} \sqrt{M^2 - 1} \quad (4.40)$$

The flow through an expansion wave is isentropic; from the local Mach number obtained from the above relations, all other flow properties are given by the isentropic flow relations discussed in Section 3.5

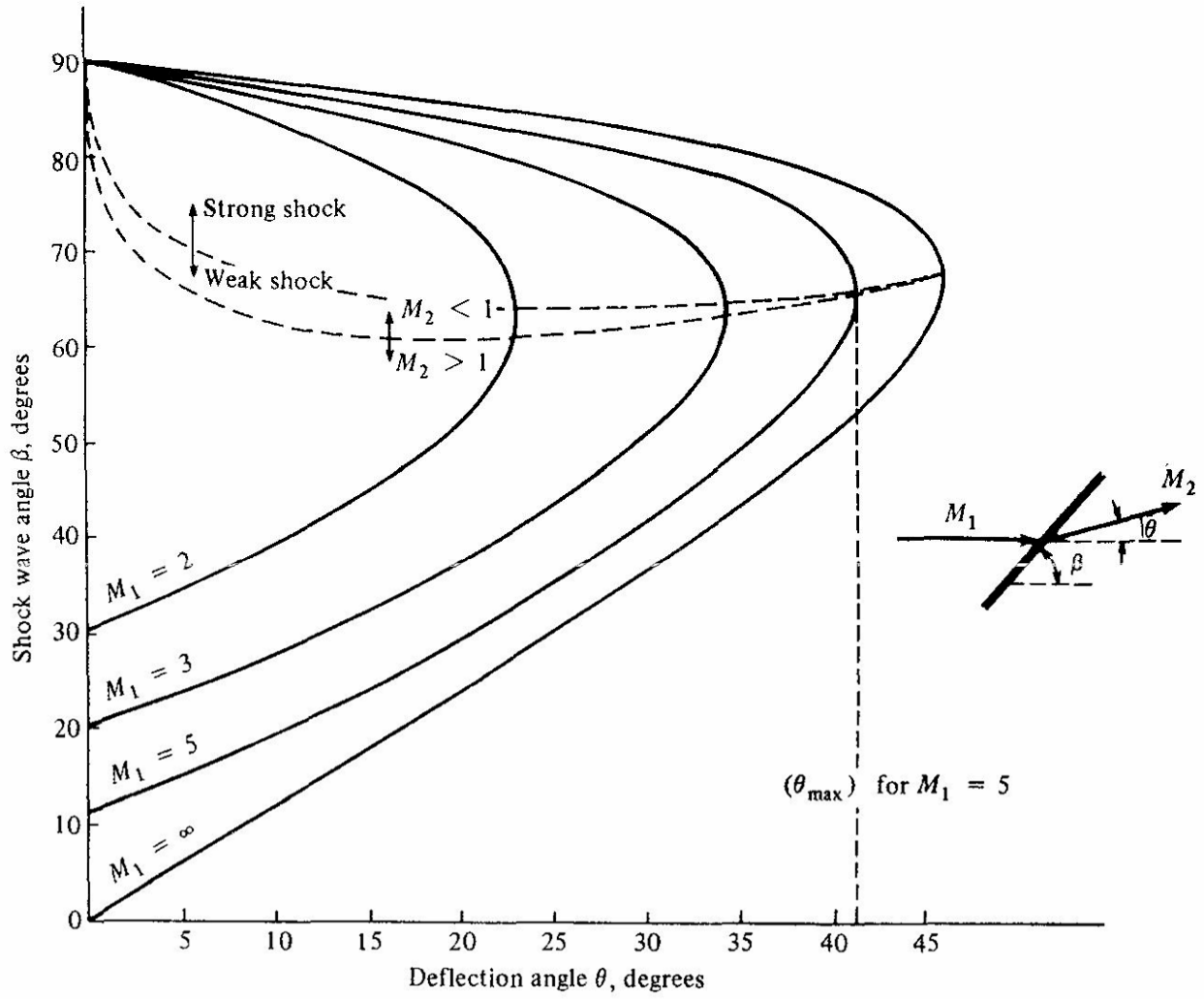


Fig. 2.14 Theta-Beta-Mach number chart.

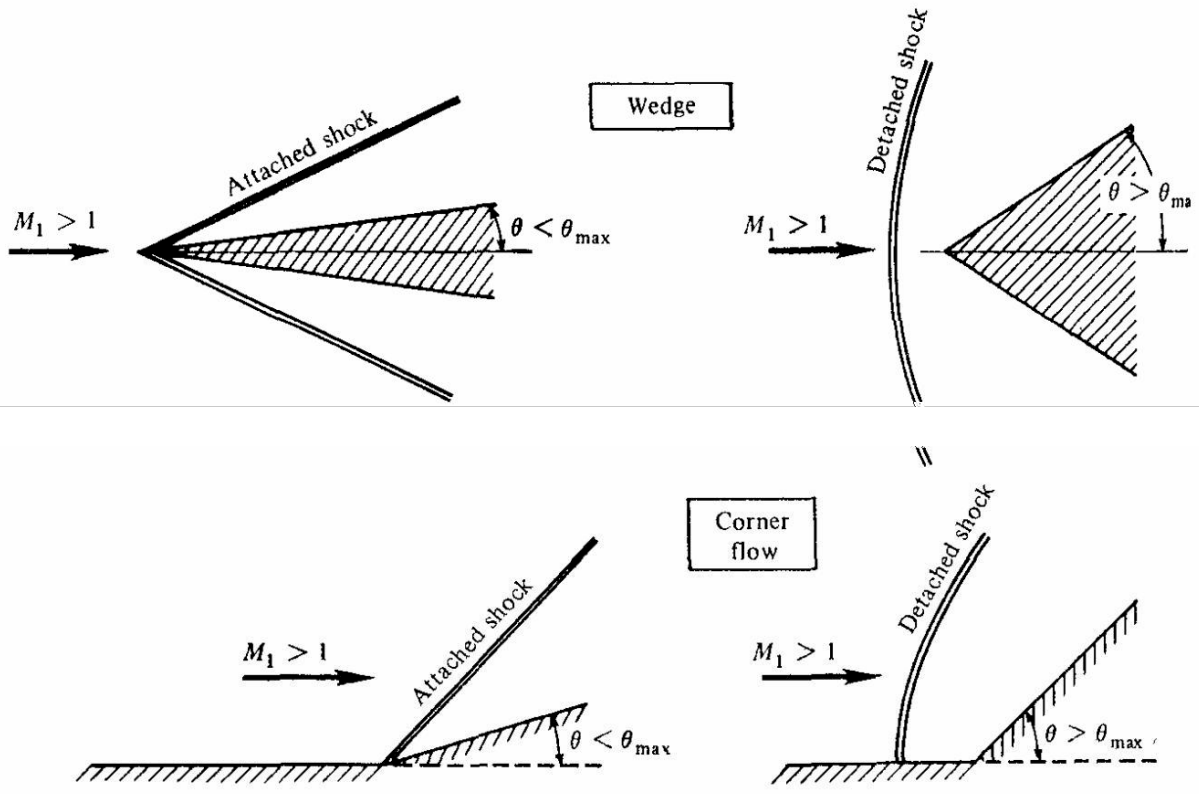


FIGURE 4 6

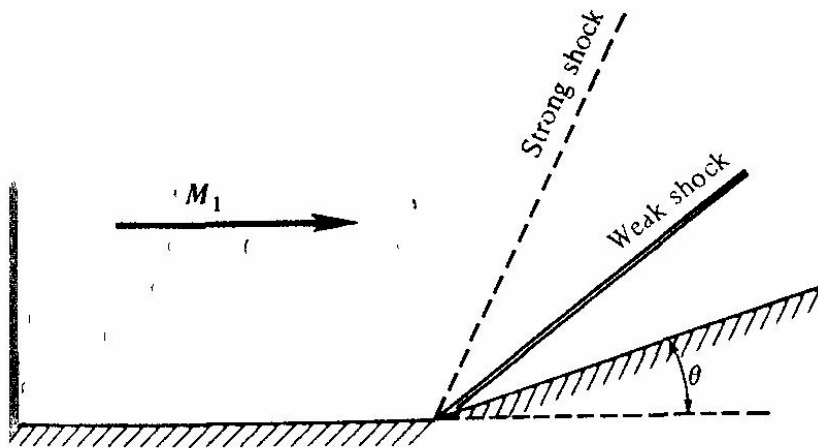


FIGURE 4.7
Weak and strong shocks

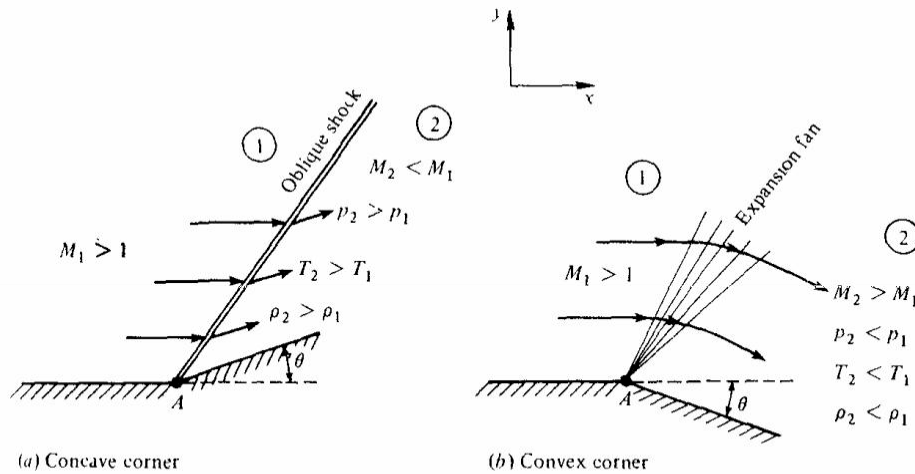


FIGURE 4.1
Supersonic flow over a corner

Example 4.1. A uniform supersonic stream with $M_1 = 3.0$, $p_1 = 1 \text{ atm}$, and $T_1 = 288 \text{ K}$ encounters a compression corner (see Fig 4.1a) which deflects the stream by an angle $\theta = 20^\circ$. Calculate the shock wave angle, and p_2 , T_2 , M_2 , p_{o_2} , and T_{o_2} behind the shock wave

Solution. For the geometrical picture, refer to Fig 4.4. Also, from Fig 4.5, for $M_1 = 3$ and $\theta = 20^\circ$, $\beta = 37.5^\circ$. Thus

$$M_{n_1} = M_1 \sin \beta = 3 \sin 37.5^\circ = 1.826$$

From Table A.2, for $M_{n_1} = 1.826$, $p_2/p_1 = 3.723$, $T_2/T_1 = 1.551$, $M_{n_2} = 0.6108$, and $p_{o_2}/p_{o_1} = 0.8011$. Hence,

$$p_2 = \frac{p_2}{p_1} p_1 = (3.723)(1) = 3.723 \text{ atm}$$

$$T_2 = \frac{T_2}{T_1} T_1 = (1.551)(288) = 446.7 \text{ K}$$

$$M_2 = \frac{M_{n_2}}{\sin(\beta - \theta)} = \frac{0.6108}{\sin 17.5^\circ} = 2.03$$

From Table A.1, for $M_1 = 3$: $p_{o_1}/p_1 = 36.73$ and $T_{o_1}/T_1 = 2.8$. Hence

$$p_{o_2} = \frac{p_{o_2}}{p_{o_1}} \frac{p_{o_1}}{p_1} p_1 = (0.8011)(36.73)(1) = 29.42 \text{ atm}$$

$$T_{o_2} = T_{o_1} = \frac{T_{o_1}}{T_1} T_1 = (2.8)(288) = 806.4 \text{ K}$$

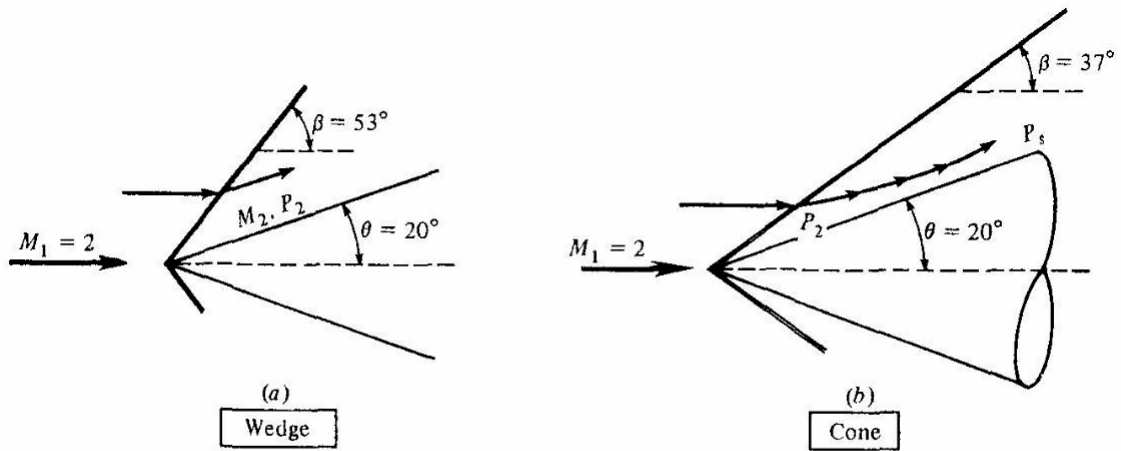


FIGURE 4 8
Comparison between wedge and cone flow; illustration of the three-dimensional relieving effect.

2.9 SHOCK POLAR

Graphical explanations go a long way towards the understanding of supersonic flow with shock waves. One such graphical representation of oblique shock properties is given by the shock polar, described below.

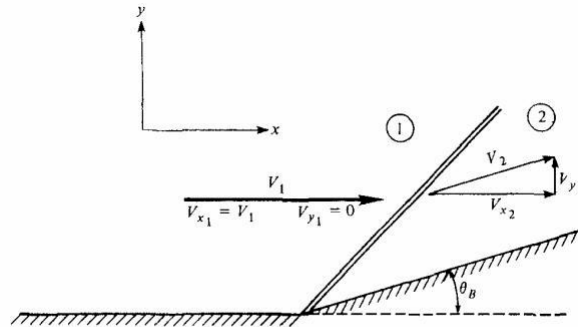


FIGURE 4.10
The physical (xv) plane

Consider an oblique shock with a given upstream velocity V_1 and deflection angle θ_B , as sketched in Fig. 4.10. Also, consider an xy cartesian coordinate system with the x axis in the direction of V_1 . Figure 4.10 is called the *physical plane*. Define V_{x1} , V_{y1} , V_{x2} , and V_{y2} as the x and y components of velocity ahead of and behind the shock, respectively. Now plot these velocities on a graph which uses V_x and V_y as axes, as shown in Fig. 4.11. This graph of velocity components is called the *hodograph plane*. The line OA represents V_1 ahead of the shock; the line OB represents V_2 behind the shock. In turn, *point A* in the hodograph plane of Fig. 4.11 represents the entire *flowfield* of region 1 in the physical plane of Fig. 4.10. Similarly, *point B* in the hodograph plane represents the entire flowfield of region 2 in the physical plane. If now the deflection angle in Fig. 4.10 is increased to a larger value, say θ_C , then the velocity V_2 is inclined further to angle θ_C , and its magnitude is decreased because the shock wave becomes stronger. This condition is shown as point C in the hodograph diagram of Fig. 4.12. Indeed, if

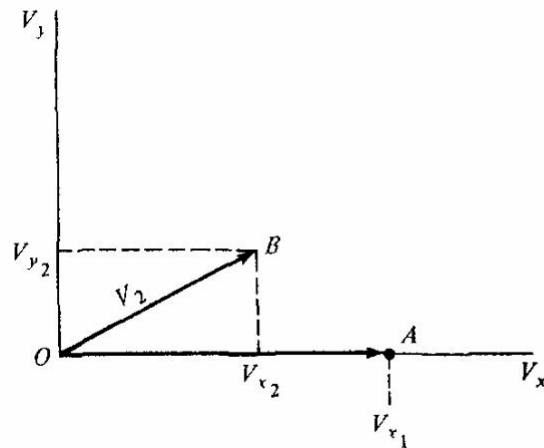
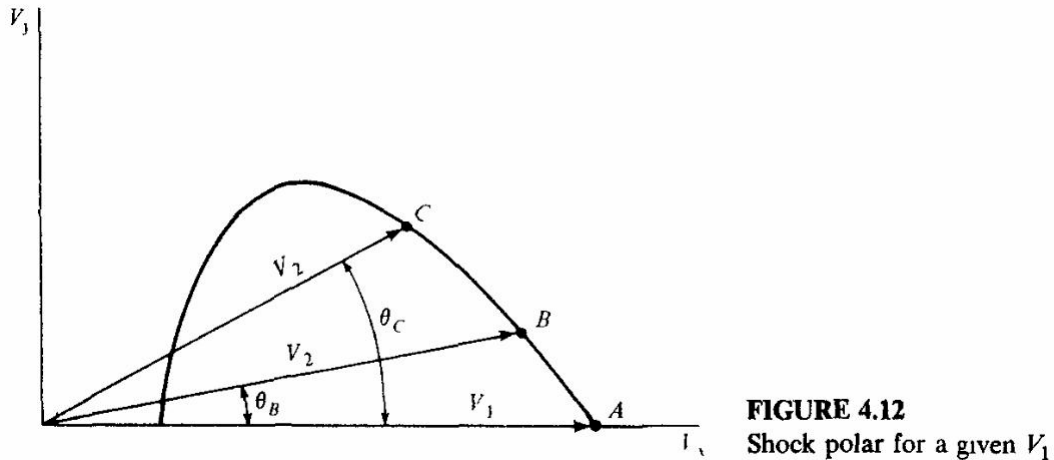
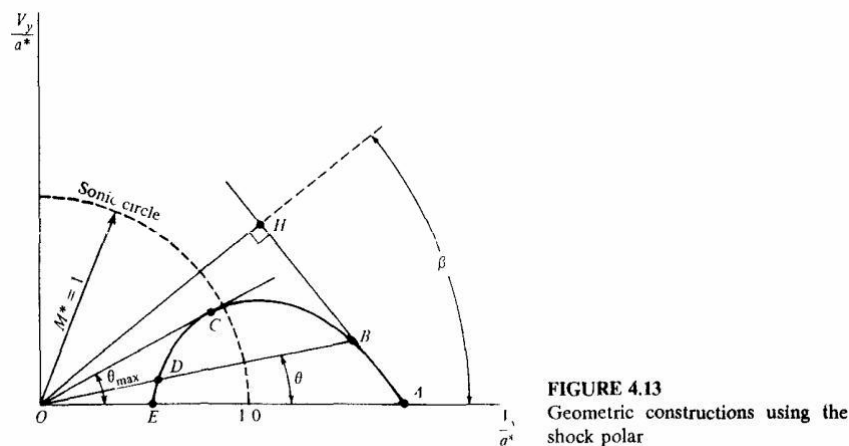


FIGURE 4.11
The hodograph plane



the deflection angle θ in Fig. 4.9 is carried through all possible values for which there is an oblique shock solution ($\theta < \theta_{\max}$), then the locus of all possible velocities behind the shock is given in Fig. 4.12. This locus is defined as a *shock polar*. Points A , B , and C in Figs. 4.11 and 4.12 are just three points on the shock polar for a given V_1 .

For convenience, let us now nondimensionalize the velocities in Fig. 4.12 by a^* , defined in Sec. 3.4. Recall that the flow across a shock is adiabatic, hence a^* is the same ahead of and behind the shock. Consequently, we obtain a shock polar which is the locus of all possible M_2^* values for a given M_1^* , as sketched in Fig. 4.13. The convenience of using M^* instead of M or V to plot the shock polar is that, as $M \rightarrow \infty$, $M^* \rightarrow 2.45$ (see Sec. 3.5). Hence, the shock polars for a wide range of Mach numbers fit compactly on the same page when plotted in terms of M^* . Also note that a circle with radius $M^* = 1$ defines the *sonic circle* shown in Fig. 4.13. Inside this circle, all velocities are subsonic; outside it, all velocities are supersonic.



Several important properties of the shock polar are illustrated in Fig. 4.13 as follows:

1. For a given deflection angle θ , the shock polar is cut at two points B and D . Points B and D represent the weak and strong shock solutions, respectively. Note that D is inside the sonic circle, as would be expected.
2. The line OC drawn tangent to the shock polar represents the maximum deflection angle θ_{\max} for the given M_1^* (hence also for the given M_1). For $\theta > \theta_{\max}$, there is no oblique shock solution.
3. Points E and A represent flow with no deflection. Point E is the normal shock solution; point A corresponds to a Mach line.
4. If a line is drawn through A and B , and line OH is drawn perpendicular to AB , then the angle HOA is the wave angle β corresponding to the shock solution at point B . This can be proved by simple geometric argument, recalling that the tangential component of velocity is preserved across the shock wave. Try it yourself.
5. The shock polars for different Mach numbers form a family of curves, as drawn in Fig. 4.14. Note that the shock polar for $M_1^* = 2.45$ ($M_1 \rightarrow \infty$) is a circle.

The analytic equation for the shock polar (V_y/a^* versus V_x/a^*) can be obtained from the oblique shock equations given in Sec. 4.3. The derivation is given in such classic texts as those by Ferri (Ref. 5) or Shapiro (Ref. 16). The

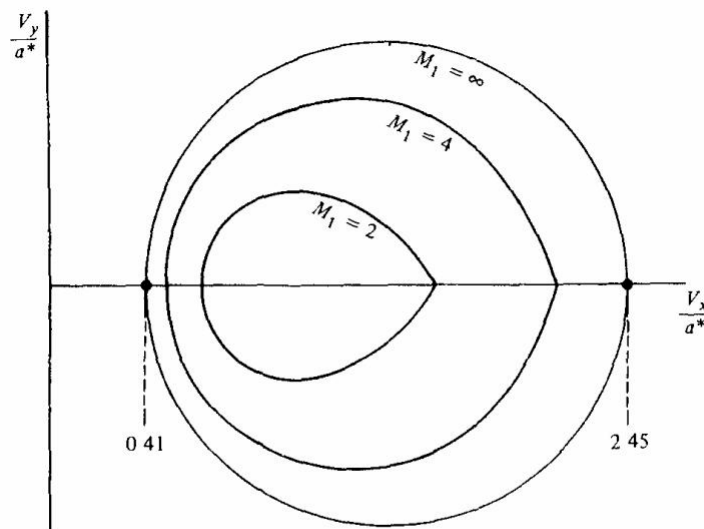


FIGURE 4.14
Shock polars for different Mach numbers

2.9 INTERSECTION OF SHOCKS OF THE SAME FAMILY

Consider the compression corner sketched in Fig. 4.20, where the supersonic flow in region 1 is deflected through an angle θ , with the consequent oblique shock wave emanating from point B . Now consider a Mach wave generated at point A ahead of the shock. Will this Mach wave interest the shock, or will it simply diverge, i.e., is μ_1 greater than or less than β ? To find out, consider Eq. (4.7), which written in terms of velocities is

$$u_1 = V_1 \sin \beta$$

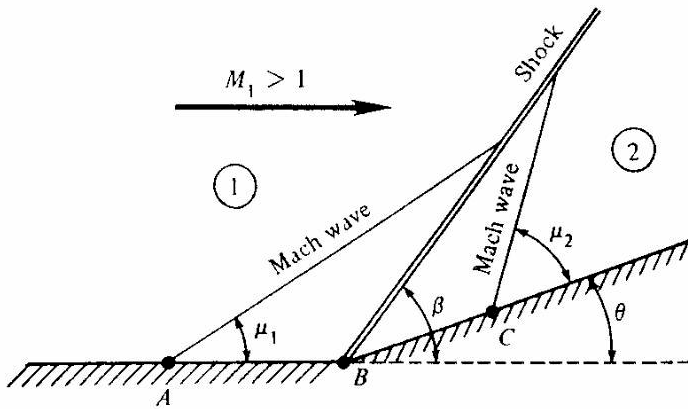


FIGURE 4.20
Mach waves ahead of and behind a shock wave

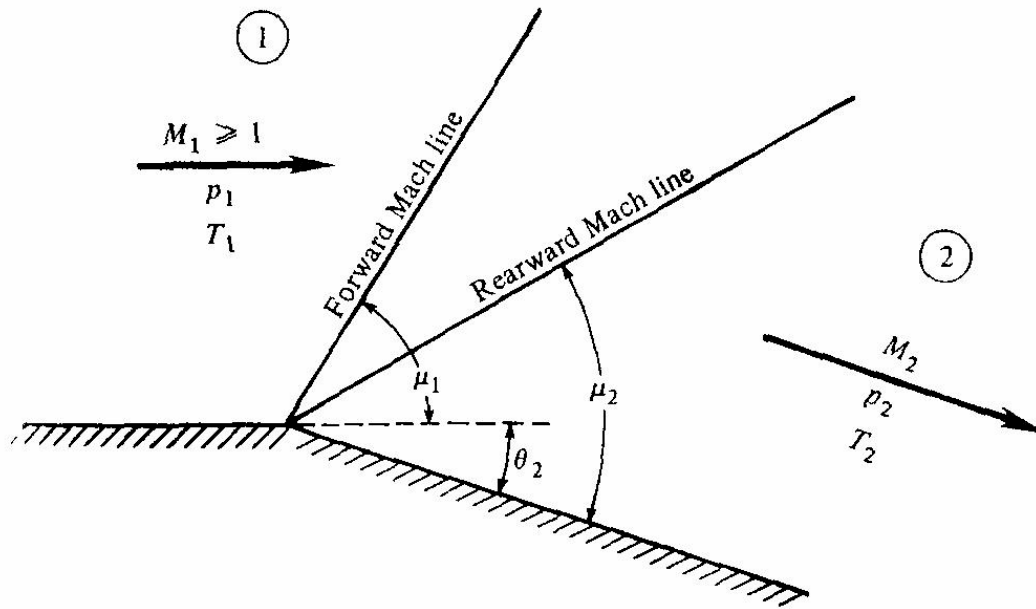


FIGURE 4.27
Prandtl-Meyer expansion

An expansion wave emanating from a sharp convex corner such as sketched in Figs. 4.1b and 4.27 is called a *centered* expansion fan. Moreover, because Prandtl in 1907, followed by Meyer in 1908, first worked out the theory for such a supersonic flow, it is denoted as a *Prandtl-Meyer expansion wave*.

The quantitative problem of a Prandtl-Meyer expansion wave can be stated as follows (referring to Fig. 4.27): For a given M_1 , p_1 , T_1 , and θ_2 , calculate M_2 , p_2 , and T_2 . The analysis can be started by considering the infinitesimal changes across a very weak wave (essentially a Mach wave) produced by an infinitesimally small flow deflection, $d\theta$, as illustrated in Fig. 4.28 From the law of sines,

$$\frac{V + dV}{V} = \frac{\sin(\pi/2 + \mu)}{\sin(\pi/2 - \mu - d\theta)} \quad (4.24)$$



SATHYABAMA

INSTITUTE OF SCIENCE AND TECHNOLOGY

(DEEMED TO BE UNIVERSITY)

Accredited "A" Grade by NAAC | 12B Status by UGC | Approved by AICTE

www.sathyabama.ac.in

**SCHOOL OF MECHANICAL ENGINEERING
DEPARTMENT OF AERONAUTICAL ENGINEERING**

HIGH SPEED AERODYNAMICS

SAEA1505

UNIT – III FLOW THROUGH DUCTS – SAEA1505

3.1. ONE-DIMENSIONAL FLOW WITH HEAT ADDITION

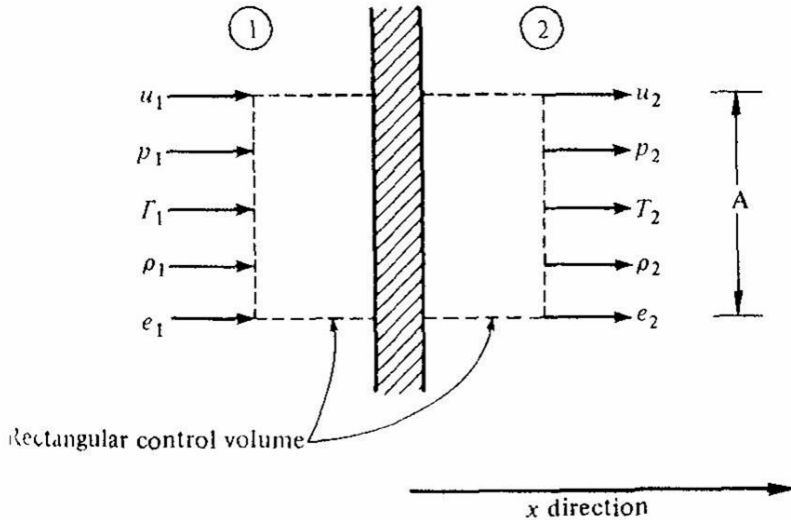


Fig. 3.1. Rectangular Control volume for one-dimensional flow.

Consider again Fig 3 1, which illustrates a control volume for one-dimensional flow Inside this control volume some action is occurring which causes the flow properties in region 2 to be different than in region 1. In the previous sections, this action has been due to a normal shock wave, where the large gradients inside the shock structure ultimately result in an increase in entropy via the effects of viscosity and thermal conduction. However, these effects are taking place inside the control volume in Fig. 3.1 and therefore the governing normal shock equations relating conditions in regions 1 and 2 did not require explicit terms accounting for friction and thermal conduction.

The action occurring inside the control volume in Fig. 3.1 can be caused by effects other than a shock wave. For example, if the flow is through a duct, friction between the moving fluid and the stationary walls of the duct causes changes between regions 1 and 2. This can be particularly important in long pipelines transferring gases over miles of land, for example. Another source of change in a one-dimensional flow is heat addition. If heat is added to or taken away from the gas inside the control volume in Fig 3.1, the properties in region 2 will be different than those in region 1. This is a governing phenomenon in turbojet and ramjet engine burners, where heat is added in the form of fuel-air combustion. It also has an important effect on the supersonic flow in the cavities of modern gas dynamic and chemical lasers, where heat is effectively added by chemical reactions and molecular vibrational energy deactivation. Another example would be the heat added to an absorbing gas by an intense beam of radiation; such an idea has been suggested for laser-heated wind tunnels. In general, therefore, changes in a one-dimensional flow can be created by both friction and heat addition without the presence of a shock wave.

Consider the one-dimensional flow in Fig. 3.5, with heat addition (or extraction) taking place between regions 1 and 2. The governing equations are repeated here for convenience,

$$\begin{aligned}\rho_1 u_1 &= \rho_2 u_2 \\ p_1 + \rho_1 u_1^2 &= p_2 + \rho_2 u_2^2 \\ h_1 + \frac{u_1^2}{2} + q &= h_2 + \frac{u_2^2}{2}\end{aligned}$$

If conditions in region 1 are known, then for a specified amount of heat added per unit mass, q , these equations along with the appropriate equations of state can be solved for conditions in region 2. In general, a numerical solution is required. However, for the specific case of a calorically perfect gas, closed-form analytical expressions can be obtained—just as in the normal shock problem. Therefore, the remainder of this section will deal with a calorically perfect gas.

$$h_1 + \frac{u_1^2}{2} + q = h_2 + \frac{u_2^2}{2} \quad (1)$$

Solving the above energy equation for q with $h = C_p T$ we get,

$$q = \left(c_p T_2 + \frac{u_2^2}{2} \right) - \left(c_p T_1 + \frac{u_1^2}{2} \right) \quad (2)$$

From the definition of total temperature, the terms on the right-hand side of the above equation simply result in

$$\boxed{q = c_p T_{o_2} - c_p T_{o_1} = c_p (T_{o_2} - T_{o_1})} \quad (3)$$

The above equation clearly indicates that the effect of heat addition is to directly change the total temperature of the flow. If heat is added, T_o increases; if heat is extracted, T_o decreases.

Let us proceed to find the ratios of properties between regions 1 and 2 in terms of the Mach numbers M_1 and M_2 . We have,

$$\boxed{p_1 + \rho_1 u_1^2 = p_2 + \rho_2 u_2^2} \quad (4)$$

Noting that

$$\rho u^2 = \rho a^2 M^2 = \rho \frac{\gamma p}{\rho} M^2 = \gamma p M^2 \quad (5)$$

We obtain,

$$p_2 - p_1 = \rho_1 u_1^2 - \rho_2 u_2^2 = \gamma p_1 M_1^2 - \gamma p_2 M_2^2 \quad (6)$$

Hence,

$$\boxed{\frac{p_2}{p_1} = \frac{1 + \gamma M_1^2}{1 + \gamma M_2^2}} \quad (7)$$

Also, from the perfect gas equation of state and the below continuity equation,

$$\boxed{\rho_1 u_1 = \rho_2 u_2} \quad (8)$$

We get,

$$\frac{T_2}{T_1} = \frac{p_2 \rho_1}{p_1 \rho_2} = \frac{p_2 u_2}{p_1 u_1} \quad (9)$$

$$\boxed{a = \sqrt{\gamma RT}} \quad (10)$$

From the above equation for velocity of sound and the definition of Mach number, we get

$$\frac{u_2}{u_1} = \frac{M_2 a_2}{M_1 a_1} = \frac{M_2}{M_1} \left(\frac{T_2}{T_1} \right)^{1/2} \quad (11)$$

Using the above equations and substituting the values of P_2/P_1 , and u_2/u_1 in T_2/T_1 we get,

$$\boxed{\frac{T_2}{T_1} = \left(\frac{1 + \gamma M_1^2}{1 + \gamma M_2^2} \right)^2 \left(\frac{M_2}{M_1} \right)^2} \quad (12)$$

Since $\rho_2/\rho_1 = (p_2/p_1)(T_1/T_2)$ (13)

We get,

$$\boxed{\frac{\rho_2}{\rho_1} = \left(\frac{1 + \gamma M_2^2}{1 + \gamma M_1^2} \right) \left(\frac{M_1}{M_2} \right)^2} \quad (14)$$

We have

$$\boxed{\frac{p_o}{p} = \left(1 + \frac{\gamma - 1}{2} M^2 \right)^{\gamma/(\gamma-1)}} \quad (15)$$

$$\boxed{\frac{p_2}{p_1} = \frac{1 + \gamma M_1^2}{1 + \gamma M_2^2}} \quad (16)$$

The ratio of total pressures is obtained directly from the above two equations,

$$\boxed{\frac{p_{o_2}}{p_{o_1}} = \frac{1 + \gamma M_1^2}{1 + \gamma M_2^2} \left(\frac{1 + \frac{\gamma - 1}{2} M_2^2}{1 + \frac{\gamma - 1}{2} M_1^2} \right)^{\gamma/(\gamma - 1)}} \quad (17)$$

We have,

$$\boxed{\frac{T_o}{T} = 1 + \frac{\gamma - 1}{2} M^2} \quad (18)$$

$$\frac{T_2}{T_1} = \left(\frac{1 + \gamma M_1^2}{1 + \gamma M_2^2} \right)^2 \left(\frac{M_2}{M_1} \right)^2 \quad (19)$$

The ratio of total temperatures is obtained directly from the above equations,

$$\frac{T_{o_2}}{T_{o_1}} = \left(\frac{1 + \gamma M_1^2}{1 + \gamma M_2^2} \right)^2 \left(\frac{M_2}{M_1} \right)^2 \left(\frac{1 + \frac{\gamma - 1}{2} M_2^2}{1 + \frac{\gamma - 1}{2} M_1^2} \right) \quad (20)$$

Finally, the entropy change can be found from the below equation with the above derived equations for T_2/T_1 and P_2/P_1 .

$$s_2 - s_1 = c_p \ln \frac{T_2}{T_1} - R \ln \frac{P_2}{P_1} \quad (21)$$

$$\frac{p_2}{p_1} = \frac{1 + \gamma M_1^2}{1 + \gamma M_2^2} \quad (3.78)$$

$$\frac{T_2}{T_1} = \left(\frac{1 + \gamma M_1^2}{1 + \gamma M_2^2} \right)^2 \left(\frac{M_2}{M_1} \right)^2 \quad (3.81)$$

$$\frac{\rho_2}{\rho_1} = \left(\frac{1 + \gamma M_2^2}{1 + \gamma M_1^2} \right) \left(\frac{M_1}{M_2} \right)^2 \quad (3.82)$$

$$\frac{p_{o2}}{p_{o1}} = \frac{1 + \gamma M_1^2}{1 + \gamma M_2^2} \left(\frac{1 + \frac{\gamma - 1}{2} M_2^2}{1 + \frac{\gamma - 1}{2} M_1^2} \right)^{\gamma/(\gamma - 1)} \quad (3.83)$$

$$\frac{T_{o2}}{T_{o1}} = \left(\frac{1 + \gamma M_1^2}{1 + \gamma M_2^2} \right)^2 \left(\frac{M_2}{M_1} \right)^2 \left(\frac{1 + \frac{\gamma - 1}{2} M_2^2}{1 + \frac{\gamma - 1}{2} M_1^2} \right) \quad (3.84)$$

For convenience of calculation, we use sonic flow as a reference condition. Let $M_1 = 1$, the corresponding flow properties are denoted by $p_1 = p^*$, $T_1 = T^*$, $\rho_1 = \rho^*$, $p_{o_1} = p_o^*$, and $T_{o_1} = T_o^*$. The flow properties at any other value of M are then obtained by inserting $M_1 = 1$ and $M_2 = M$ into Eq (3.78) and Eqs (3.81) to (3.84), yielding

$$\frac{p}{p^*} = \frac{1 + \gamma}{1 + \gamma M^2}$$

$$\frac{T}{T^*} = M^2 \left(\frac{1 + \gamma}{1 + \gamma M^2} \right)^2$$

$$\frac{\rho}{\rho^*} = \frac{1}{M^2} \left(\frac{1 + \gamma M^2}{1 + \gamma} \right)$$

$$\frac{p_o}{p_o^*} = \frac{1 + \gamma}{1 + \gamma M^2} \left[\frac{2 + (\gamma - 1) M^2}{\gamma + 1} \right]^{\gamma/(\gamma - 1)}$$

$$\frac{T_o}{T_o^*} = \frac{(\gamma + 1) M^2}{(1 + \gamma M^2)^2} \left[2 + (\gamma - 1) M^2 \right]$$

Example 3.8. Air enters a constant-area duct at $M_1 = 0.2$, $p_1 = 1 \text{ atm}$, and $T_1 = 273 \text{ K}$. Inside the duct, the heat added per unit mass is $q = 1.0 \times 10^6 \text{ J/kg}$. Calculate the flow properties M_2 , p_2 , T_2 , ρ_2 , T_{o_2} , and p_{o_2} at the exit of the duct.

Solution. From Table A.1, for $M_1 = 0.2$, $T_{o_1}/T_1 = 1.008$ and $p_{o_1}/p_1 = 1.028$. Hence

$$T_{o_1} = 1.008T_1 = 1.008(273) = 275.2 \text{ K}$$

$$p_{o_1} = 1.028p_1 = 1.028(1 \text{ atm}) = 1.028 \text{ atm}$$

$$c_p = \frac{\gamma R}{\gamma - 1} = \frac{(1.4)(287)}{0.4} = 1005 \text{ J/kg} \cdot \text{K}$$

We have

$$q = c_p T_{o_2} - c_p T_{o_1} = c_p (T_{o_2} - T_{o_1})$$

$$T_{o_2} = \frac{q}{c_p} + T_{o_1} = \frac{1.0 \times 10^6}{1005} + 275.2 = \boxed{1270 \text{ K}}$$

From Gas Table

From Table A 3, for $M_1 = 0.2$ $T_1/T^* = 0.2066$, $p_1/p^* = 2.273$, $p_{o1}/p_o^* = 1.235$, and $T_{o1}/T_o^* = 0.1736$ Hence

$$\frac{T_{o2}}{T_o^*} = \frac{T_{o2}}{T_{o1}} \frac{T_{o1}}{T_o^*} = \frac{1270}{275.2} (0.1736) = 0.8013$$

From Table A.3, this corresponds to $M_2 = 0.58$

Also from Table A3, for $M_2 = 0.58$ $T_2/T^* = 0.8955$, $p_2/p^* = 1.632$, $p_{o2}/p_o^* = 1.083$ Hence

$$T_2 = \frac{T_2}{T^*} \frac{T^*}{T_1} T_1 = (0.8955) \left(\frac{1}{0.2066} \right) (273) = 1183 \text{ K}$$

$$p_2 = \frac{p_2}{p^*} \frac{p^*}{p_1} p_1 = 1.632 \frac{1}{2.273} 1 \text{ atm} = 0.718 \text{ atm}$$

$$p_{o2} = \frac{p_{o2}}{p_o^*} \frac{p_o^*}{p_{o1}} p_{o1} = 1.083 \frac{1}{1.235} 1.028 = 0.902 \text{ atm}$$

Since $1 \text{ atm} = 1.01 \times 10^5 \text{ N/m}^2$,

$$\rho_2 = \frac{p_2}{RT_2} = \frac{(0.718)(1.01 \times 10^5)}{(278)(1183)} = 0.214 \text{ kg/m}^3$$

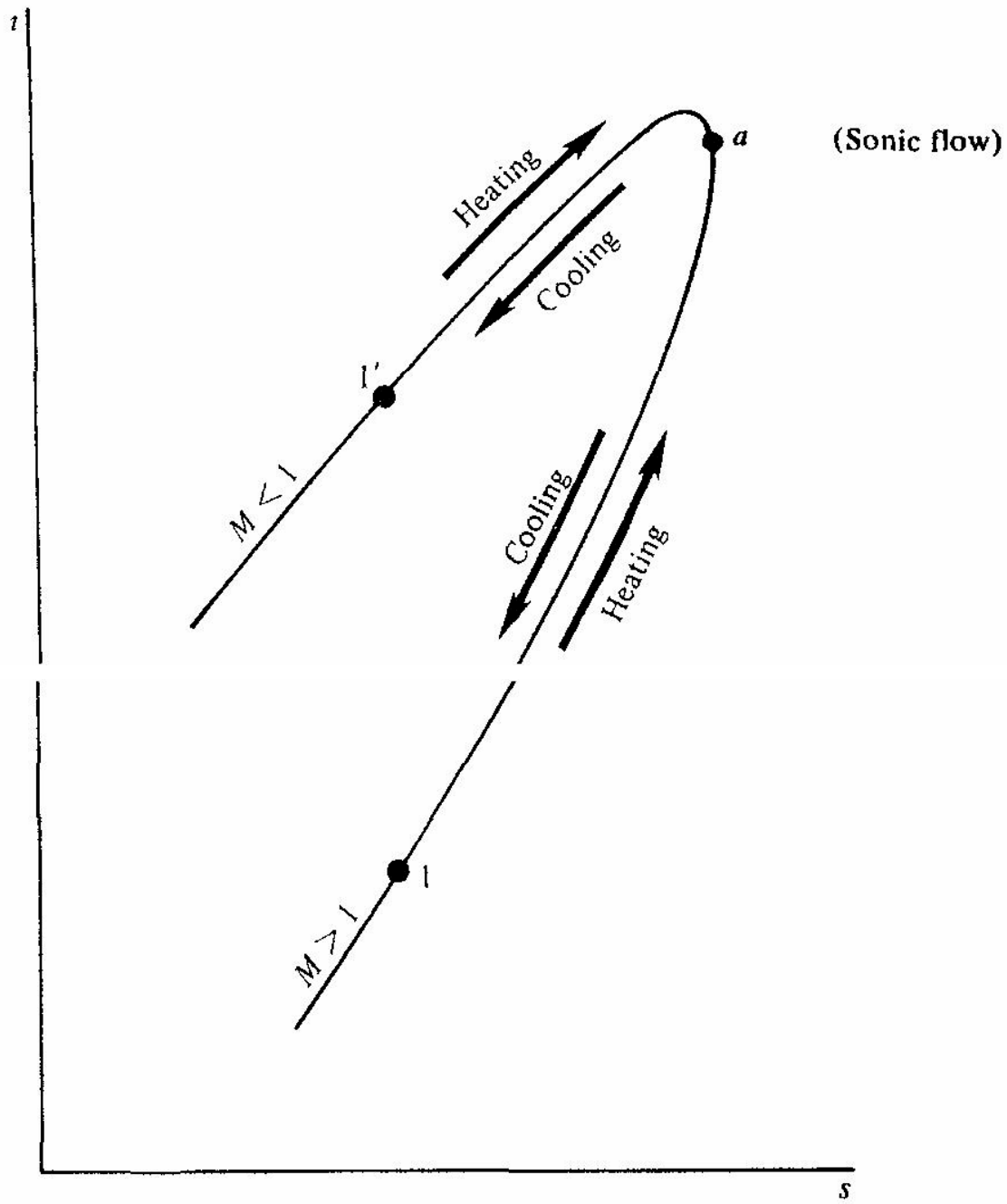


FIGURE 3.12
The Rayleigh curve

From the above, it is important to note that heat addition always drives the Mach numbers toward 1, decelerating a supersonic flow and accelerating a subsonic flow. This is emphasized in Fig. 3.12, which is a Mollier diagram (enthalpy versus entropy) of the one-dimensional heat-addition process. The curve in Fig. 3.12 is called the *Rayleigh curve*, and is drawn for a set of given initial conditions. If the conditions in region 1 are given by point 1 in Fig. 3.12, then the particular Rayleigh curve through point 1 is the locus of all possible states in region 2. Each point on the curve corresponds to a different value of q added or taken away. Point a corresponds to maximum entropy, also at point a the flow is sonic. The lower branch of the Rayleigh curve below point a corresponds to supersonic flow; the upper branch above point a corresponds to subsonic flow. If the flow in region 1 of Fig. 3.5 is supersonic and corresponds to point 1 in Fig. 3.12, then heat addition will cause conditions in region 2 to move closer to point a , with a consequent decrease of Mach number towards unity. As a is made larger, conditions in region 2 get closer and closer to point a . Finally, for a certain value of q , the flow will become sonic in region 2. For this

condition, the flow is said to be *choked*, because any further increase in q is not possible without a drastic revision of the upstream conditions in region 1. For example, if the initial supersonic conditions in region 1 were obtained by expansion through a supersonic nozzle, and if a value of q is added to the flow above that allowed for attaining Mach 1 in region 2, then a normal shock will form inside the nozzle and conditions in region 1 will suddenly become subsonic.

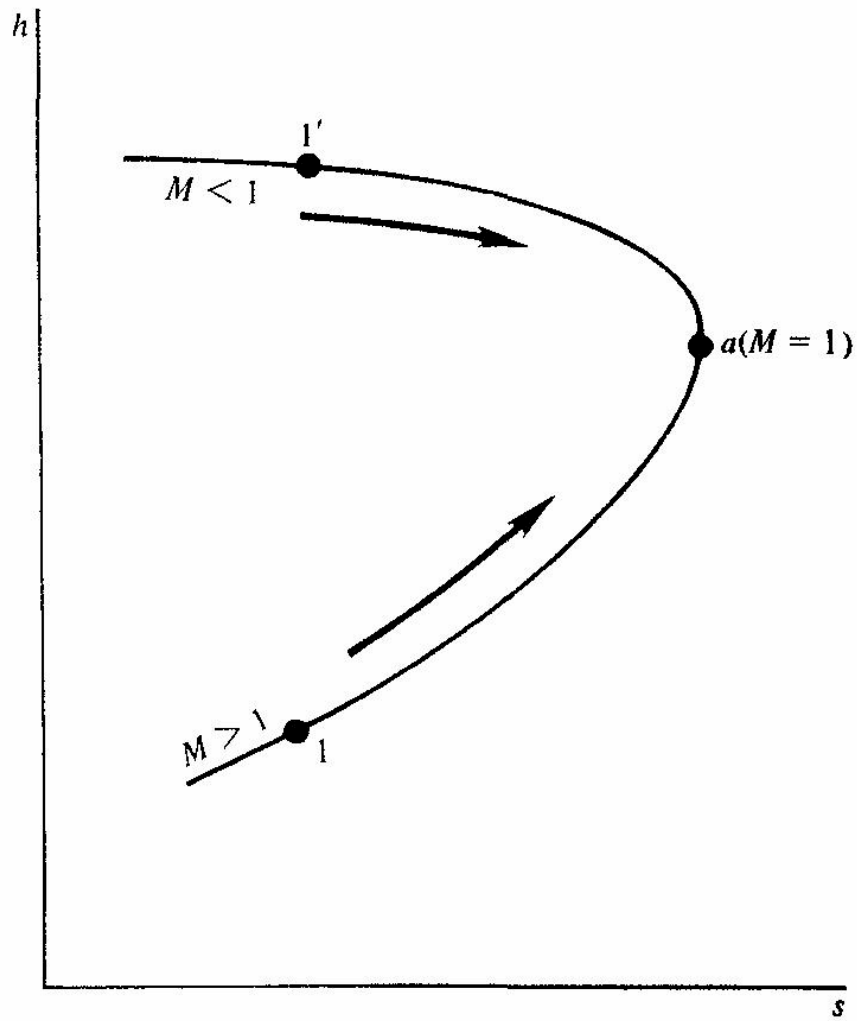


FIGURE 3.14
The Fanno curve

From the above, note that friction always drives the Mach number toward 1, decelerating a supersonic flow and accelerating a subsonic flow. This is emphasized in Fig 3.14, which is a Mollier diagram of one-dimensional flow with friction. The curve in Fig 3.14 is called the *Fanno curve*, and is drawn for a set of given initial conditions. Point *a* corresponds to maximum entropy, where the flow is sonic. This point splits the Fanno curve into subsonic (upper) and

supersonic (lower) portions. If the inlet flow is supersonic and corresponds to point 1 in Fig 3.14, then friction causes the downstream flow to move closer to point *a*, with a consequent decrease of Mach number towards unity. Each point on the curve between points 1 and *a* corresponds to a certain duct length *L*. As *L* is made larger, the conditions at the exit move closer to point *a*. Finally, for a certain value of *L*, the flow becomes sonic. For this condition, the flow is *choked*, because any further increase in *L* is not possible without a drastic revision of the inlet conditions. For example, if the inlet conditions at point 1 were obtained by expansion through a supersonic nozzle, and if *L* were larger than that allowed for attaining Mach 1 at the exit, then a normal shock would form inside the nozzle, and the duct inlet conditions would suddenly become subsonic.

Example 3.9. Air enters a constant-area duct at $M_1 = 3$, $p_1 = 1$ atm, and $T_1 = 300$ K. Inside the duct, the heat added per unit mass is $q = 3 \times 10^5$ J/kg. Calculate the flow properties M_2 , p_2 , T_2 , ρ_2 , T_{o_2} , and p_{o_2} at the exit of the duct

Also find how much heat per unit mass must be added to choke the flow.

Solution. From Table A 1, for $M_1 = 3$ $T_{o_1}/T_1 = 2.8$ Hence

$$T_{o_1} = 2.8(300) = 840 \text{ K}$$

$$c_p = \frac{\gamma R}{\gamma - 1} = \frac{(1.4)(287)}{0.4} = 1004.5 \text{ J/kg K}$$

From Eq. (3.77)

$$q = c_p(T_{o_2} - T_{o_1})$$

Thus

$$T_{o_2} = \frac{q}{c_p} + T_{o_1} = \frac{3 \times 10^5}{1004.5} + 840 = \boxed{1139 \text{ K}}$$

From Table A 3, for $M_1 = 3$ $p_1/p^* = 0.1765$, $T_1/T^* = 0.2803$, and $T_{o_1}/T^* = 0.6540$ Hence

$$\frac{T_{o_2}}{T_o^*} = \frac{T_{o_2}}{T_{o_1}} \frac{T_{o_1}}{T_o^*} = \frac{1139}{840} (0.6540) = 0.8868$$

From Table A 3, for $T_{o_2}/T_o^* = 0.8868$ $M_2 = \boxed{1.58}$ Also from Table A 3, $p_2/p^* = 0.5339$ and $T_2/T^* = 0.7117$ Thus

$$p_2 = \frac{p_2}{p^*} \frac{p^*}{p_1} p_1 = 0.5339 \left(\frac{1}{0.1765} \right) (1 \text{ atm}) = \boxed{3.025 \text{ atm}}$$

$$T_2 = \frac{T_2}{T^*} \frac{T^*}{T_1} T_1 = 0.7117 \left(\frac{1}{0.2803} \right) (300) = \boxed{761.7 \text{ K}}$$

$$\rho_2 = \frac{p_2}{RT_2} = \frac{(3.025)(1.01 \times 10^5)}{(287)(761.7)} = \boxed{1.398 \text{ kg/m}^3}$$

Example-5.

Consider a point in a supersonic flow where the static pressure is 0.4 atm. When a Pitot tube is inserted in the flow at this point, the pressure measured by the Pitot tube is 3 atm. Calculate the Mach number at this point. Calculate the entropy change across the shock (Hint: Normal shock occurs in front of the Pitot tube).

Solution.

The pressure measured by a Pitot tube is the total pressure. However, when the tube is inserted into a supersonic flow, a normal shock is formed a short distance ahead of the mouth of the tube. In this case, the Pitot tube is sensing the total pressure behind the normal shock.

Hence

$$\frac{p_{o_2}}{p_1} = \frac{3}{0.4} = 7.5$$

From Table A 2, for $p_{o_2}/p_1 = 7.5$ $M_1 = \boxed{2.35}$

From Table A 2, for $M_1 = 2.35$ $p_{o_2}/p_{o_1} = 0.5615$

Using the following equation,

$$\frac{s_2 - s_1}{R} = -\ln \frac{p_{o_2}}{p_{o_1}} = -\ln(0.5615) = 0.577$$

$$s_2 - s_1 = 0.577R$$

Example-6:

A supersonic wind tunnel settling chamber expands air or Freon-21 through a nozzle from a pressure of 10 bar to 4 bar in the test section. Calculate the stagnation temperature to be maintained in the settling chamber to obtain a velocity of 500 m/s in the test section for,

- (a) Air, $C_p = 1.025 \text{ kJ/kg K}$, $C_v = 0.735 \text{ kJ/kg K}$
- (b) Freon – 21, $C_p = 0.785 \text{ kJ/kg K}$, $C_v = 0.675 \text{ kJ/kg K}$

What is the test section Mach number in each case?

Ans: $M (\text{air}) = 1.225$

$M (\text{Freon}) = 1.296$

Example-7:

A nozzle in a wind tunnel gives a test-section Mach number of 2.0. air enters the nozzle from a large reservoir at 0.69 bar and 310 K. The cross-sectional area of the throat is 1000 cm² . Determine the following quantities for the tunnel for one dimensional isentropic flow:

- (i) pressure, temperature and velocities at the throat and test section
- (ii) area of cross-section of the test section
- (iii) mass flow rate
- (iv) power required to drive the compressor.

Solution:

Given: $P_0 = 0.69$ bar, $T_0 = 310$ K, $A^* = 1000$ cm²

Find $\rho_0 = P_0/RT_0$, and a_0

From Gas table at $M = 1$ (throat section)

Find P^*/P_0 , T^*/T_0 , ρ^*/ρ_0

$P^* = 0.365$ bar (Ans.)

$T^* = 258$ K (Ans.)

$\rho^* = 0.49$ kg/m³ (Ans.)

$C^* = a^* = 323$ m/s (Ans.)

From Gas table at $M_t = 2.0$ (test section)

$$P/P_0 = 0.128 \quad P = 0.0885 \text{ bar (Ans.)}$$

$$T/T_0 = 0.555 \quad T = 175 \text{ K (Ans.)}$$

$$A/A^* = 1.687; \quad A = 1687 \text{ cm}^2$$

$$\text{Velocity at test section} = M a = 2 \times 264 = 528 \text{ m/s (Ans.)} \quad \text{Mass flow rate} = 15.9 \text{ kg/s}$$

$$\begin{aligned} \text{Compressor work} &= \text{mass flow rate} \times C_p \times \text{temperature drop} \\ &= 2182 \text{ kW} \end{aligned}$$

3.2. NORMAL, OBLIQUE SHOCKS AND EXPANSION WAVES

Prandtl equation and Rankine – Hugoniot relation, Normal shock equations, Pitot static tube, corrections for subsonic and supersonic flows, Oblique shocks and corresponding equations, Hodograph and pressure turning angle, shock polars, flow past wedges and concave corners, strong, weak and detached shocks, Raleigh and Fanno Flow. Flow past convex corners, Expansion hodograph, Reflection and interaction of shocks and expansion, waves, Families of shocks, Methods of Characteristics, Two dimensional supersonic nozzle contours.

From **Table A.3**, for $M_1 = 3$. $p_{o_1}/p_o^* = 3.424$ For $M_2 = 1.58$: $p_{o_2}/p_o^* = 1.164$
Thus

$$\frac{p_{o_2}}{p_{o_1}} = \frac{p_{o_2}/p_o^*}{p_{o_1}/p_o^*} = \frac{1.164}{3.424} = 0.340$$

From **Table A.1**, For $M_1 = 3$: $p_{o_1}/p_1 = 36.73$ Hence

$$p_{o_2} = \frac{p_{o_2}}{p_{o_1}} \frac{p_{o_1}}{p_1} p_1 = (0.340)(36.73)(1 \text{ atm}) = \boxed{12.49 \text{ atm}}$$

Solution. From Example 3.9, $T_{o_1} = 840 \text{ K}$ Also from **Table A.3**, for $M_1 = 3$:
 $T_{o_1}/T_o^* = 0.6540$ Thus

$$T_o^* = \frac{T_{o_1}}{0.6540} = \frac{840}{0.6540} = 1284 \text{ K}$$

When the flow is choked, the Mach number at the end of the duct is $M_2 = 1$ Thus

$$T_{o_2} = T_o^* = 1284 \text{ K}$$

$$q = c_p(T_{o_2} - T_{o_1}) = (1004.5)(1284 - 840) = \boxed{4.46 \times 10^5 \text{ J/kg}}$$



SATHYABAMA

INSTITUTE OF SCIENCE AND TECHNOLOGY
(DEEMED TO BE UNIVERSITY)

Accredited "A" Grade by NAAC | 12B Status by UGC | Approved by AICTE

www.sathyabama.ac.in

**SCHOOL OF MECHANICAL ENGINEERING
DEPARTMENT OF AERONAUTICAL ENGINEERING**

HIGH SPEED AERODYNAMICS

SAEA1505

UNIT – IV AIRFOILS IN HIGH SPEED FLOWS – SAEA1505

4.1. Small perturbation potential theory

4.1.1 LINEARIZED FLOW

Transport yourself back in time to the year 1940, and imagine that you are an aerodynamicist responsible for calculating the lift on the wing of high-performance fighter plane. You recognize that the airspeed is high enough so that the well-established incompressible flow techniques of the day will give inaccurate results. Compressibility must be taken into account. However, you also recognize that the governing equations for compressible flow are nonlinear, and that no general solution exists for these equations. Numerical solutions are out of the question! So, what do you do? The only practical recourse is to seek assumptions regarding the physics of the flow which will allow the governing equations to become linear, but which at the same time do not totally compromise the accuracy of the real problem. In turn, these linear equations can be attacked by conventional mathematical techniques.

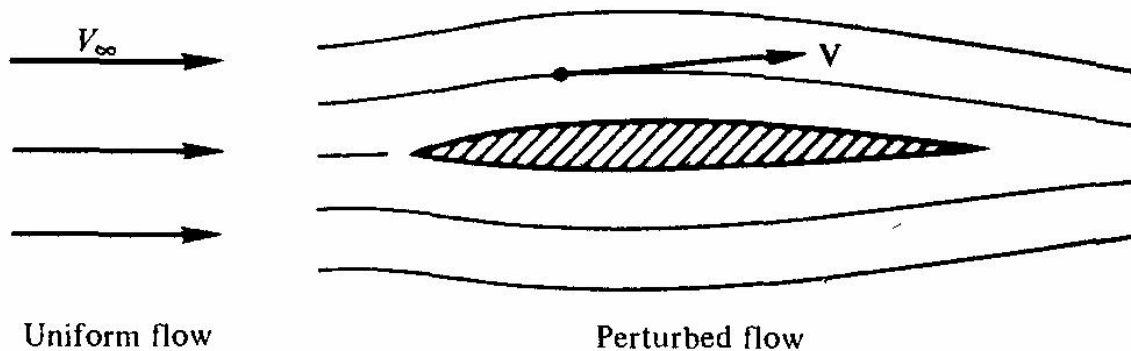


Fig. 4.1 Comparison between uniform and perturbed flows

There are a number of practical aerodynamic problems where, on a physical basis, a uniform flow is changed, or perturbed, only slightly. One such example is the flow over a thin airfoil illustrated in in the above figure. The flow is characterized by only a small deviation of the flow from its original uniform state. The analyses of such flows are usually called small-perturbation theories. Small-perturbation theory is frequently (but not always) linear theory, an example is the acoustic theory, where the assumption of small perturbations allowed a linearized solution. Linearized solutions in compressible flow always contain the assumption of small perturbations, but small perturbations do not always guarantee that the governing equations can be linearized.

4.1.2. LINEARIZED PRESSURE COEFFICIENT

The pressure coefficient C_p is defined as

$$C_p \equiv \frac{p - p_\infty}{\frac{1}{2} \rho_\infty V_\infty^2} \quad (1)$$

where p is the local pressure, and p_∞ , ρ_∞ , and V_∞ are the pressure, density, and velocity, respectively, in the uniform free stream. The pressure coefficient is simply a non-dimensional pressure difference; it is extremely useful in fluid dynamics.

An alternative form of the pressure coefficient, convenient for compressible flow, can be obtained as follows

$$\frac{1}{2} \rho_\infty V_\infty^2 = \frac{1}{2} \frac{\gamma p_\infty}{\gamma p_\infty} \rho_\infty V_\infty^2 = \frac{\gamma}{2} p_\infty \frac{V_\infty^2}{a_\infty^2} = \frac{\gamma}{2} p_\infty M_\infty^2 \quad (2)$$

Substitute it in the above equation, we get

$$C_p = \frac{p - p_\infty}{(\gamma/2) \rho_\infty M_\infty^2} = \frac{p_\infty (p/p_\infty - 1)}{(\gamma/2) \rho_\infty M_\infty^2} \quad (3)$$

$$\boxed{C_p = \frac{2}{\gamma M_\infty^2} \left(\frac{p}{p_\infty} - 1 \right)} \quad (4)$$

The above equation is an alternative form of C_p expressed in terms of γ and M_∞ rather than ρ_∞ , and V_∞ . It is still an exact representation of C_p .

We now proceed to obtain an approximate expression for C_p which is consistent with linearized theory. Since the total enthalpy is constant,

$$h + \frac{V^2}{2} = h_\infty + \frac{V_\infty^2}{2}$$

For a calorically perfect gas, this becomes

$$T + \frac{V^2}{2c_p} = T_\infty + \frac{V_\infty^2}{2c_p}$$

$$T - T_\infty = \frac{V_\infty^2 - V^2}{2c_p} = \frac{V_\infty^2 - V^2}{2\gamma R/(\gamma - 1)}$$

$$\frac{T}{T_\infty} - 1 = \frac{\gamma - 1}{2} \frac{V_\infty^2 - V^2}{\gamma R T_\infty} = \frac{\gamma - 1}{2} \frac{V_\infty^2 - V^2}{a_\infty^2}$$

Since

$$V^2 = (V_\infty + u')^2 + v'^2 + w'^2$$

The above equation becomes,

$$\frac{T}{T_\infty} = 1 - \frac{\gamma - 1}{2a_\infty^2} (2u'V_\infty + u'^2 + v'^2 + w'^2) \quad (6)$$

Since the flow is isentropic, $p/p_\infty = (T/T_\infty)^{\gamma/(\gamma-1)}$

and the above equation gives,

$$\frac{p}{p_\infty} = \left[1 - \frac{\gamma - 1}{2a_\infty^2} (2u'V_\infty + u'^2 + v'^2 + w'^2) \right]^{\gamma/(\gamma-1)}$$

or

$$\frac{p}{p_\infty} = \left[1 - \frac{\gamma - 1}{2} M_\infty^2 \left(\frac{2u'}{V_\infty} + \frac{u'^2 + v'^2 + w'^2}{V_\infty^2} \right) \right]^{\gamma/(\gamma-1)} \quad (7)$$

The above equation is still an exact expression.

However considering small perturbations:

$$u'/V_\infty \ll 1; \quad u'^2/V_\infty, \quad v'^2/V_\infty^2, \quad \text{and} \quad w'^2/V_\infty^2 \lll 1.$$

Hence the above equation is of the form

$$\frac{p}{p_\infty} = (1 - \varepsilon)^{\gamma/(\gamma-1)} \quad (8)$$

where ε is small. Hence, from the binomial expansion, neglecting higher-order terms,

$$\frac{p}{p_\infty} = 1 - \frac{\gamma}{\gamma - 1} \varepsilon + \dots$$

Thus, the previous equation can be expressed in the form of the above equation as follows, neglecting higher-order terms:

$$\frac{p}{p_\infty} = 1 - \frac{\gamma}{2} M_\infty^2 \left(\frac{2u'}{V_\infty} + \frac{u'^2 + v'^2 + w'^2}{V_\infty^2} \right) + \dots \quad (9)$$

Substituting the above equation in the below equation,

$$C_p = \frac{2}{\gamma M_\infty^2} \left(\frac{p}{p_\infty} - 1 \right)$$

We get,

$$C_p = \frac{2}{\gamma M_\infty^2} \left[1 - \frac{\gamma}{2} M_\infty^2 \left(\frac{2u'}{V_\infty} + \frac{u'^2 + v'^2 + w'^2}{V_\infty^2} \right) + \dots - 1 \right]$$

$$= - \frac{2u'}{V_\infty} - \frac{u'^2 + v'^2 + w'^2}{V_\infty^2} + \dots$$

Since u'^2/V_∞^2 , v'^2/V_∞^2 , and $w'^2/V_\infty^2 \lll 1$, (10)

The above equation becomes,

$$C_p = - \frac{2u'}{V_\infty} \quad (11)$$

The above equation gives the linearized pressure coefficient, valid for small perturbations. Note its particularly simple form; the linearized pressure coefficient depends only on the x component of the perturbation velocity.

4.2. Prandtl-Glauert rule

It is a similarity rule, which relates incompressible flow over a given two-dimensional profile to subsonic compressible flow over the same profile.

$$C_p = \frac{C_{p_0}}{\sqrt{1 - M_\infty^2}} \quad (1)$$

where C_{p_0} is the incompressible pressure coefficient.

The above equation is called the Prandtl-Glauert rule.

Consider the compressible subsonic flow over a thin airfoil at small angle of attack (hence small perturbations), as sketched in the Fig 4.1. The usual inviscid flow boundary condition must hold at the surface, i e., the flow velocity must be tangent to the surface. Referring to Fig. 4.1 , at the surface this boundary condition is

$$\frac{df}{dx} = \frac{v'}{V_\infty + u'} = \tan \theta \quad (2)$$

We have the linearized perturbation-velocity potential equation.

$$(1 - M_\infty^2) \frac{\partial^2 \phi}{\partial x^2} + \frac{\partial^2 \phi}{\partial y^2} + \frac{\partial^2 \phi}{\partial z^2} = 0 \quad (3)$$

Note that this is an approximate equation and no longer represent the exact physics of the flow.

- (b) The perturbations must be small.
- (c) Transonic flow $0.8 \leq M_\infty \leq 1.2$) is excluded.
- (d) Hypersonic flow ($M_\infty \geq 5$) is excluded.

This equation is valid for subsonic and supersonic flow only. However, this equation has the striking advantage that it is linear.

In summary, we have demonstrated that subsonic and supersonic flows lend themselves to approximate, linearized theory for the case of irrotational, isentropic flow with small perturbations. In contrast, **transonic and hypersonic flows cannot be linearized, even with small perturbations. This is another example of the consistency of nature.**

Note some of the physical problems associated with transonic flow (mixed subsonic-supersonic regions with possible shocks, and extreme sensitivity to geometry changes at sonic conditions) and with hypersonic flow (strong shock waves close to the geometric boundaries, i e., thin shock layers, as well as high enthalpy, and hence high-temperature conditions in the flow). Just on an intuitive basis, we would expect such physically complicated flows to be inherently nonlinear. For the remainder of this chapter, we will consider linear flows only; thus, we will deal with subsonic and supersonic flows.

$$C_p = \frac{C_{p_0}}{\sqrt{1 - M_\infty^2}} \quad (4)$$

Equation (9.36) is called the *Prandtl-Glauert* rule; it is a similarity rule which relates *incompressible* flow over a given two-dimensional profile to *subsonic compressible* flow over the *same* profile. Moreover, consider the aerodynamic lift L and moment M on this airfoil. We define the lift and moment coefficients, C_L and C_M , respectively, as

$$C_L = \frac{L}{\frac{1}{2}\rho_\infty V_\infty^2 S}$$

$$C_M = \frac{M}{\frac{1}{2}\rho_\infty V_\infty^2 S l}$$

$$C_L = \frac{C_{L_0}}{\sqrt{1 - M_\infty^2}} \quad (5)$$

$$C_M = \frac{C_{M_0}}{\sqrt{1 - M_\infty^2}} \quad (6)$$

In an effort to obtain an improved compressibility correction, Laitone (see Ref. 23) applied Eq (9.36) locally in the flow, i.e.,

$$C_p = \frac{C_{p_o}}{\sqrt{1 - M^2}}$$

where M is the local Mach number. In turn, M can be related to M_∞ and the pressure coefficient through the isentropic flow relations. The resulting compressibility correction is

$$C_p = - \frac{C_{p_o}}{\sqrt{1 - M_\infty^2} + \left[M_\infty^2 \left(1 + \frac{\gamma - 1}{2} M_\infty^2 \right) / 2\sqrt{1 - M_\infty^2} \right] C_{p_o}} \quad (9.39)$$

Note that, as C_{p_o} becomes small, Eq. (9.39) approaches the Prandtl-Glauert rule.

Another compressibility correction that has been adopted widely is that due to von Karman and Tsien (see Refs. 24 and 25). Utilizing a hodograph solution of the nonlinear equations of motion along with a simplified “tangent gas” equation of state, the following result was obtained:

$$C_p = \frac{C_{p_o}}{\sqrt{1 - M_\infty^2} + \left(\frac{M_\infty^2}{1 + \sqrt{1 - M_\infty^2}} \right) \frac{C_{p_o}}{2}} \quad (9.40)$$

Equation (9.40) is called the *Karman-Tsien rule*.

4.3. CRITICAL MACH NUMBER

By definition, the critical Mach number M_{cr} is that free-stream Mach number at which sonic flow is first encountered on the airfoil.

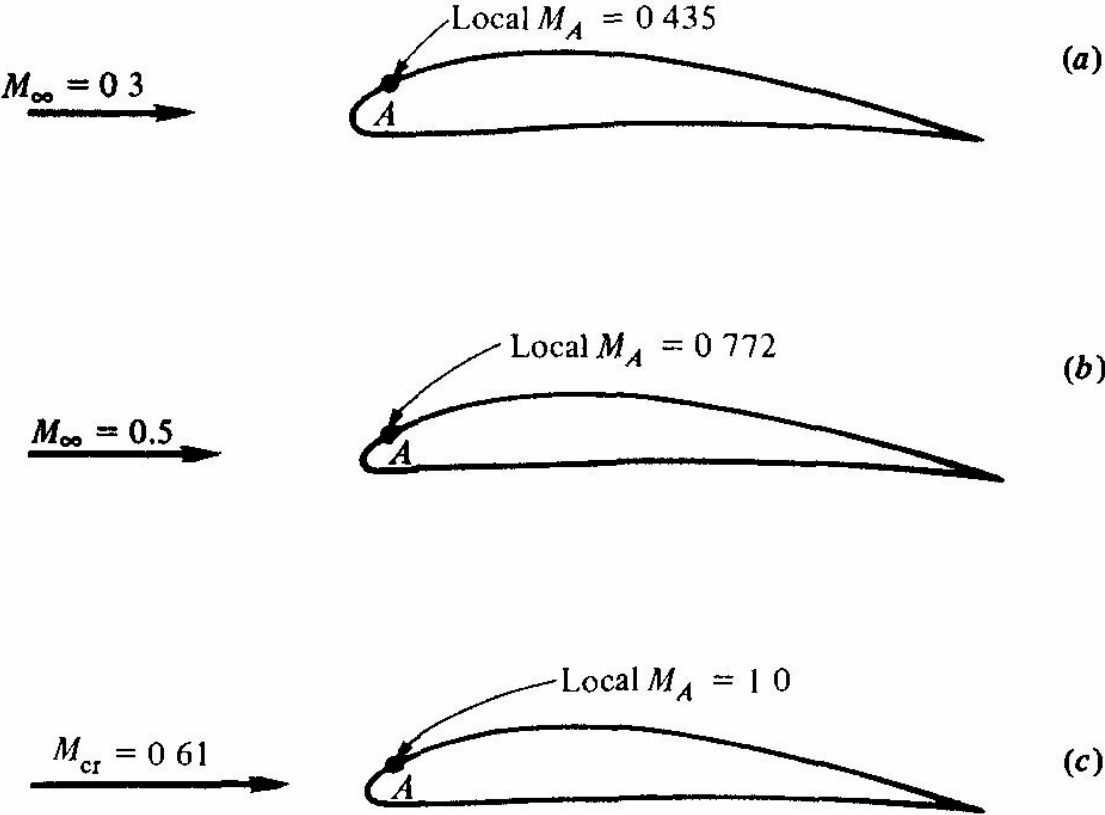


Fig. 4.2 Definition of critical Mach number Point A is the location of minimum pressure on the top surface of the airfoil

The critical Mach number can be calculated as follows. Assuming isentropic flow throughout the flow field and using the following equation derived from the previous isentropic flow relationship, we get

$$\frac{P_A}{P_\infty} = \left(\frac{1 + \frac{\gamma - 1}{2} M_\infty^2}{1 + \frac{\gamma - 1}{2} M_A^2} \right)^{\gamma/(\gamma-1)}$$

We have,

$$C_p = \frac{2}{\gamma M_\infty^2} \left(\frac{P}{P_\infty} - 1 \right)$$

Combining the above two equations the pressure coefficient at point A is

$$C_{pA} = \frac{2}{\gamma M_\infty^2} \left[\left(\frac{1 + \frac{\gamma-1}{2} M_\infty^2}{1 + \frac{\gamma-1}{2} M_A^2} \right)^{\gamma/(\gamma-1)} - 1 \right]$$

From Eq. (9.54), for a given M_∞ the values of local pressure coefficient and local Mach number are uniquely related at any given point A . Now assume as before that point A is the minimum-pressure (hence maximum-velocity) point on the airfoil. Furthermore, assume $M_A = 1$. Then, by definition, $M_\infty \equiv M_{cr}$. Also, for this case the value of the pressure coefficient is defined as the critical pressure coefficient $C_{p_{cr}}$. Setting $M_A = 1$, $M_\infty = M_{cr}$, and $C_p \equiv C_{p_{cr}}$ in Eq. (9.54), we obtain

$$C_{p_{cr}} = \frac{2}{\gamma M_{cr}^2} \left[\left(\frac{1 + \frac{\gamma-1}{2} M_{cr}^2}{1 + \frac{\gamma-1}{2}} \right)^{\gamma/(\gamma-1)} - 1 \right]$$

Note that $C_{p_{cr}}$ is a unique function of M_{cr} ; this variation is plotted as curve C in Fig. 9.14

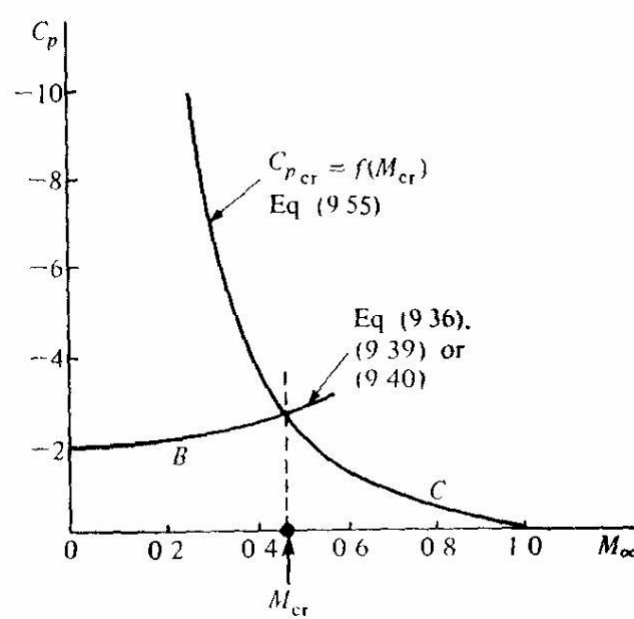


Fig. 4.3 Calculation of critical Mach number

Note in Fig 4.3 that curve C [from eq. for $C_{P_{cr}}$] is a result of the fundamental gas dynamics of the flow; it is unique, and does not depend on the size or shape of the airfoil. In contrast, curve B is different for different airfoils. For example, consider two airfoils, one thin and one thick. For the thin airfoil, the flow experiences only a mild expansion over the top surface, and hence C_{p_0} is small. Combined with the chosen compressibility correction, curve B in Fig 4.3 is low on the graph, resulting in a high value of M_{cr} . For the thick airfoil, $|C_p|$ is naturally larger because the flow experiences a stronger expansion over the top surface. Curve B is higher on the graph, resulting in a lower value of M_{cr} . Hence, an airfoil designed for a high critical Mach number must have a thin profile.

When the free-stream Mach number exceeds M_{cr} , a finite region of supersonic flow exists on the top surface of the airfoil. At a high enough subsonic Mach number, this embedded supersonic region will be terminated by a weak shock wave. The total pressure loss associated with the shock will be small, however, the adverse pressure gradient induced by the shock tends to separate the boundary layer on the top surface, causing a large pressure drag. The net result is a dramatic increase in drag. The free-stream Mach number at which the large drag rise begins is defined as the drag-divergence Mach number, it is always slightly larger than M_{cr} . The massive increase in drag encountered at the drag-divergence Mach number is the technical base of the "sound barrier" which was viewed with much trepidation before 1947.

4.3.1 Drag divergence Mach number

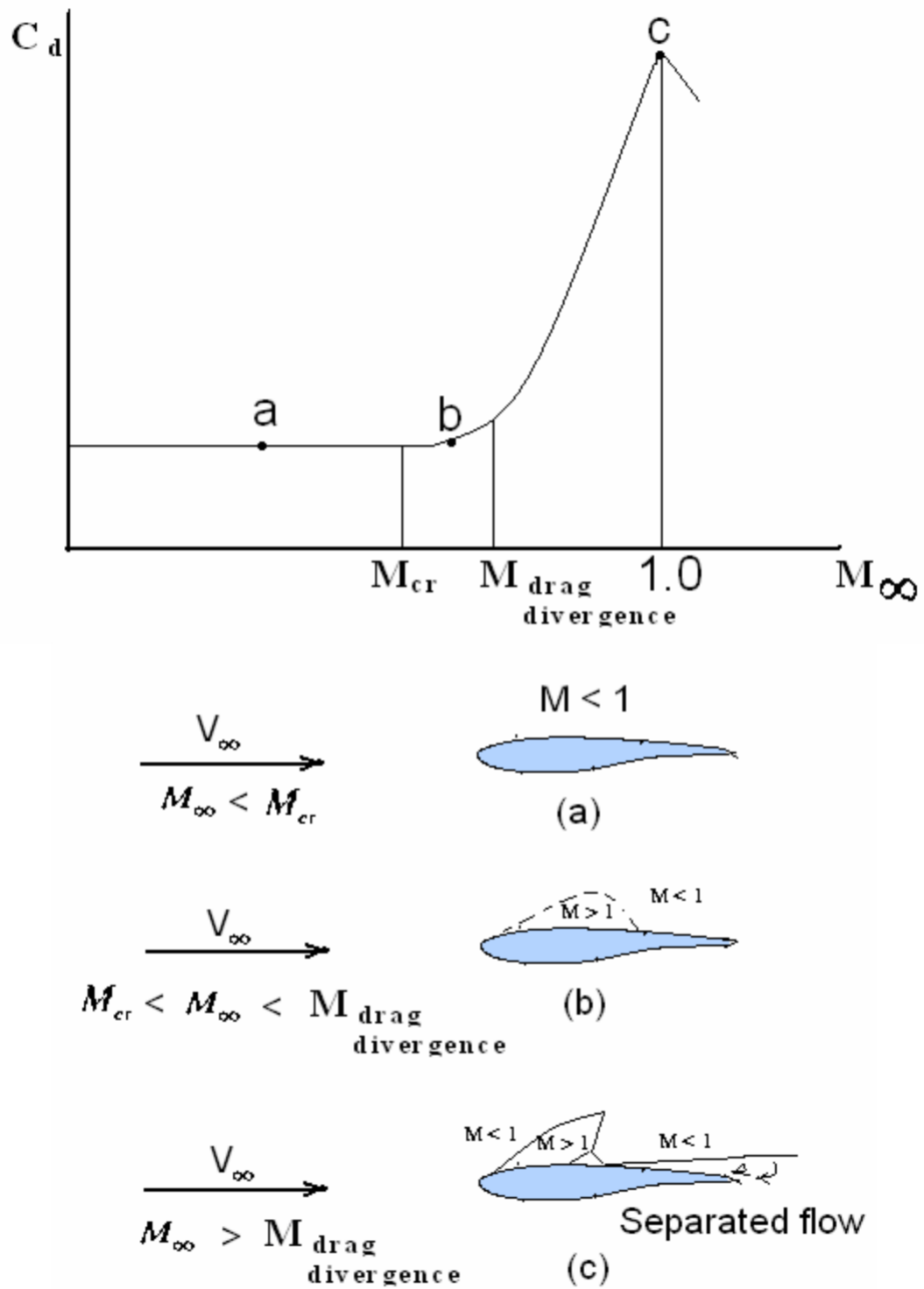


Fig. 4.4 C_d vs Mach number curve

If M_∞ increases slightly above M_{cr} , a bubble of supersonic flow will occur, surrounding the minimum pressure point (see above figure 4.4 (b)). Correspondingly, C_d will still remain reasonably low, as indicated by point b in the above figure. However, if M_∞ is still further increased, a very sudden and dramatic rise in the drag coefficient will be observed as noted by point c in the above figure 4.4. The effect of the shock wave on the surface pressure distribution can be seen.

The shock waves themselves are dissipative phenomena, which result in an increase in drag on the airfoil. But in addition, the sharp pressure increase across the shock wave creates a strong adverse gradient, causing the flow to separate from the surface. Such flow separation can create substantial increases in drag. Thus, the sharp increase in C_d shown in the above figure 4.4 is a combined effect of shock waves and flow separation. The free stream Mach number at which C_d begins to increase rapidly is defined as drag-divergence Mach number.

Note that $M_{cr} < M_{drag\ divergence} < 1.0$

The flow pattern sketched above is characteristic of a flight regime called transonic. When $0.8 \leq M_\infty \leq 1.2$, the flow is generally designated as transonic flow, and it is characterized by some complex effects only hinted in the above figure 4.5.

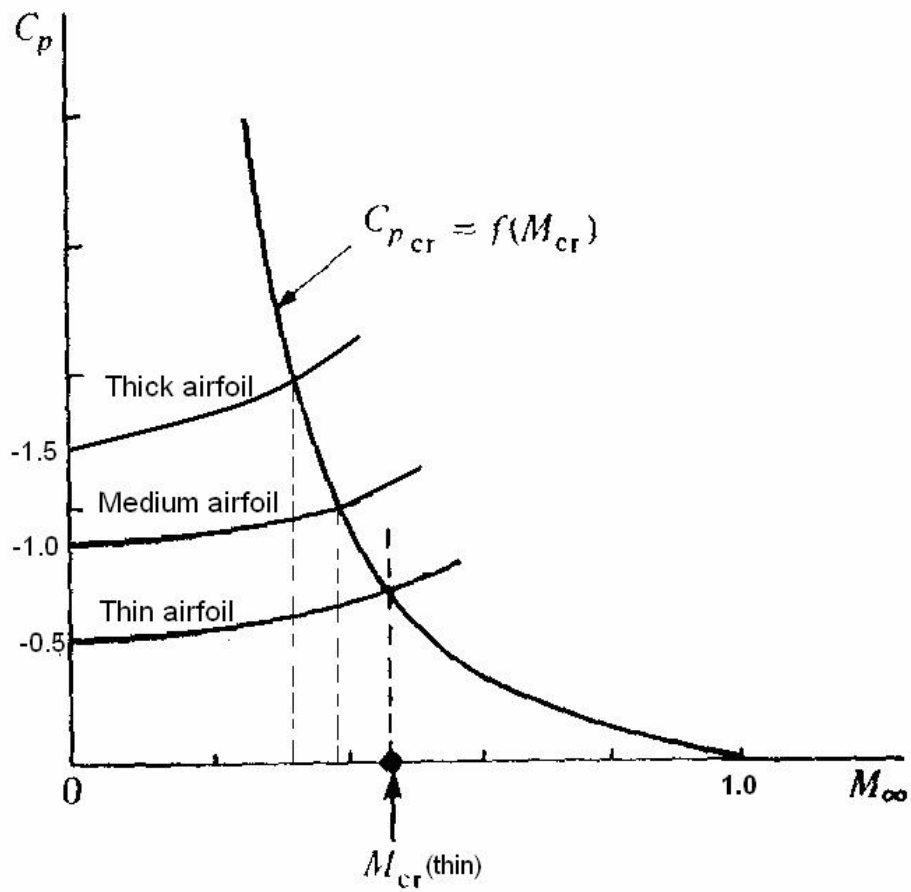


Fig. 4.5. Variation of critical Mach number with thickness of the airfoil

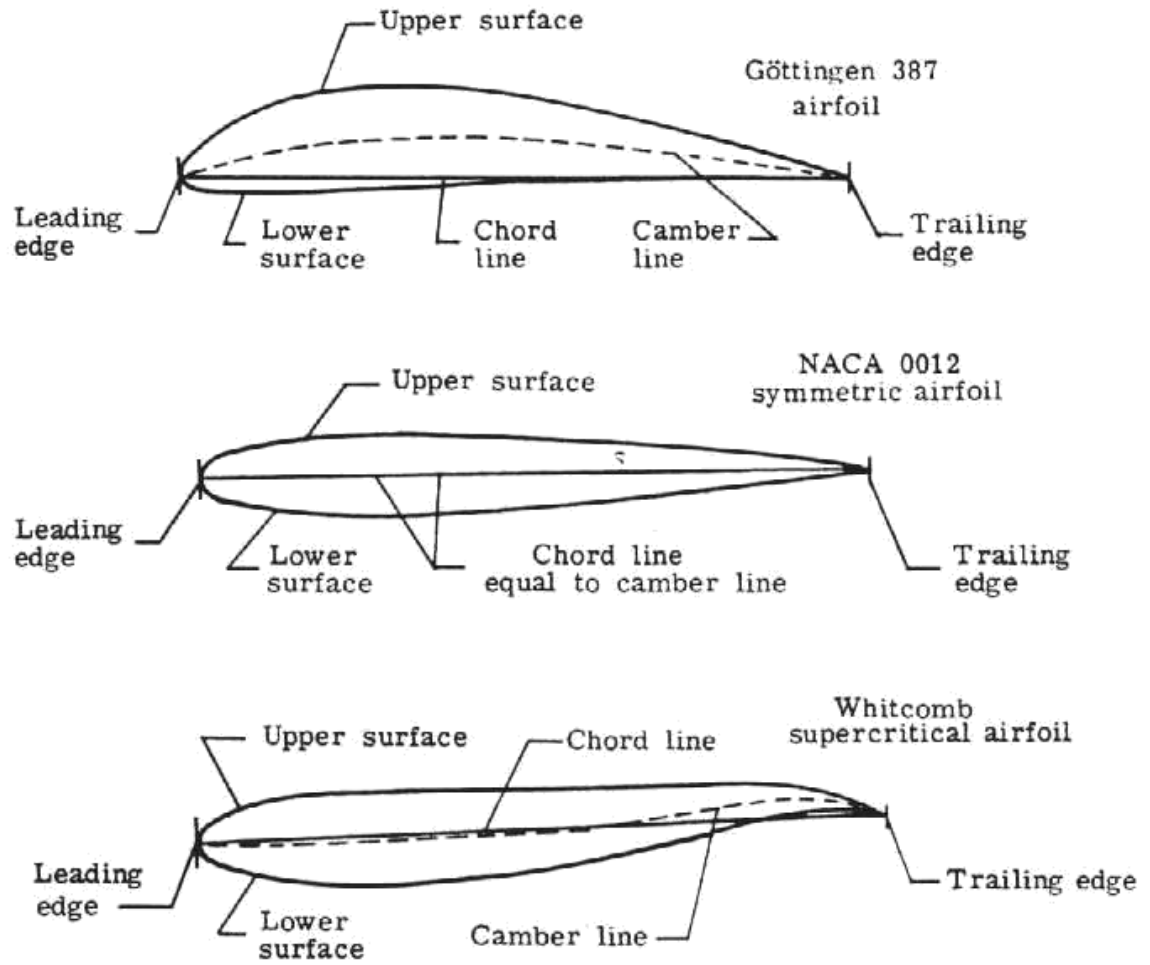


Fig. 4.6. Variation of critical Mach number with normal vs supercritical airfoil.

4.4. Supercritical airfoil

The supercritical airfoil is a different approach to the increase in drag-divergence Mach number. Here, the shape of the airfoil is designed with a relatively flat top surface as shown in the below figure 4.7.

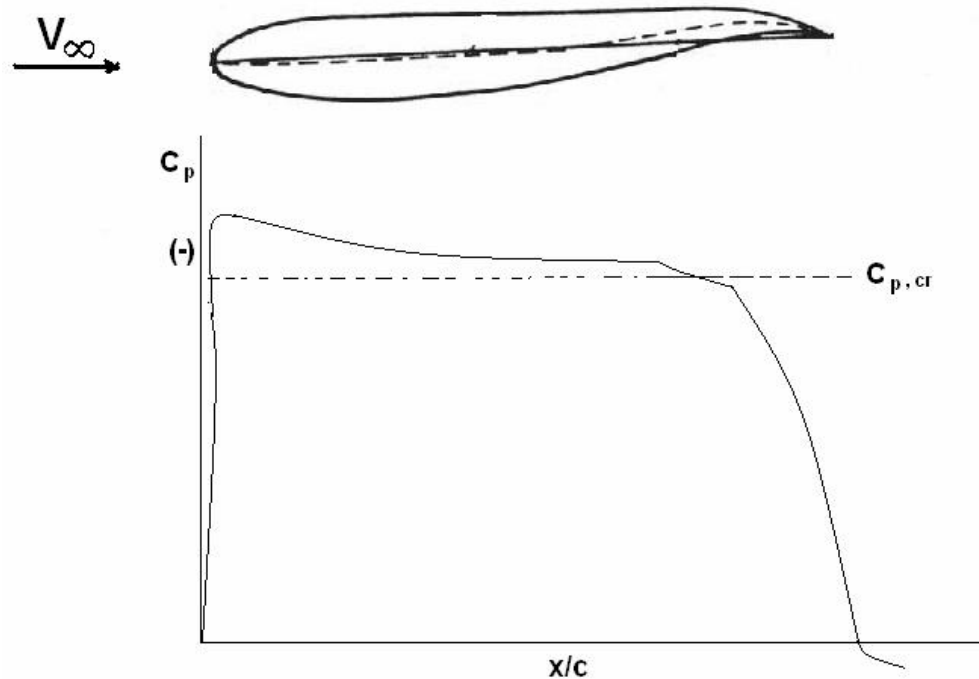


Fig. 4.7 Shape of a typical supercritical airfoil and its pressure coefficient distribution over the top surface

When the free stream Mach number exceeds M_{cr} , a pocket of supersonic flow occurs over the top surface as usual; but because of the top is relatively flat, the local supersonic Mach number is a lower value than would exist in the case of a conventional

As a result, the shock wave that terminates the pocket of supersonic flow is weaker. In turn, the super critical airfoil can penetrate closer to Mach 1 before drag divergence occurs. In essence, the increment in Mach number (the “grace period”) between M_{cr} and $M_{drag\ divergence}$ is increased by the shape of the supercritical airfoil. One way to think about this is that the supercritical airfoil is “more comfortable” than conventional airfoils in the region above M_{cr} , and it can fly closer to Mach 1 before drag divergence is encountered. Because they are more comfortable in the flight regime above the critical Mach number and because they can penetrate closer to Mach 1 after exceeding M_{cr} these airfoils are called supercritical airfoils. They are designed to cruise in the Mach number range above M_{cr} . The pressure coefficient distribution over the top surface of a supercritical airfoil flying above M_{cr} but below $M_{drag\ divergence}$ is sketched in the above figure. After a sharp decrease in pressure around the leading edge, the pressure remains relatively constant over a substantial portion of the top surface. This is in contrast to the pressure coefficient distribution for a conventional airfoil flying above M_{cr} , as shown below (wind Tunnel data) for NACA 0012 airfoil for $M_{\infty} = 0.808$, which is above the critical Mach number.

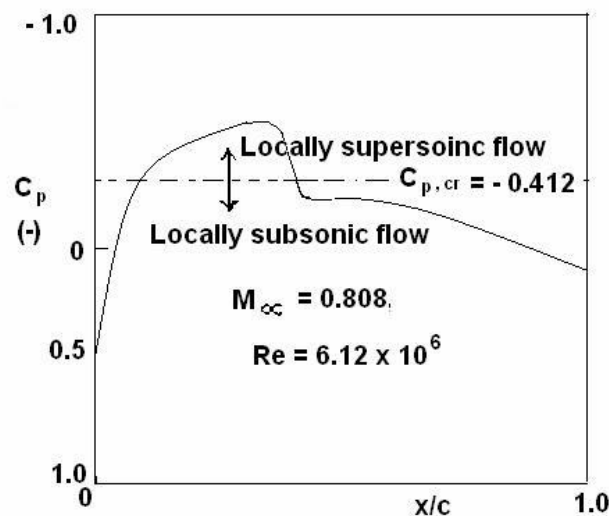


Fig. 4.8 Wind Tunnel measurements of the surface pressure coefficient distribution for the NACA0012 airfoil at zero angle of attack for $M_{\infty} = 0.808$, which is above the critical Mach number.

Clearly, the flow over the supercritical airfoil is carefully tailored to achieve the desired result.

The early aerodynamic research on supercritical airfoils was carried out by Whitecomb's an aeronautical engineer at NASA Langly Research Center, during the middle 1960s. Designers of transonic aircraft can use supercritical airfoils to accomplish one of two objectives:

For a given airfoil thickness, the supercritical airfoil shape allows a higher cruise velocity; or for a given lower cruise velocity, airfoil thickness can be larger.

The later option has some design advantages. The structural design of a thicker wing is more straightforward and actually results in a more light weight (albeit thicker) wing. Also a thicker wing provides more volume for an increased fuel capacity. Clearly, the use of a supercritical airfoil provides a larger design space for transonic airplanes.

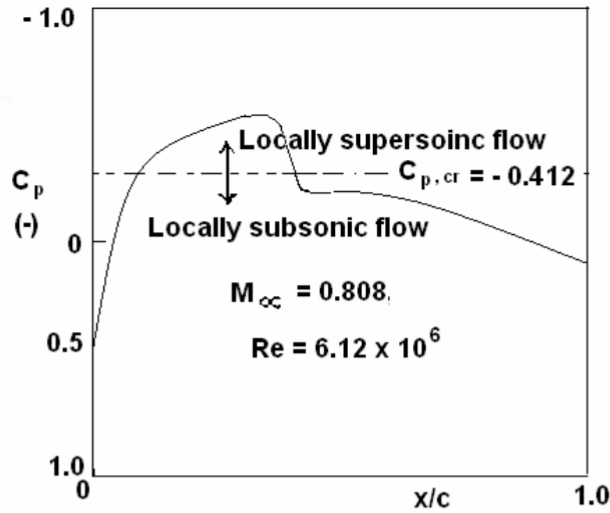


Fig. 4.9 Wind Tunnel measurements of the surface pressure coefficient distribution for the NACA0012 airfoil at zero angle of attack for $M_\infty = 0.808$, which is above the critical Mach number.

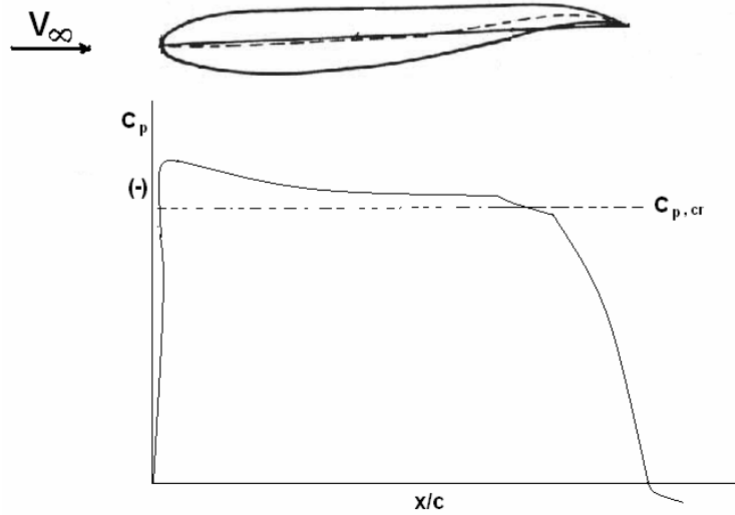


Fig. 4.10 Shape of a typical supercritical airfoil and its pressure coefficient distribution over the top surface

Nature places the maximum velocity at a point that satisfies the physics of the whole flow field not just what is happening in a local region of flow. The point of maximum velocity is dictated by the complete shape of the airfoil, not just by the shape in a local region.

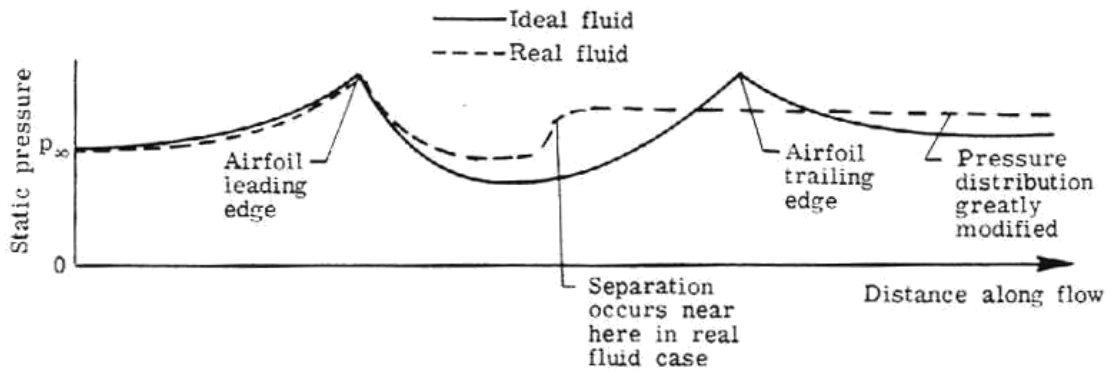
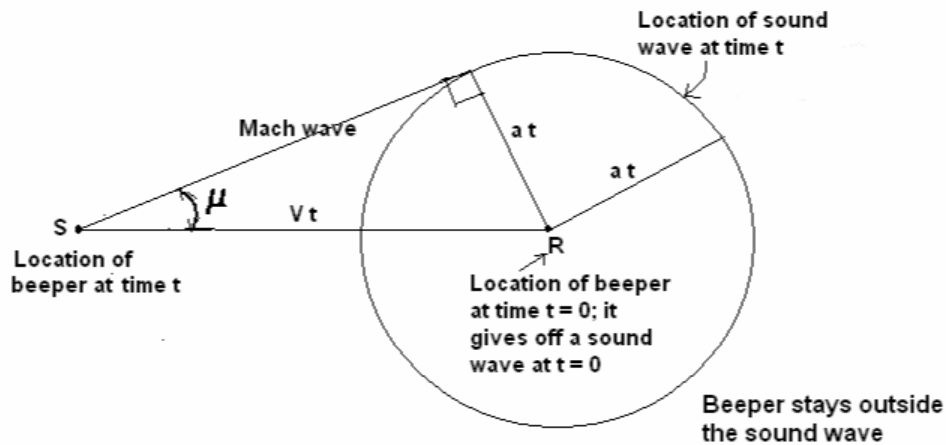


Fig. 4.11 (a) Airfoil upper surface static-pressure distributions.

4.5 Wave Drag (At supersonic speeds)

With respect to airfoils (as well as all other aerodynamics bodies), shock waves in supersonic flow create a new source of drag, called wave drag.

Wave drag is an aerodynamics term that refers to a sudden and very powerful form of drag that appears on aircraft and blade tips moving at high-subsonic and supersonic speeds....



**The origin of Mach waves and shock waves.
Beeper is moving faster than the speed of sound**

Mach angle

It is defined as $\mu = \arcsin 1/M$

4.5.1. Drag divergence Mach number

It is that free-stream Mach number at which the drag coefficient begins to rapidly increase due to occurrence of transonic shock waves. For a given body, the drag divergence Mach number is slightly higher than the critical Mach number.

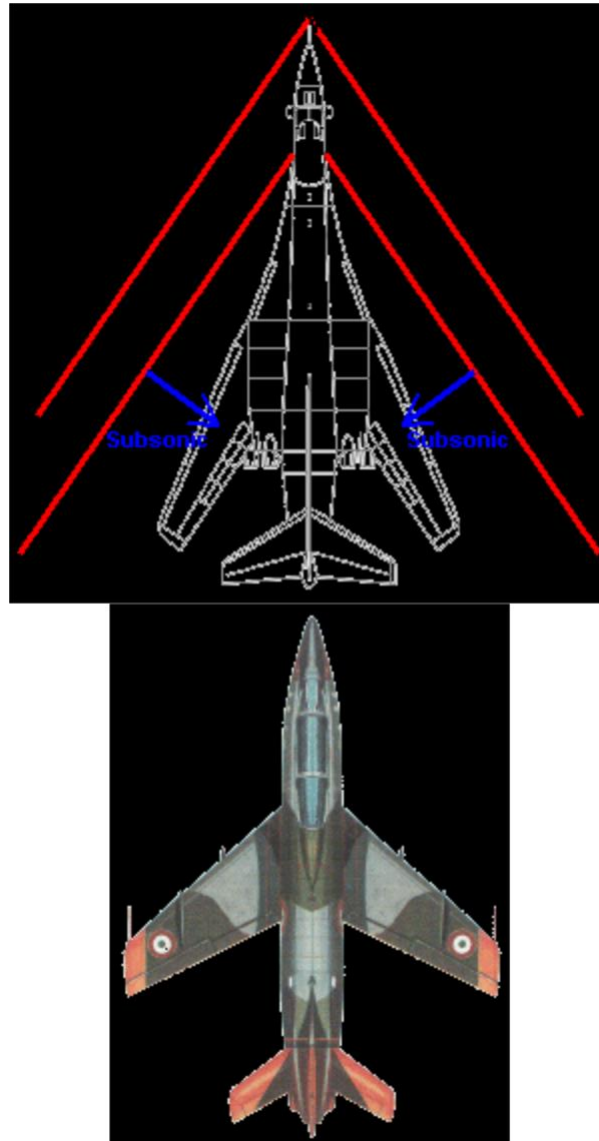


Fig. 4.12. Wave angle and Shock angle relation

The whole idea of sweeping an aircraft's wing is to delay the drag rise caused by the formation of shock waves. The swept-wing concept had been appreciated by German aerodynamicists since the mid-1930s, and by 1942 a considerable amount of research had gone into it. However, in the United States and Great Britain, the concept of the swept wing remained virtually unknown until the end of the war. Due to the early research in this area, this allowed Germany to successfully introduce the swept wing in the jet fighter Messerschmitt ME-262 as early as 1941.

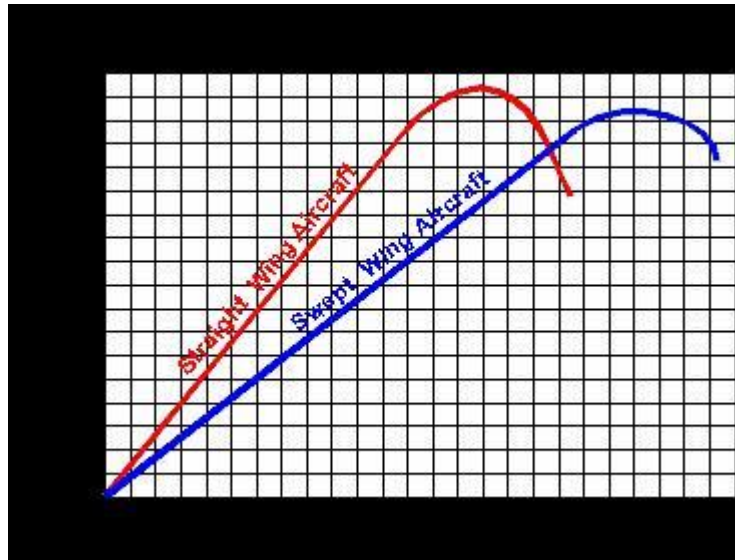
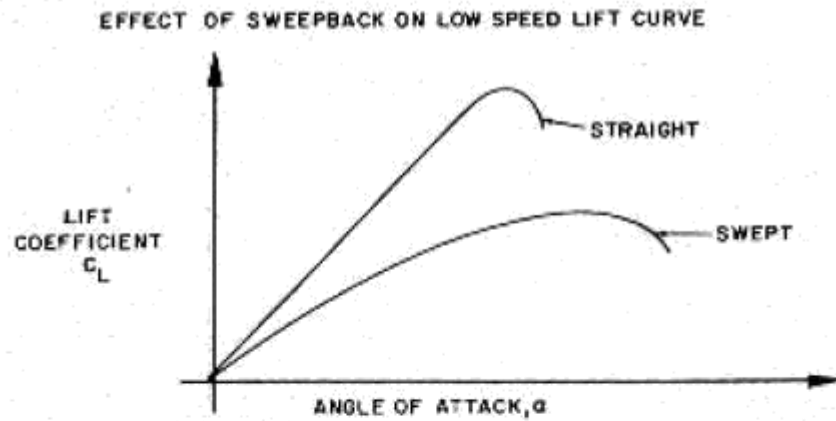


Fig. 4.13. Swept vs Straight wing configuration



EFFECT OF SWEEPBACK ON YAW AND ROLL MOMENTS

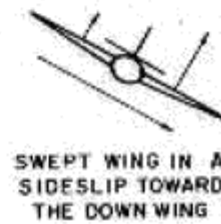
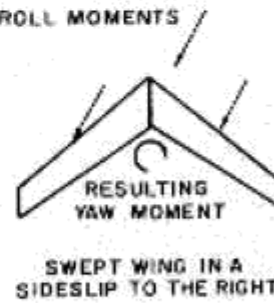
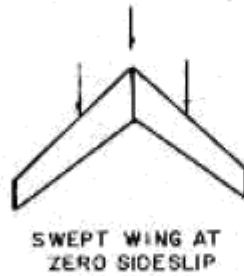


Fig. 4. 14 Aerodynamic Effects due to sweepback.

4.6. Transonic Area Rule

Within the limitations of small perturbation theory, at a given transonic Mach number, aircraft with the same longitudinal distribution of cross-sectional area, including fuselage, wings and all appendages will, at zero lift, have the same wave drag.

Why: Mach waves under transonic conditions are perpendicular to flow.

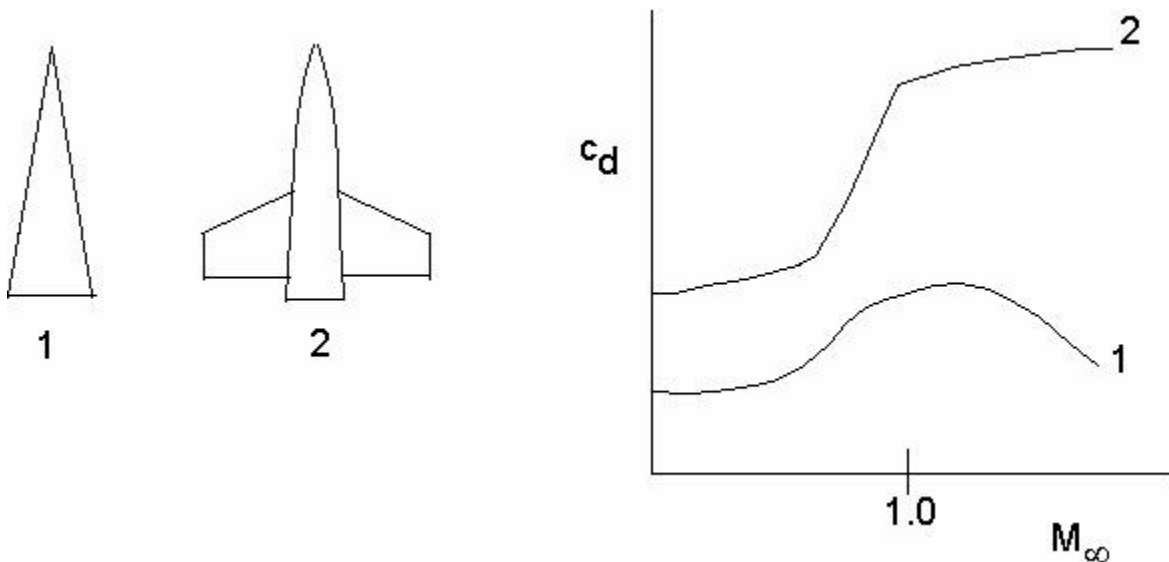


Fig. 4.15 Area Rule, Minimizing Drag.

Keep area distribution smooth, constant if possible. Else, strong shocks and hence drag result.

Wing-body interaction leading to shock formation:

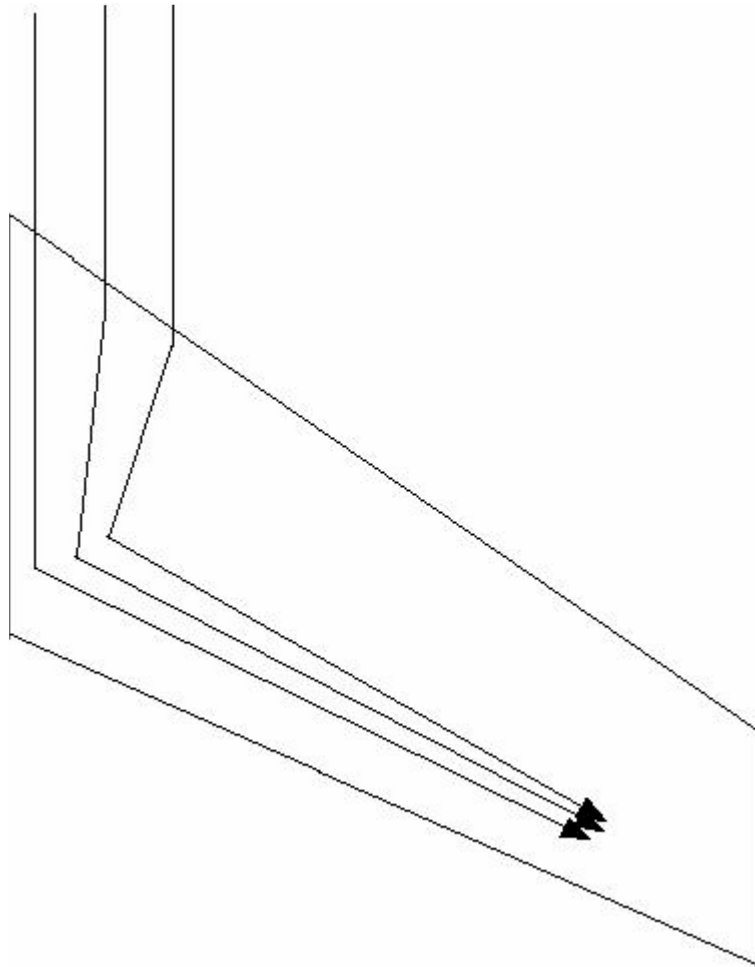


Fig. 4.16 Wing-body interaction leading to shock formation

Observed: c_p distributions are such that maximum velocity is reached far aft at root and far forward at tip. Hence, streamlines curve in at the root, compress, shock propagates out.

The **Whitcomb area rule**, also called the **transonic area rule**, is a design technique used to reduce an aircraft's drag at transonic and supersonic speeds, particularly between Mach 0.8 and 1.2. This is the operating speed range of the majority of commercial and military fixed-wing aircraft today. At high-subsonic flight speeds, supersonic airflow can develop in areas where the flow accelerates around the aircraft body and wings. The speed at which this occurs varies from aircraft to aircraft, and is known as the critical Mach number. The resulting shock waves formed at these points of supersonic flow can bleed away a considerable amount of power, which is experienced by the aircraft as a sudden and very powerful form of drag, called wave drag. To reduce the number and power of these shock waves, an aerodynamic shape should change in cross sectional area as smoothly as possible. This leads to a "perfect" aerodynamic shape known as the **Sears-Haack body**, roughly shaped like a cigar but pointed at both ends.

The area rule says that an airplane designed with the same cross-sectional area as the Sears-Haack body generates the same wave drag as this body, largely independent of the actual shape. As a result, aircraft have to be carefully arranged so that large volumes like wings are positioned at the widest area of the equivalent Sears-Haack body, and

that the cockpit, tailplane, intakes and other "bumps" are spread out along the fuselage and or that the rest of the fuselage along these "bumps" is correspondingly thinned.

The area rule also holds true at speeds higher than the speed of sound, but in this case the body arrangement is in respect to the Mach line for the design speed. For instance, at Mach 1.3 the angle of the Mach cone formed off the body of the aircraft will be at about $\mu = \arcsin (1/M) = 50,3 \text{ deg}$ (μ is the sweep angle of the Mach cone). In this case the "perfect shape" is biased rearward, which is why aircraft designed for high speed cruise tend to be arranged with the wings at the rear. A classic example of such a design is Concorde.

Anti-shock bodies or **Küchemann carrots** are pods placed at the trailing edge of a transonic aircraft's wings in order to reduce wave drag, thus improving fuel economy, as the aircraft enters the transonic flight regime (Mach 0.8–1.2). Most jet airliners have a cruising speed between Mach 0.8 and 0.85. For aircraft operating in the transonic regime, wave drag can be minimized by having a cross-sectional area which changes smoothly along the length of the aircraft. This is known as the area rule, and is the operating principle behind the design of anti-shock bodies.

On most jet airliners, the mechanisms for deploying the wing flaps are enclosed in fairings, called "flap track fairings", which also serve as anti-shock bodies.

Anti-shock bodies were concurrently developed by Richard Whitcomb at NASA and Dietrich Küchemann, a German aerodynamicist, in the early 1950s. The Handley-Page Victor bomber was particularly well-known for featuring a conspicuous pair of Küchemann carrots, so-called because of their distinctive shape.

4.6 Area Rule

The Area Rule was discovered by NASA aerodynamicist Richard Whitcomb in 1950. The rule states that, in order to produce the least amount of drag when approaching supersonic flight, the cross-sectional area of an aircraft body should be consistent throughout the aircraft's length. To compensate for the place on an aircraft where the wings are attached to the fuselage, the fuselage needs to be made narrower so that the cross-section remains the same. This is why aircraft that are designed to fly around the speed of sound have a pinched fuselage where the wings are attached to the body.

4.8. Wing Types

Aircraft designers have designed several wing types that have different aerodynamic properties. These have different shapes and attach to the aircraft body at different angles at different points along the fuselage. Not all of these planes have a practical use-some have just been use for research.

The conventional straight wing extends out from the fuselage at approximately right angles. On early biplanes, one wing often was suspended above the fuselage by some sort of bracing supports while the second crossed directly under the fuselage. On monoplanes, designers positioned the wings at different heights depending on the design-some crossed above the fuselage while others were attached at the lower part of the fuselage. The swept-back wing extends backward from the fuselage at an angle.

The delta wing looks much like a triangle when viewed from above (or the Greek letter "delta" Δ .) It sweeps sharply back from the fuselage with the angle between the front of the wing (the leading edge) often as high as 60 degrees and the angle between the fuselage and the trailing edge (the back edge of the wing) at around 90 degrees. The tip of a delta wing is often, but not always, cut off.

The forward-swept wing gives an airplane the appearance of flying backward. The wing is angled toward the front of the aircraft and is usually attached to the airplane far back on the fuselage. A small wing called a canard is often attached to the fuselage near the front on this type of aircraft.

A variable-sweep wing can be moved during flight-usually between a swept-back position and a straight position.

The flying wing is an aircraft design where the wing forms virtually the entire airplane and it sweeps back from the center of the aircraft. The fuselage is a very narrow section in the center that joins the wings without any seams.

The term "dihedral" is used to describe wings that are angled upward from the fuselage. Dihedral is the angle at which the wings are slanted upward from the root of the wing (where it is attached to the fuselage) to the wing tip. "Canards" are small wings placed toward the front of the fuselage.

4.8. Types of Wings and Transonic Flow

There are a number of ways of delaying the increase in drag encountered when an aircraft travels at high speeds, i.e., the transonic wave drag rise, or of increasing the drag-divergence Mach number (the free-stream Mach number at which drag rises precipitously) so that it is closer to 1. One way is by the use of *thin airfoils*: increase in drag associated with transonic flow is roughly proportional to the square of the thickness-chord ratio (t/c). If a thinner airfoil section is used, the airflow speeds around the airfoil will be less than those for the thicker airfoil. Thus, one may fly at a higher free-stream Mach number before a sonic point appears and before one reaches the drag-divergence Mach number. The disadvantages of using thin wings are that they are less effective (in terms of lift produced) in the subsonic speed range and they can accommodate less structure (wing fuel tanks, structural support members, armament stations, etc.) than a thicker wing.

In 1935, the German aerodynamicist Adolf Busemann proposed that a swept wing might delay and reduce the effects of compressibility. A *swept wing* would delay the formation of the shock waves encountered in transonic flow to a higher Mach number. Additionally, it would reduce the wave drag over all Mach numbers.

A swept wing would have virtually the same effect as a thinner airfoil section (the thickness-chord ratio (t/c) is reduced). The maximum ratio of thickness to chord for a swept wing is less than for a straight wing with the same airflow. One is effectively using a thinner airfoil section as the flow has more time in which to adjust to the high-speed situation. The critical Mach number (at which a sonic point appears) and the drag-divergence Mach number are delayed to higher values; Sweep forward or

sweepback will accomplish these desired results. Forward sweep has disadvantages, however, in the stability and handling characteristics at low speeds.

A major disadvantage of swept wings is that there is a spanwise flow along the wing, and the boundary layer will thicken toward the wingtips for sweepback and toward the roots (the part of the wing closest to the fuselage) for sweep-forward. In the case of sweepback, there is an early separation and stall of the wingtip sections and the ailerons lose their roll control effectiveness. The spanwise flow may be reduced by the use of stall fences, which are thin plates parallel to the axis of symmetry of the airplane. In this manner a strong boundary layer builds up over the ailerons is prevented. Wing twist is another possible solution to this spanwise flow condition.

The wing's *aspect ratio* is another parameter that influences the critical Mach number and the transonic drag rise. Substantial increases in the critical Mach number (the subsonic Mach number at which sonic flow occurs at some point on the wing for the first time) occur when using an aspect ratio less than about four. However, low-aspect-ratio wings are at a disadvantage at subsonic speeds because of the higher induced drag.

By bleeding off some of the boundary layer along an airfoils surface, the drag-divergence Mach number can be increased. This increase results from the reduction or elimination of shock interactions between the subsonic boundary layer and the supersonic flow outside of it.

Vortex generators are small plates, mounted along the surface of a wing and protruding perpendicularly to the surface. They are basically small wings, and by creating a strong tip vortex, the vortex generators feed high-energy air from outside the boundary layer into the slow moving air inside the boundary layer. This condition reduces the adverse

pressure gradients and prevents the boundary layer from stalling. A small increase in the drag-divergence Mach number can be achieved. This method is economically beneficial to airplanes designed for cruise at the highest possible drag-divergence Mach number.

A more recent development in transonic technology, and destined to be an important influence on future wing design, is the *supercritical wing* developed by Dr. Richard T. Whitcomb of NASA's Langley Research Center. With the supercritical wing, a substantial rise in the drag-divergence Mach number is realized and the critical Mach number is delayed even up to 0.99. This delay represents a major increase in commercial airplane performance.

The curvature of a wing gives the wing its lift. Because of the flattened upper surface of the supercritical airfoil, lift is reduced. However, to counteract this, the new supercritical wing has increased camber at the trailing edge.

There are two main advantages of the supercritical airfoil. First, by using the same thickness-chord ratio, the supercritical airfoil permits high subsonic cruise near Mach 1 before the transonic drag rise. Alternatively, at lower drag divergence Mach numbers, the supercritical airfoil permits a thicker wing section to be used without a drag penalty. This airfoil reduces structural weight and permits higher lift at lower speeds.

Coupled to supercritical technology is the "area-rule" concept also developed by Dr. Richard T. Whitcomb in the early 1950s for transonic airplanes and later applied to supersonic flight in general.

Basically, the area rule states that minimum transonic and supersonic drag is obtained when the cross-sectional area distribution of the airplane along the longitudinal axis can be projected into a body of revolution that is smooth and shows no abrupt changes in cross section along its length. Or, if a graph is made of the cross-sectional area against body position, the resulting curve is smooth. If it is not a smooth curve, then the cross section is changed accordingly.

The original Convair F-102A was simply a scaled-up version of the XF-92A with a pure delta wing. But early tests indicated that supersonic flight was beyond its capability because of excessive transonic drag and the project was about to be cancelled. Area ruling, however, saved the airplane from this fate. In the original YF-102A, the curve of the cross-sectional area plotted against body station was not very smooth as there was a large increase in cross-sectional area when the wings were attached. The redesigned F-102A had a “coke-bottle”-waist-shaped fuselage and bulges added aft of the wing on each side of the tail to give a better area-rule distribution. The F-102A could then reach supersonic speeds because of the greatly reduced drag and entered military service in great numbers.

Later, the area-rule concept was applied to design of a near-sonic transport capable of cruising at Mach numbers around 0.99. In addition to area ruling, a supercritical wing was used.

Transonic is an aeronautics term referring to a range of velocities just below and above the speed of sound. It is defined as the range of speeds between the critical mach, when some parts of the airflow over an aircraft become supersonic, and a higher speed, typically near Mach number, when all of the airflow is supersonic....

speed range. Supercritical airfoils are characterized by their flattened upper surface, highly cambered (curved) aft section, and greater leading edge

The **leading edge** is a line connecting the forward-most points of a wing's profile. In other words, it's the front edge of the wing. When an aircraft is moving forward, the leading edge is that part of the wing that first contacts the air....

4.9 Geometric and aerodynamic twist

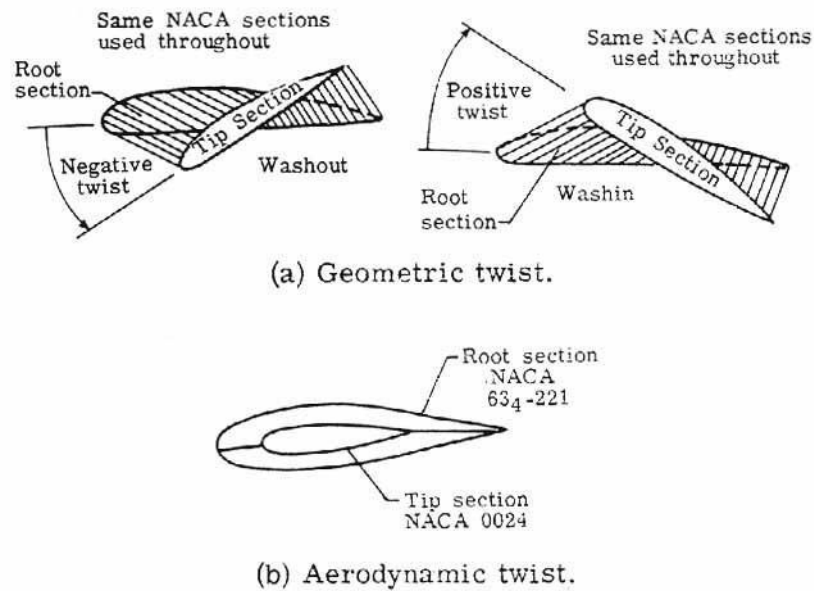


Fig. 4.17 Twisted wing Configuration

Wings are given twist so that the angle of attack varies along the span. A decrease in angle of attack toward the wing tip is called washout whereas an increase in angle of attack toward the wing tip is called washin. Geometric twist (fig. 4.17 (a)) represents a geometric method of changing the lift distribution, whereas aerodynamic twist, by using different airfoil sections along the span represents an aerodynamic method of changing the lift distribution in a spanwise manner (fig. 4.17 (b)). To give minimum induced drag it was demonstrated that the spanwise efficiency factor e should be as close to 1 as possible. This is the case of an elliptic spanwise lift distribution. A number of methods are available to modify the spanwise distribution of lift.

4.9. Vortex flow effects

Note that upwash and downwash are due to both the bound vortex and the tip vortices.

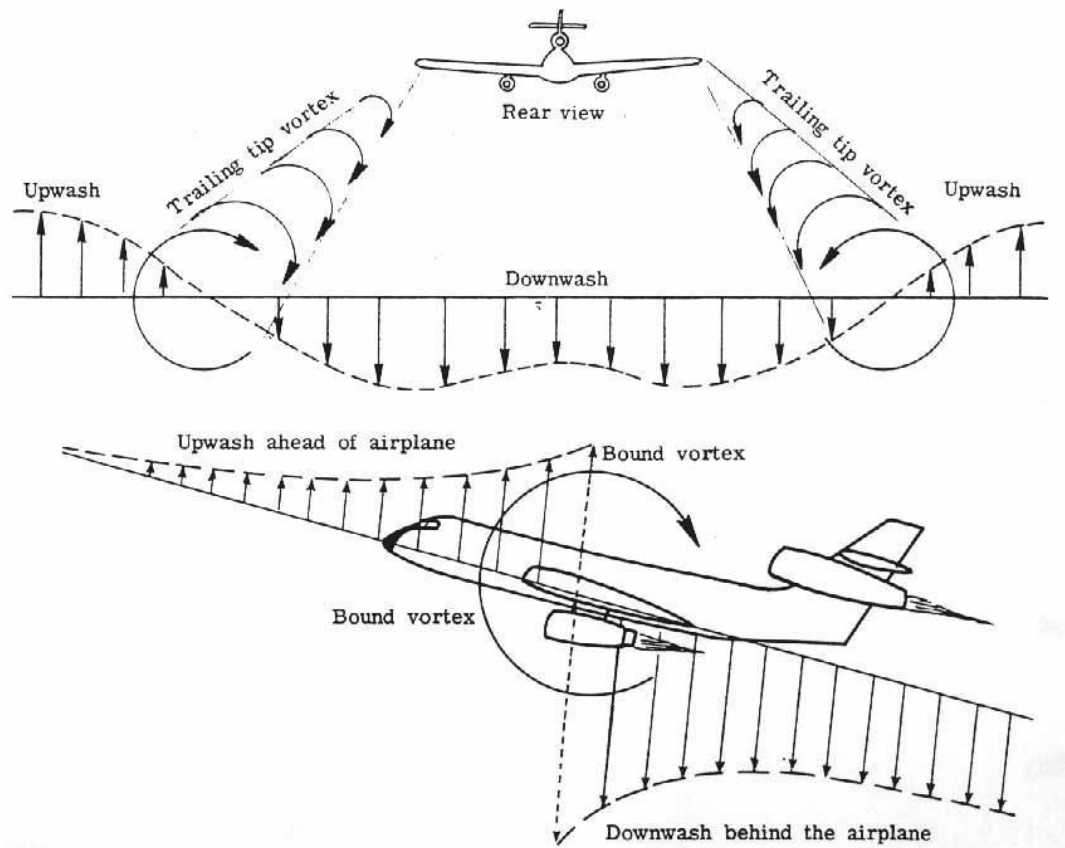


Fig. 4.18. Bound vortex and downwash effects of 3D wing.

The important effects of the vortex system are shown in figure. Indicated are the directions of air movement due to the vortex system. The left-tip vortex rotates clockwise, the right-tip vortex rotates counter clockwise (when viewed from behind), and the bound vortex rotates clockwise (when viewed from the left side). The bound vortex is directly related to the lift on the wing as in the dimensional case.

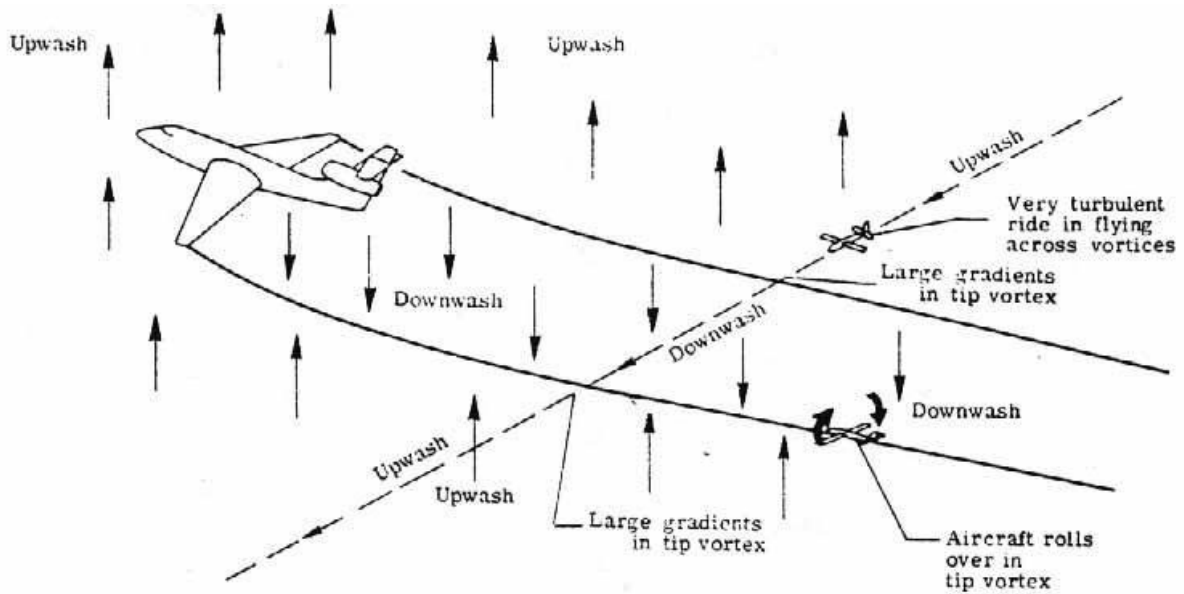


Fig. 4.19 Upwash and downwash fields around an airplane

In both the 2D and 3D cases the upflow (or upwash) in front of the wing balanced the downflow (or downwash) in back of the wing caused by the bound vortex. But, in the finite-wing case one must also take into account the tip vortices (assuming that the influence of the starting vortex is negligible). The tip vortices cause additional downwash behind the wing within the wing span. One can see that, for an observer fixed in the air (fig. 4.18) all the air within the vortex system is moving downwards (this is called downwash) whereas all the air outside the vortex system is moving upwards (this is called upwash). Note that an aircraft flying perpendicular to the flight path of the airplane creating the vortex pattern will encounter upwash, downwash, and upwash in that order. The gradient, or change of downwash to upwash, can become very large at the tip vortices and cause extreme motions in the airplane flying through it. Also shown is an airplane flying into a tip vortex. Note that there is a large tendency for the airplane to roll over. If the control surfaces of the airplane are not effective enough to counteract

the airplane roll tendency, the pilot may lose control or in a violent case experience structural failure.

The problems of severe tip vortices are compounded by the take-off and landings of the new generation of jumbo jets. During these times the speed of the airplane is low and the airplane is operating at high lift coefficients to maintain flight. The Federal Aviation Agency has shown that for a 0.27 MN (600 000 lb) plane, the tip...

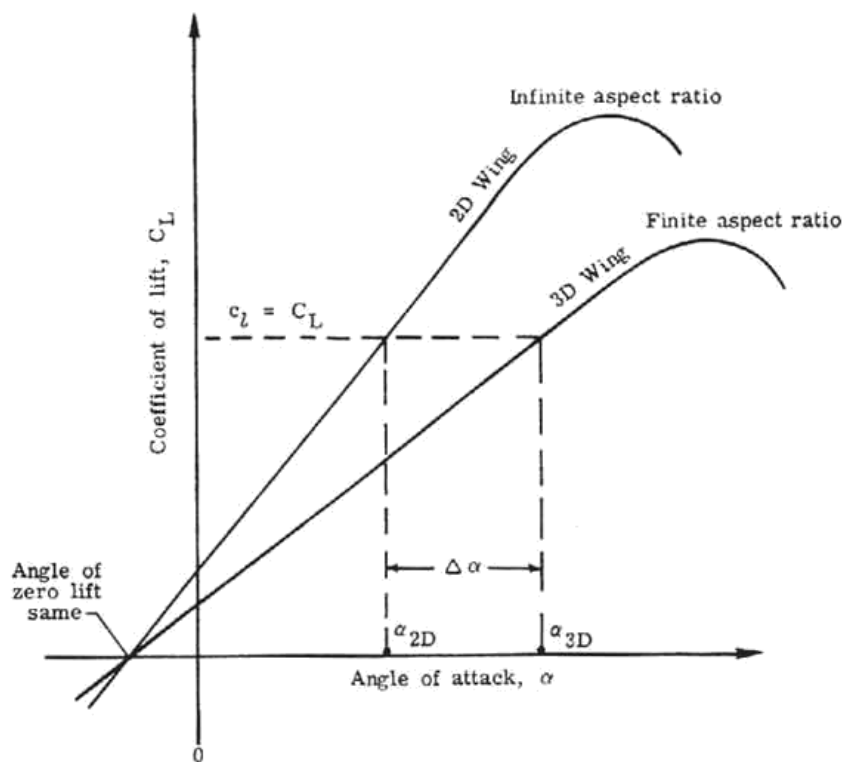


Fig. 4.20 Effect of aspect ratio on coefficient of lift

Figure 4.20 shows the coefficient of lift curves ("lift curves") obtained for both wings by experiment. Readily evident is the effect that the tip vortices have in creating the additional downwash w at the wing; the lift curve is flattened out so that at the same angle of attack less lift is obtained for the smaller aspect ratio wing. This is not a beneficial effect.



SATHYABAMA

INSTITUTE OF SCIENCE AND TECHNOLOGY
(DEEMED TO BE UNIVERSITY)

Accredited "A" Grade by NAAC | 12B Status by UGC | Approved by AICTE

www.sathyabama.ac.in

**SCHOOL OF MECHANICAL ENGINEERING
DEPARTMENT OF AERONAUTICAL ENGINEERING**

HIGH SPEED AERODYNAMICS

SAEA1505

**UNIT – V EXPERIMENTAL TECHNIQUES IN HIGH SPEED
FLOWS – SAEA1505**

5. 1. INTRODUCTION:

Wind tunnels are designed for a specific purpose and speed regime. Therefore, there are different types of wind tunnels and several ways to classify wind tunnels. In this section we shall present some basics of these wind tunnels. Experimental facilities of supersonic and hypersonic flow speeds can be called high speed wind tunnels. In high speed flows it is essential to consider Mach number as a more appropriate parameter than velocity. For hypersonic flows, additional considerations should be taken for the chemical state of the gas. It is because of the fact that the influence of compressibility is significant. Wind tunnels with Mach number range from 1 to 5 are classified as supersonic tunnels and those with Mach number more than 5 are termed as hypersonic tunnels.

5.1.1.CLASSIFICATION OF WIND TUNNELS:

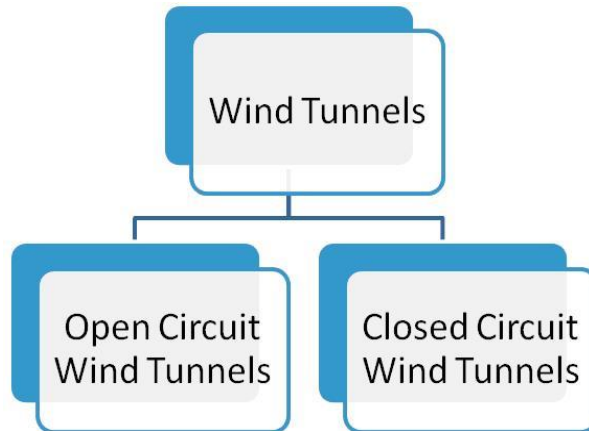


Fig. 5.1. Classification of wind tunnels.

5.1.1.2 HIGH SPEED WIND TUNNELS:

A high speed wind tunnels may be of open circuit type which draw air from outside atmosphere. Wind tunnels of closed circuit type re-circulate the inside air. Higher construction cost is one of the disadvantages of the closed circuit wind tunnel. These tunnels are generally used for continuous or long test durations. However, power required to run a supersonic wind tunnel is enormous and is proportional to the cube of the velocity. For this reason high speed wind tunnels of continuous running type are not generally preferred. Hence most of them operate intermittently either using high pressure tanks or vacuum tanks. The wind tunnels which use high pressure reservoirs are called as intermittent supersonic blowdown wind tunnels. Another way of achieving the huge power output is with the use of a vacuum storage tank. These tunnels are called Indraft or Induction supersonic wind tunnels. Following tree shows the types of intermittent wind tunnels.

5.1.1.3 CLASSIFICATION OF INTERMITTENT TUNNEL:

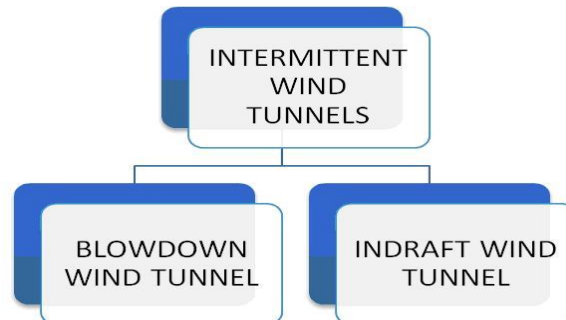
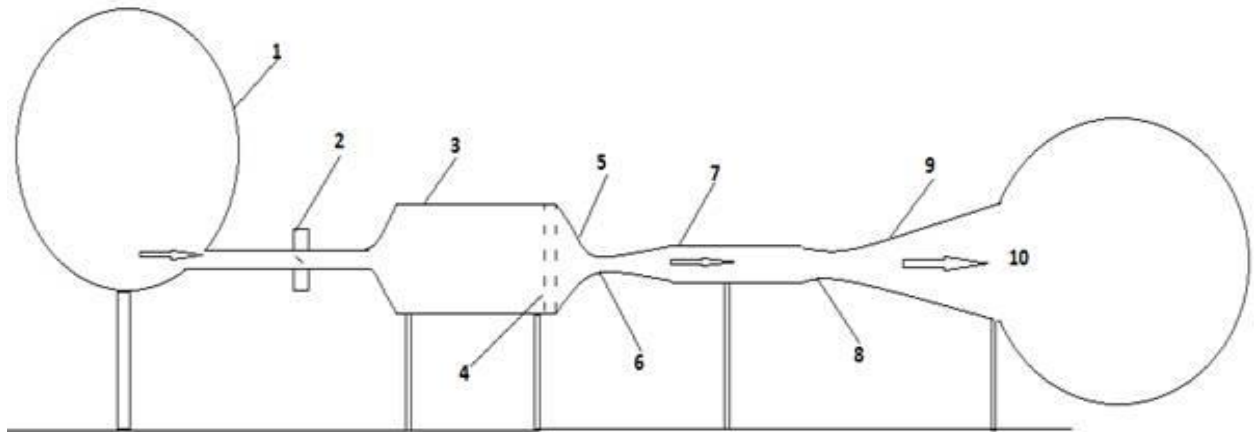


Fig. 5.2 Classification of Intermittent supersonic tunnel.

**5.1.2.BLOWDOWN TUNNEL:
Schematic of Blowdown Tunnel:**



- | | |
|------------------------------|-------------------------------|
| 1. High pressure air storage | 2. Pressure regulator |
| 3. Settling chamber | 4. Screens |
| 5. Nozzle | 6. Sonic throat |
| 7. Test-section | 8. Second throat |
| 9. Diffuser | 10. Low pressure air chamber. |

Fig. 5.3 Schematic diagram of blow down tunnel.

Tunnel Characteristics:

A schematic drawing of a blowdown wind tunnel with above parts is given in the figure. During operation of this blowdown tunnel, air taken from the atmosphere is compressed and stored in the high pressure air storage. Low pressure air chamber is then set with a specific lower pressure.

During the experiment, air flow from high pressure to low pressure end of the tunnel. Pressure regulator is installed to regulate the flow from reservoir to the settling chamber to maintain the desired constant pressure in the settling chamber.

Settling chamber acts as the constant high pressure reservoir during operation of the tunnel. The Mach number in the test section is therefore function of this driving pressure difference (difference between high pressure in settling chamber and low pressure air chamber).

Nozzle expands the air flow from the settling chamber and provides desired flow Mach number in to the test section where test models of interest are mounted with necessary instruments for various measurements. Second throat decelerates the air at the exit of the test section.

Blowdown tunnel circuit:

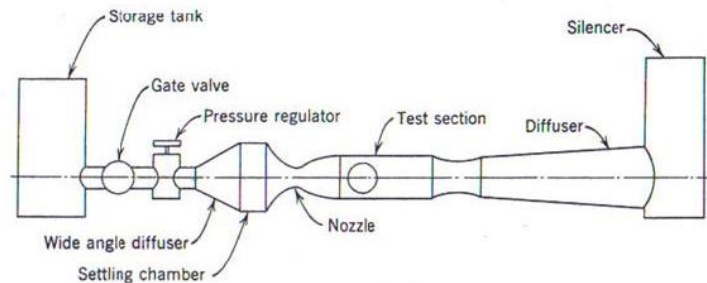


Fig. 5.4 Schematic diagram of Blowdown tunnel circuit.

Advantages and Disadvantages:

Duration of the experiments or test times are limited in blowdown wind tunnels. The blowdown tunnels have many advantages over continuous wind tunnels such as High Mach capability (up to $M=4$), easy tunnel "starting", large size test section, lower construction and operating costs, superior design for propulsion and smoke visualization. It is also important to note that there is no accumulation of exhaust products in an open tunnel. Limitations of the blowdown tunnels includes requirement of faster (often more expensive) instrumentation due to shorter test times, need for pressure regulator valves, noisy operation.

5.1.3. INDRAFT TUNNEL:

Indraft Tunnel circuit:

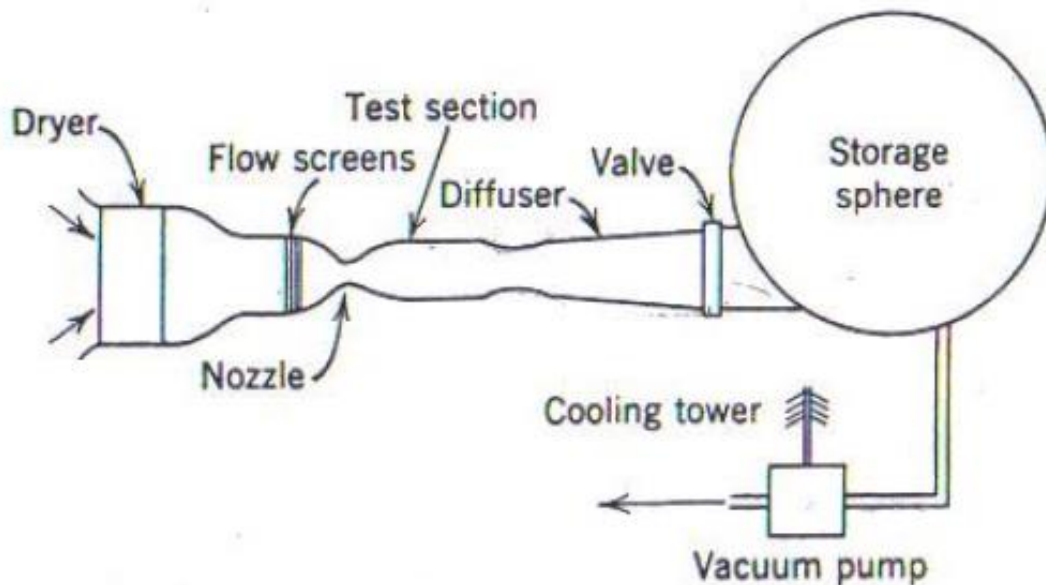


Fig. 5.4 Indraft tunnel circuit diagram.

Tunnel Characteristics:

- Intermittent indraft wind tunnels use the difference between a low pressure tank and the atmosphere to create a low.
- A vacuum tank is pumped down to a very low pressure, and the other end of the tunnel is open to the atmosphere. When the desired vacuum pressure is reached, a valve is opened, and air rushes from outside the tunnel, in through the test section, into the vacuum chamber.
- The end of the run occurs when the pressure differential is no longer great enough to drive the tunnel at the desired test section Mach number.
- One of the benefits of an indraft tunnel is that the **stagnation temperature can be considered constant throughout a run.**

Advantages:

- Additionally, the flow is free of contaminants from equipment used by other wind tunnel types. For example, there is **no need for the pressure regulators required by blowdown tunnels.**
- In comparison to other types of tunnels, indraft tunnels can operate at higher Mach numbers before a **heater is necessary to prevent flow liquefaction during expansion.**
- Lastly, using a vacuum is safer than using high pressures. High pressure tanks face the risk of exploding, while the **reversed pressure differential of a vacuum chamber only results in the risk of an implosion.**
- Indraft tunnels typically have nine major components: a vacuum tank, pump, test section, diffuser, settling chamber, nozzle, one or two valves (between the test section and tank), and a drier.

Disadvantages:

- One of the major disadvantages of indraft wind tunnels is that they can be up to four times as expensive as their blowdown counterparts. Additionally, the Reynolds number for a particular Mach number can be varied over a greater range with a blowdown tunnel. Finally, while indraft tunnels are capable of running without air driers, they may only do so up to Mach 1.6 without condensation. In order to address this problem, air can be slowly dried and stored in a ballonet over time, or it can be dried as it is used.

5.1.4. CONTINUOUS WIND TUNNEL:**Tunnel Characteristics:**

- Continuous wind tunnels are essentially a closed-circuit system and can be used to achieve a wide range of Mach numbers. They are designed so that the air that passes through the tunnel does not exhaust to the atmosphere; instead, it enters through a return passage and is cycled through the test section repeatedly as pictured in Figure.
- This type of wind tunnel is beneficial because the operator has more control of the conditions in the test section than with other approaches since the tunnel is cut off from the environmental conditions once running.
- In comparison to other wind tunnel types, continuous wind tunnels have superior flow quality due to the different facets of the tunnel's construction. The turning vanes in the corners and flow straighteners near the test section ensure that relatively uniform flow passes through the test section.

Continuous Tunnel Circuit:

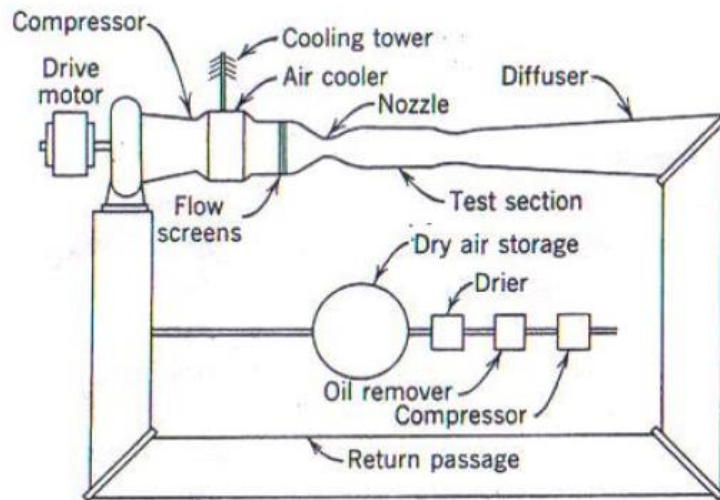


Fig. 5.5 Continuous Tunnel circuit.

Advantages & Disadvantages:

- Continuous tunnels also operate relatively quietly. Finally, the testing conditions can be held constant for extended periods of time, and the overall time for each run is typically longer than with other approaches. Unfortunately, some continuous tunnel designs require two or more hours to reach the desired pressure, and their construction is complicated and expensive.

5.2. CALIBRATION OF A TRANSONIC TUNNEL:

Introduction:

- Transonic wind tunnels operate in the range $0.5 < M < 1.4$ and have slotted or porous test-section walls.
- A plenum chamber surrounds the test section and the bleed-off air is either fed back into the stream at the downstream end of the test section or pumped externally to the tunnel.
- Stagnation pressures typically run from **15 to 50 lb/in.2 absolute**.
- The slotted walls yield almost no blocking, making it possible to run the tunnel right through sonic speed. The porous walls do this also and, in addition, greatly **diminish the reflection of shock or expansion waves**.
- **A model frontal area of 1% of the test-section area is customary.**

Calibration Steps:

- Setting of Mach number in a ventilated tunnel
- Measurement of total head
- Measurement of pitot pressure
- Measurement of Static pressure

- Measurement of temperature
- Determining the mach number and its distribution
- Determining flow angularity
- Determining the longitudinal static pressure gradient
- Determining turbulence
- Condensation of moisture
- Wave cancellation

SETTING MACH NUMBER IN A VENTILATED TUNNEL

Most ventilated tunnels set their Mach number by one of, or a combination of, six devices:

- (a) Changing the drive pressure ratio;
- (b) Changing the position of the ejector flaps (these guide the flow of the air bled through the ventilation back into the main stream) which, in turn, vary the amount of mass flow through the ventilated walls;
- (c) Changing the amount of air pumped out of the plenum chamber surrounding the test section through the use of auxiliary pumping;
- (d) Changing the area of a second throat, i.e., using a 'choke';
- (e) Changing the wall angle; this changes both the geometrical channel expansion and the flow through the ventilation;
- (f) Changing the contour of a flexible nozzle, or changing fixed supersonic nozzle blocks.

Almost any combination of the first four parameters may be employed to set a particular Mach number with sonic nozzle blocks, the choice being determined by a combination of which gives the best flow and which uses the least air. Since the ejectors influence the division of main stream and bleed-off air, a choke is not the unique determiner of Mach number that it is in a solid-wall tunnel. In some ventilated tunnels, the choke is mostly used in the range $0.7 < M < 1.1$. At the lower speeds, the pressure ratio is used to vary Mach number; at the higher ranges, the bleed-off (i.e., the flow expansion) has to be helped by pumping on the plenum chamber, or a nozzle change is made.

MEASURING TOTAL HEAD IN A TRANSONIC TUNNEL

Due to the loss that occurs through the shock wave which forms across the front face of a total-head tube, the total head is not directly measurable above $M = 1.0$, although losses are initially small, being only 0.1% at $M = 1.1$ and 0.3% at $M = 1.5$. It is the usual procedure to measure the total head in the settling chamber where the true value is available.

MEASURING PITOT PRESSURE IN A TRANSONIC TUNNEL

The pressure measured by an open-ended tube facing into the airstream is the total pressure, as long as the stream Mach number is less than 1.0. Above that value, a shock forms across the front of the tube and the reading then becomes 'pitot pressure', equivalent to the total pressure less the normal shock loss. In the transonic range, the pitot pressure is only slightly less than the total pressure. It is normally not used for Mach-number determinations, but may be measured for turbulence studies.

MEASURING STATIC PRESSURE IN A TRANSONIC TUNNEL

For nearsonic flow, the device of balancing stem and tip errors for a static probe useful in subsonic flow is more difficult in transonic flow. One may use long static probes, with the static holes 8 diameters back of a 10-degree included-angle conical nose (or 12.5 diameters back of a 6-diameter ogival nose), and 20 diameters ahead of the stem or support, but such probes are very long and flexible. The addition of a pitot orifice on such static probes does not hurt the static pressure reading. It has been found that a static pipe, reaching all the way into the settling chamber and having orifices along its side is very useful, as are wall pressures. The static pipe must be aligned with the airstream and have a smooth surface near its orifices. Since the static pipe is hard to move around, one almost never finds contour plots of test-section static pressure for a transonic tunnel.

MEASURING TEMPERATURE IN A TRANSONIC TUNNEL

It is pointed out that one cannot measure the stream static temperature directly because, as the air is slowed in the boundary layer on any measuring device, its temperature will rise towards the stagnation value. The answer is to reduce probe radiation and conduction losses in order to measure the true stagnation temperature and then, through the use of the energy equation, compute the stream static temperature. Another approach would be to use the settling-chamber stagnation temperature and the local Mach number (from the Mach-number calibration) to compute the stream static temperature. Should direct measurement of the stagnation temperature be desired, a single shielded unheated stagnation-temperature probe, for the moderate temperatures usually found in transonic tunnels, yield the stagnation temperature with very small error.

DETERMINING THE MACH NUMBER AND ITS DISTRIBUTION IN A TRANSONIC TUNNEL

The determination of the Mach number in a transonic stream is best accomplished through the use of the ratio of static to stagnation pressure. This is because the difference between stagnation and pitot pressures is too small for good accuracy and the angle of bow waves, when they exist, are not useful as accurate Indicators of Mach number. An added difficulty is that static pressure probes for the transonic range are very long and hard to use for calibration. The most satisfactory procedure is to use a tube sufficiently long that its upstream end is in the subsonic portion of the entrance cone where it can be supported, and its downstream end is somewhat downstream of the model location. Plush orifices are located about every 0.02 to 0.05 tunnel width, and their readings, along with the settling-chamber stagnation pressure, are used to compute the local Mach number. Mach numbers computed from wall pressure taps are also obtained. The calibration then consists of static-pipe and wall-pressure readings for a range of tunnel Mach numbers. Most of the time it is so difficult to locate the static pipe at other than the tunnel centerline that no further measurements are made. The assumption that no irregularities exist between centerline and wall is strengthened by the fact that most transonic tunnels have large contraction ratios and hence good flow. Difficulties with the flow-spreading wide-angle diffuser in an intermittent tunnel may add to calibration troubles. The specific calibration is accomplished by running the tunnel through a range of stagnation pressures and measuring the local centerline Mach number M , using the settling-chamber stagnation pressure, the static-pipe local static pressure.

DETERMINING THE FLOW ANGULARITY

The general yawmeters applies as well to transonic flow. The same simple shapes, which are calibrated by being rotated in a steady stream, work transonically too. The problem again is one of sensitivity, and the transonic calibration of two types of probes, both of which work well although having detached shock waves in the region near $M = 1$. Serious angularity troubles may arise from ventilated wind tunnels whose top and bottom plenum chambers are not connected together, and such designs should be avoided.

DETERMINING TURBULENCE IN A TRANSONIC TUNNEL

Both hot-wire anemometry and direct-pressure transducers may be used to determine the turbulence in a transonic tunnel. The hot-wire data in many cases have the advantage of being amenable to component separation. The direct-pressure work discussed below is simple and seems to yield a parameter of use. The technique is as follows: a transducer is mounted flush with the surface of a supporting structure (lead in pipes is

subject to organ piping) and normal to the stream. The data taken are then expressed as a fraction of the stagnation pressure. The variation in stagnation pressure runs as high as 3% of the settling-chamber value in some tunnels; 1% is believed to be a more desirable limit.

CONDENSATION OF MOISTURE

The condensation of moisture is that tunnel heating to moderate levels (say 150°F) usually suffices to reduce greatly or even eliminate condensation in the nearsonic range. This procedure becomes borderline in a transonic tunnel, and all variable-pressure transonic tunnels with which the author is familiar dry the air rather than depend on heating. Since dewpoints of around -40°F are obtainable with commercial equipment, it is suggested that this criterion be met if tunnel leakage does not present a problem. If it does, a comprehensive study of the errors due to varying amounts of moisture for the particular tunnel size and operating temperature must be made. Air-exchange tunnels do not have this ability, and the tunnel temperature must be permitted to rise.

WAVE CANCELLATION

Theory and experience have shown that optimum cancellation for particular shock strength occurs with a porous wall only when the proper plenum suction is matched with a particular wall deflection angle. If the wall convergence is too large, or if the suction is too low, shock-wave cancellation is reduced. If the convergence is too little, or if the suction is too high, a shock can be 'reflected' as an expansion wave. The normal measuring procedure is to use the pressure distribution over a body whose free-air distribution is known or calculable, and to note when excessive size starts to produce unacceptable changes. Cone-cylinders are frequently employed, say of 1/4%, 1/2% and 1% blockage. Sometimes an indication of proper wave cancellation may be obtained with a schlieren or shadowgraph system, although the difficulty here is that, as the cancellation gets better, the optical system becomes less effective.

5.3 CALIBRATION OF SUPERSONIC TUNNEL:

Supersonic wind tunnels are those which operate in the Mach-number range from 1.4 to around 5.0, usually having stagnation pressures from 14.7 to 300 lb/in.² abs. and stagnation temperatures from ambient to 250°F. For this range of Mach numbers, a tunnel requires a contoured nozzle to produce a uniform stream, and the test section usually has solid walls. Model frontal areas run from 4% to 10% (or more) of the test-section area.

In general, the supersonic tunnel is easier to calibrate than the transonic one because:

- (a) There are fewer variables (such as wall movement, changing bleed ratio, etc.);
- (b) There is less buffeting;
- (c) The dynamic pressures are usually no larger, making the instrument loads for the typically smaller tunnels easier to handle;
- (d) Interference is less, and calibration probes or rakes can be proportionately larger.

The flow in a supersonic tunnel is normally free of large-scale fluctuations. Severe unsteadiness from upstream is squeezed out by the large contraction ratio, and diffuser fluctuations are unable to proceed upstream against the supersonic velocity. Even in continuous-flow tunnels, the pressure recovery is so low that diffuser fluctuations rarely affect the compressors. High-frequency pressure fluctuations (mostly from the boundary layer) probably exist in all supersonic tunnels.

The calibration of a supersonic wind tunnel is complete when the following quantities are known:

- (a) The distribution of Mach number in the test section for each of the available speeds
- (b) The change of nominal Mach number with stagnation pressure

- (c) The flow angularity
- (d) The dryness needed for negligible measuring difficulties
- (e) The longitudinal static-pressure gradient
- (f) The turbulence level and cone-transition Reynolds number.

SETTING MACH NUMBER IN A SUPERSONIC TUNNEL

One does not adjust Mach number in a supersonic tunnel by changing drive-pressure ratio, as the test-section Mach number is determined by the nozzle-area ratio within the limitations of the small changes associated with changes in nozzle-boundary layer thickness (Reynolds number). The Mach number is hence 'set' by the tunnel geometry and turning on the drive. However, one is interested in knowing that the tunnel has 'started'. By that it is meant that the starting normal shock has passed through the test section and supersonic flow now exists. Starting is accompanied by a large drop in test-section static pressure and may be so noted from wall pressure taps or using a flow visualization system to see the shock system pass. Over a period of time, the tunnel operators learn to recognize a change in tunnel noise level associated with establishing flow or simply learn typical pressure or rpm settings which insure starting at a particular Mach number.

MEASURING TOTAL HEAD IN A SUPERSONIC TUNNEL

The total head cannot be measured directly in a supersonic stream since the probe itself has a shock wave at its nose which reduces the measured total pressure. The total head in the test section is the same as that in the settling chamber, where measurement requires a simple open-ended probe.

MEASURING PITOT PRESSURE IN A SUPERSONIC TUNNEL

The pitot pressure, for transonic conditions turns out to be a most valuable parameter for the calibration of supersonic tunnels and is almost exclusively used for Mach-number determinations. It is also used directly in pressure fluctuation measurements. Pitot tubes are both simple and error-free for the flow angularity normally found in supersonic tunnels. Tunnels operating at low stagnation pressures may fall into the range where, for very small pitot probes, viscous effects can result in errors in the pitot readings.

MEASURING STATIC PRESSURE IN A SUPERSONIC TUNNEL

The presence of a probe in a supersonic stream will, of course, result in a bow wave on its nose such that there will be a static-pressure rise effect on the forward part of the probe. Two approaches exist for getting around this effect. The first is to use the probe, which balances off the pressure rise with an expansion to end up with very small error in static pressure; the second is to make the bow shock so weak and so far from the static holes that its effect is negligible. Considering the first approach, Vaughn has developed a probe with a tapering body such that its rising pressure and that of the nose shock balances the under pressure aft of the conical nose. The result is an accurate probe of moderate length, suitable for wind tunnel or flight. The probe error in static pressure is a fraction of the static pressure and as a fraction of the dynamic pressure. One may use the calibration curves directly or the relation (based on the mean values) of

$$p = 0.992 p_m \text{ (accuracy of 0.008 } q)$$

or

$$p = p_m - 0.002 q \text{ (accuracy of 0.002 } q)$$

where p_m = measured pressure, p = true pressure.

This probe should not be used below $M = 1.1$, as the shock-wave build-up is then passing over the static orifices and errors of several percent of the static pressure then develop.

MEASURING TEMPERATURE IN A SUPERSONIC TUNNEL

The measurement of temperatures in an airstream is that stream temperature cannot easily be measured due to the boundary layer temperature which arises, but that the stagnation temperature can be measured to an

excellent degree of accuracy. Single-shielded probes will give recovery factors of 0.997 for the range of Mach numbers and stagnation temperatures usually found in supersonic tunnels. It is not customary to make either settling-chamber or test-section temperature surveys in supersonic tunnels, although it certainly would not hurt. The point is that, for moderate temperatures, very small heat loss will occur, and the gradients are rarely serious. Should a check run reveal gradations, (1) the cooler should be appropriately adjusted or (2) the settling-chamber size should be reduced to reduce free convection through an increase in stream speed. Stagnation temperatures should be read at several axial stations approaching the nozzle throat. The value at the throat (measured or extrapolated) may be taken as the test-section stagnation value.

DETERMINING THE MACH NUMBER AND ITS DISTRIBUTION IN A SUPERSONIC TUNNEL

Mach number, being the ratio of the stream velocity to the local speed of sound, is not measured directly but may be computed from flow conditions which depend on it. Five procedures are in common use. These involve the determination of:

- (a) The ratio of settling-chamber stagnation pressure to test-section pitot pressure;
- (b) The ratio of settling-chamber stagnation pressure to test-section static pressure;
- (c) The ratio of test-section pitot pressure to test section static pressure;
- (d) The ratio of some body-surface pressure to stagnation pressure;
- (e) The wave angle off some body whose dimensions are known - usually a wedge or cone.

(a) Mach Number from Pitot to Stagnation-Pressure Ratio

The Mach number in a supersonic tunnel may be determined most accurately above a Mach number of about 1.6 by measuring the pitot pressure in the test section and the stagnation pressure in the settling chamber, computing their ratio, and determining the Mach number by the normal shock relation.

The pitot tubes are squared-off open-ended tubes which have negligible errors as long as the flow angularity is small - less than a degree or so.

The Mach number is then computed from

$$s_2 - s_1 = c_p \ln \frac{T_2}{T_1} - R \ln \frac{p_2}{p_1}$$

$$\text{but } s_2 - s_1 = R \ln \frac{p_{01}}{p_{02}}$$

where $\frac{T_2}{T_1}$ & $\frac{p_2}{p_1}$ are static pressure ratios of normal shock can be substituted to get

$$\frac{p_{02}}{p_{01}} = \left[\frac{(\gamma + 1)M_1^2}{(\gamma - 1)M_1^2 + 2} \right]^{\frac{\gamma}{\gamma - 1}} \left[\frac{\gamma + 1}{2\gamma M_1^2 - (\gamma - 1)} \right]^{\frac{1}{\gamma - 1}}$$

Which simplifies for $\gamma=1.4$,

$$\frac{p_{02}}{p_{01}} = \left[\frac{6M_1^2}{M_1^2 + 5} \right]^{\frac{7}{2}} \left[\frac{6}{7M_1^2 - 1} \right]^{\frac{5}{2}}$$

Below $M = 1.6$, the difference between pitot pressure and stagnation pressure becomes increasingly small (it is zero at $M = 1.0$) an error in pressure reading becomes a large percent of the ratio which, in turn, produces a large-error Mach number. The ratio of stagnation to static pressure is still large in this region and reading errors have less effect.

(b) Mach Number from Static to Stagnation - Pressure Ratio

Using the local static pressure, as measured with one of the static probes and making the good assumption that the test-section stagnation pressure is the same as that in the settling chamber; the local Mach number may be computed from Equation below. Equation is also used for computing Mach numbers from wall or nozzle orifices.

$$M = \sqrt{\frac{2}{\gamma - 1} \left[\left(\frac{p_0}{p} \right)^{\frac{\gamma - 1}{\gamma}} - 1 \right]}$$

(C) Mach Number from Static to Pitot - Pressure Ratios

Equation of static to stagnation pressure may be divided by Equation of stagnation pressure ratios to yield a relation for obtaining the Mach number from the test section static pressure p and the test section pitot pressure p_0 :

$$\frac{p}{p_{02}} = \frac{\left[\frac{2\gamma M_1^2 - (\gamma - 1)}{(\gamma + 1)} \right]^{\frac{1}{\gamma - 1}}}{\left[\frac{\gamma + 1}{2} M_1^2 \right]^{\frac{\gamma}{\gamma - 1}}}$$

(d) Mach Number from Body Surface Pressures

The body surface pressures from almost any body amenable to theory may be used along with the settling-chamber stagnation pressure to determine the Mach number. The difficulties of such a system include possible model inaccuracies and certain boundary-layer effects. The method of reducing the data from a 40-degree included-angle cone having a total-head orifice in its nose and four static-pressure orifices 90 degrees apart on its surface. It should be noted that the presence of a total-head orifice in the nose of a cone affects its conic flow, the static pressures then reading as if the cone angle were slightly enlarged. If a 'pressure' wedge is employed it is interesting to note that the free-stream Mach number may be obtained from the tables in the literature more accurately than by using the customary flow charts. The procedure is as follows, assuming that the stagnation pressure, the wedge surface pressure and the wedge semi-angle are known:

- (1) Compute p_2/p_{02}
- (2) Estimate the stream Mach number, M , and, from oblique shock tables using M and Θ find the shock angle, β
- (3) Compute the normal Mach number, $M_N = M \sin \beta$
- (4) Read the static pressure ratio for a normal shock at M_N . p_2/p_1
- (5) Read the isentropic expansion for M , p_1/p_{01} .
- (6) Compute

$$\frac{p_2}{p_{01}} = \frac{p_2}{p_1} \times \frac{p_1}{p_{01}}$$

- (7) Iterate the estimation of Mach number until the computed pressure ratio equals the measured one.

The above procedure, in a typical calibration, is made easier by the fact that M_1 will not vary much and will be known to a fair degree of accuracy from the tunnel design.

(e) Mach Number from Wave Angles

The local Mach number may be determined by measuring the wave angle off a body of known dimensions from shadowgraph or schlieren photographs and reading the corresponding Mach number from tables of supersonic flow. This method is frequently used for quick and not-too-accurate values, but suffers from three substantial inaccuracies:

- (1) The wave angle is hard to measure with a high degree of accuracy;
- (2) Any picture is probably an average value across the test section, or, putting it differently, using wave angles over any reasonable distance assumes that the Mach number is uniform;
- (3) Some optical distortion results from the three-dimensional density changes accompanying cone flow. The wedge or cone employed to produce the wave to be measured will have a boundary layer on it, and hence should have an angle equal to the rate of growth of the boundary layer displacement thickness added to the body

angle. If there is not time to determine this, adding 0.2° for a laminar-flow displacement thickness would be a good approximation for each side of a wedge.

DETERMINING THE FLOW ANGULARITY

The principles of yawmeters for measuring the flow angularity in a subsonic wind tunnel apply to supersonic tunnels as well as to subsonic ones. Usually one finds 90-degree included-angle cones used instead of spheres or bent tubes. The use of an 8-degree included-angle wedge is reported. The rise of pressure differential is such that the sensitivity of an 8-degree included-angle wedge is roughly the same as that for a 30-degree included-angle cone in the range $2.5 < M < 5$. Pressure differentials per degree of misalignment for several cones and a wedge are measured. The work-up of cone pressures for a 40-degree included angle cone is to determine the flow angularity. The use of a telescope to measure wedge angles (accuracy $\pm 0.05^\circ$), and notes that shock waves crossing the orifices do not seem to affect the calibration linearity. The readings are taken with the yawmeter both normal and inverted, the midpoint between the two runs indicating the true flow direction. Due to the peculiarities of supersonic flow, the angularity on the test-section centerline is apt to be better than off it. Angularities in a supersonic stream are associated with changes in Mach number. It follows, then, that a tunnel with very small Mach-number variation will also have small angularities. A very acceptable flow variation of less than $\pm 0.1^\circ$ is possible. Many tunnels have as much as $\pm 0.5^\circ$, believed to be close to the maximum variation permissible for high-quality work.

COMBINED INSTRUMENTS AND RAKES

A total-head opening may be added to the front of a pressure cone to make a combined Mach number and angularity head, with a resulting saving in runs needed to calibrate a tunnel. One may also make a rake of such heads to essentially calibrate a whole cross section simultaneously. The difficulties associated with such combined heads include the boundary-layer troubles, and the added possibility of choking the tunnel. Using a rake of total-head tubes is just as accurate as using one probe and moving it around the test section.

DETERMINING THE LONGITUDINAL STATIC PRESSURE GRADIENT

In some supersonic tunnels, the longitudinal static-pressure gradient is large enough for corrections for buoyancy to have to be applied to the data. The longitudinal static-pressure gradient is usually obtained from the Mach-number distribution and the total pressure.

DETERMINING TURBULENCE IN A SUPERSONIC WIND TUNNEL

Measurements with a hot-wire anemometer demonstrate that there are high-frequency fluctuations in the airstream of supersonic tunnels that do not occur in free air. These fluctuations, broadly grouped under the heading of 'turbulence', consist of small oscillations in velocity, stream temperature (entropy), and static pressure (sound). Values from one tunnel are given

Turbulence in Settling Chamber and Test Section of a Supersonic Tunnel

	S e t t l i n g chamber	T e s t section
Mach number	All	2.2 4.5
Sound, Dpt/pt	less than 0.1%	0.2 1%
Entropy, DTt/Tt	less than 0.1%	less than 0.1%
Vorticity, Dv/V	0.5 to 1%	less than 0.1%

The fluctuations arise from a variety of causes, mostly from the drive system, the radiator, and the test-section boundary layer. Velocity fluctuations emanating from upstream causes may be reduced at low and moderate Mach numbers by the addition of screens in the settling chamber. At high Mach numbers, upstream pressure and velocity effects are usually less, since the large nozzle contraction ratios damp them out.

Temperature fluctuations are unaffected by the contraction ratio. The existence of such fluctuations is, of course, of less interest than their effect. Here the calibration procedure has been to determine the transition Reynolds number on smooth 5- or 10-degree (included-angle) cones and to compare this with other tunnels. The procedure, described below, yields the fact that transition Reynolds number may vary in an unpredictable manner in a particular tunnel although, in general, there seems to be a general decrease with increasing Mach number.

In general, the procedure is to measure the transition Reynolds numbers with a transition cone over the range of the tunnel Mach numbers, Reynolds numbers, and drive combinations, and to compare the data with those from other tunnels. A decision may then be made as to whether or not additional screens or other tunnel alterations are called for. These steps are described below.

(a) The Transition Cone

By common usage, transition cones have either a 5- or 10-degree included angle, and transition is determined by optical methods, pitot pressure at a constant distance from the surface, cone surface temperatures, hot-wire surveys in the boundary layer, boundary-layer thickness measurements, or evaporation techniques.

In general, their size should be selected so that a local Reynolds number of from 2 to 7 x 10⁶ can occur on the surface. Minimum heat-sink capacity and extreme surface smoothness are essential.

The cone was hollow and constructed of fiberglass, except for a steel tip and a short micarta section back of the tip. Thirty copper constantan thermocouples were located in the surface at 2-centimeter intervals. (Unless the cone transition number can be pretty well estimated, there does not seem to be much reason to group the thermocouples more closely in any particular region).

The finished surface was obtained by applying several coats of a W.P.Fuller product known as 'Fullerplast' , machining the surface to a true conical shape, and polishing with a thin coat of wax. A heating coil was applied to the cone-support sting to reduce heat losses through the sting mount, since the sting would normally take longer to heat up than the cone.

(b) Testing Procedure

The transition cone is first calibrated in an oven to ascertain that the thermocouples are working and that their readings agree. It is next mounted in the wind tunnel and runs made for the range of Mach numbers and Reynolds numbers of which the tunnel is capable. If alternative tunnel-drive combinations are available, they should be measured too. It should also be noted that transition can be caused by shock waves, thus leading to completely erroneous data. The existence of shock waves can be determined either by using an optical device or by placing the cone in another location. The change of transition Reynolds number from one point to another in a particular test section does not appear to be enough to justify such tests according to Franklin.

(c) Use of the Data

The thermocouple readings from a run may be plotted directly against local Reynolds number or converted into a 'recovery factor' using the stream and stagnation temperatures. The stream temperature is obtained from the stagnation temperature and the Mach number of the free stream. The recovery factor, Rx, is defined as

$$R_x = \frac{T_{aw} - T}{T_t - T}$$

where T_{aw} - adiabatic wall temperature, °R

T_t = stream stagnation temperature, °R

T = stream static temperature, °R

A plot of the data from a typical run will appear. There is first a laminar flow recovery value of around 0.85, then a transition to a maximum value, and finally a fall-off to the turbulent value. The determination of the transition 'point' is shown on the Figure. It should also be noted that complete agreement as to the 'length' to use in computing the Reynolds number has not been reached. Some researchers use the end of the sharp rise in recovery factor, rather than the transition 'point'. Others use the start of boundary-layer thickening. The variation in methods can result in a variation of one to two million in Reynolds numbers and should be watched for.

(d) Hot-Wire Anemometry

While the above sections have dealt with determining the effect of turbulence, direct measurement of the type, frequency and magnitude can lead to a better understanding of the fluctuations and possibly to their reduction if advisable. As is well known, the hot-wire anemometer is a device through which this may be accomplished. Basically, the system makes use of the varying electrical currents which occur in an electrically heated wire of small heat capacity when it is exposed to an oscillating airstream. This technique was developed for use in low-speed tunnels and was initially unavailable to supersonic researchers due to wire breakage, but increased wire strength, better removal of dust particles in the airstream, and the technique of translating the wire into the boundary layer to reduce starting loads on it have extended its use into the supersonic range.

DETERMINING TEST-SECTION NOISE

The contribution of the pressure fluctuations due to wavelets from the boundary layer (called 'noise') may be determined through hot-wire measurements in the test section. The first step is to measure the fluctuations of temperature, velocity and pressure in the settling chamber. It is necessary that the temperature variations be small, and that the velocity variation be small enough not to mask the boundary-layer effects after passing through the contraction.

CONDENSATION OF MOISTURE

The discussion of condensation of moisture in an airstream is pointed out that the expansion of the air as it proceeds to higher Mach numbers produces a drop in temperature which, in turn, lessens the air's ability to hold moisture. The moisture present then condenses out, leaving the airstream hotter and with discrete droplets in it. The hotter air is then at a lower Mach number and higher static pressure. To confuse the data further, there may be local areas in which condensation exists or re-evaporation can occur locally as the air changes speed near the model being tested. Since condensation effects at a particular Mach number are a function of stagnation temperature, stagnation pressure and specific humidity, and tunnel size, one cannot present typical condensation effects to be expected.

5.4 HELIUM AND GUN TUNNELS:

A gas gun differs from a conventional powder gun in that the energy required to accelerate the projectile is derived from a compressed gas reservoir rather than the combustion of a propellant charge. Quantitative studies of the gas gun (e.g. Seigel, 1965) have shown that reducing the molecular weight of the propelling gas can increase projectile muzzle velocity. This is because the gas must accelerate itself along with the projectile. In fact, a simple analysis (Seigel, 1965) will show that the maximum theoretical muzzle velocity is directly related to the speed of sound in the driving chamber,

$$u_{p \max} = \frac{2}{\gamma - 1} a_o$$

Hence by reducing the molecular weight, the speed of sound increases and a higher muzzle velocity is achieved. Further increases in muzzle velocity can be realised by heating the driving gas. Many different methods can be used to heat the driver gas, such as combustion, arc heating or detonation. In the two-stage light gas gun, the driving gas is heated by free-piston compression in a tube mounted upstream of the barrel. Free-piston compression has been used extensively for propellant gas heating (Charters, 1987, Stilp, 1987) and also successfully for driving shock waves in hypervelocity shock tunnels (Stalker, 1967) and expansion tubes (Doolan and Morgan, 1999).

The two stages of operation are illustrated in the schematic shown in Fig. 1. The first stage uses a compressed air reservoir to propel a piston into a tube that contains a light driver gas such as helium. The piston is of sufficient mass so that the helium compression is achieved at a relatively slow rate for the driver gas to be compressed polytropically with no shock wave formation. The piston compresses the gas 40 to 100 times smaller than its initial volume. This process creates very high temperatures. The second stage begins when the driver gas reaches the desired driving pressure. At this point, a diaphragm bursts, allowing the driver gas to accelerate the projectile to high velocity.

The performance increase by using compressive heating can be better understood through the results of a simple analysis. If ideal gas behaviour is assumed, the pressure-volume relationship can be described by,

$$p_1 V_1^\gamma = p_2 V_2^\gamma \quad (2)$$

$$p = \rho RT \quad (3)$$

The compression ratio of the driver gas can be defined as the ratio of the initial and final volumes,

$$\lambda = V_1 / V_2 \quad (4)$$

Combining equations (2), (3) and (4) and assuming the speed of sound is related to the root of the temperature,

$$\frac{a_2}{a_1} = \lambda^{\frac{\gamma-1}{2}} \quad (5)$$

Equation (5) gives the theoretical speed of sound increase in the driver gas for a given compression ratio and is plotted in Fig. 2 for monatomic and diatomic driver gases. Figure 2 indicates that considerable increases in sound speed can be achieved and therefore higher muzzle velocities can be obtained (Equation (1)) by using the free piston compression technique. It should also be noted that the free-piston compressor is a convenient way of achieving the high pressures required to launch the projectiles. It would be considerably more difficult to construct apparatus based on conventional pumps and compressors to achieve and store the high pressures required for hypervelocity launch.

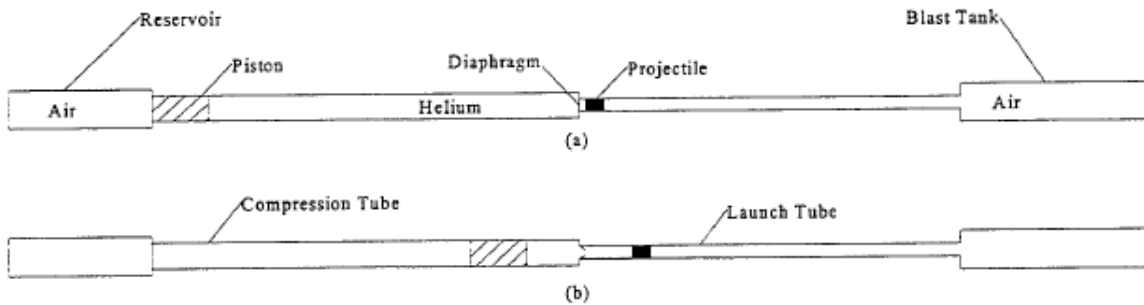


Figure 1. Schematic of two-stage light gas gun operation; (a) Initial state before shot; (b) Piston compresses helium to high pressure, bursts diaphragm and launches projectile.

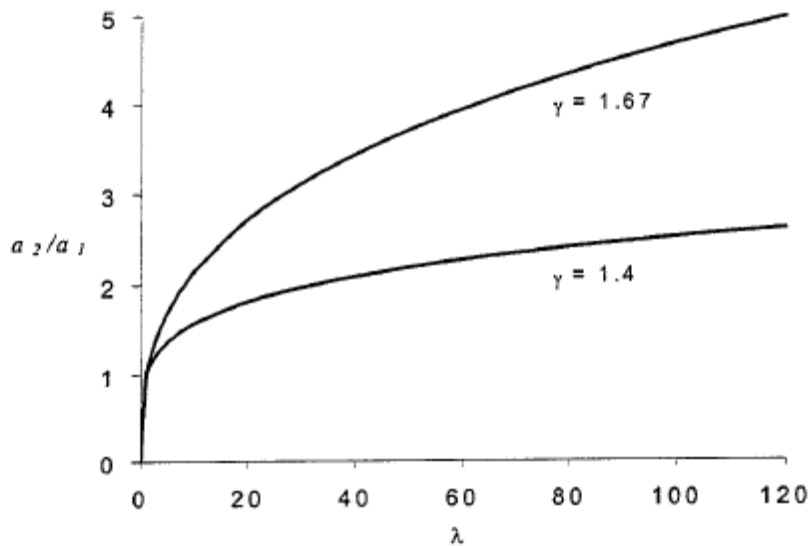


Figure 2. Theoretical speed of sound increase due to piston compression.

The free-piston compressor design used here differs from conventional two-stage light gas guns. In very high performance guns, a deformable piston is used in the breech in order to maintain a high pressure behind the projectile. The piston has a high residual velocity after the projectile is launched and is typically allowed to extrude into a specially designed internal cavity within the breech. Although this design is very successful in attaining high muzzle velocities (up to 12 kms⁻¹), it is an expensive and time consuming process to extract and fabricate pistons for each shot. In the present configuration operation and costs are improved by using a fully

reusable piston. Final muzzle velocities are somewhat lower, however performance can be optimized by proper selection of operating conditions to 'tune' the piston motion. By selecting the right combination of reservoir and driver fill pressures along with diaphragm burst pressure and projectile mass, maximum muzzle velocity can be obtained with minimal Residual piston velocity at the end of its stroke. Performance can be predicted using analytical and numerical techniques. Section 4 summarizes a quasi-one-dimensional numerical technique, which is used to analyze the two-stage light gas gun facility.

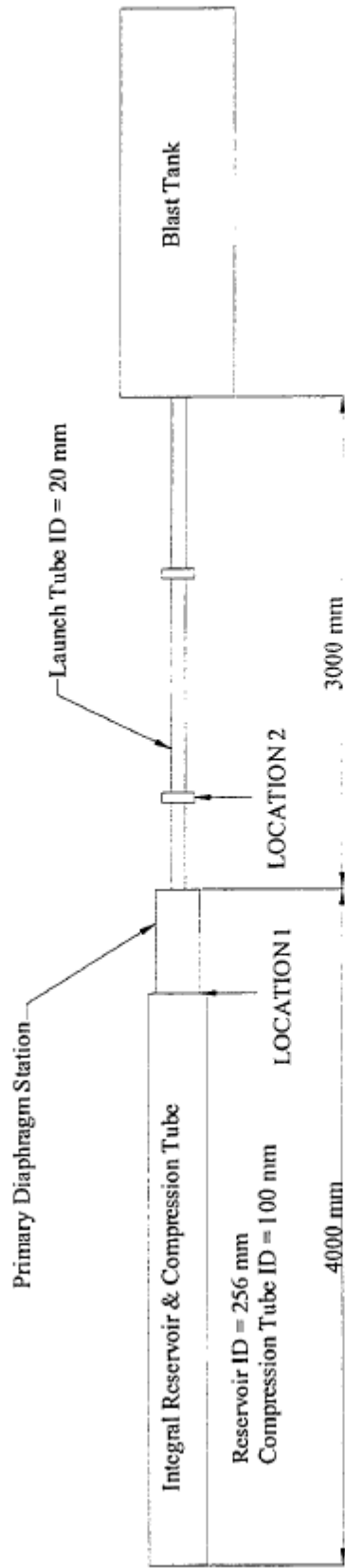


Figure 3. Schematic of the two-stage light gas gun.

5.5. FLOW VISUALIZATION

INTRODUCTION:

Visualization is essential for exploring, and understanding fluid behavior and can be both qualitative and quantitative. The flows described in the first part of this article were considered as incompressible flows with a constant, uniform density. The other group of flows, i.e. compressible flows have variable density which depends on flow velocity. The optical index of refraction $n(x,y,z)$ of a gas is a function of the gas density. For practical purposes, the density difference of 2% can be considered as an appropriate limit between incompressible and compressible flows. This occurs if $M_\infty > 0.2$.

Rapid advances during the past decades concerning issues associated with high speed flights have brought into focus the need for competent treatment of the fundamental aspects of aerodynamics and the need for application of basic sciences in solving practical problems. The different physical methods and techniques are employed to measure density, pressure, velocity and temperature in gas dynamics. The main methods for visualization of these flows are optical methods. The three principal optical methods are: **shadow, schlieren and interferometry**. The optical flow visualization has been expanded due to the innovation of the optical laser. Laser light is highly monochromatic and coherent with high-energy concentration. The laser light sources have successfully been used in conventional optical visualization systems, but they have led to the development of completely new methods. The lasers are attractive as light sources especially for interferometer.

Compressible air field as an optical object

Airflow around aerodynamical models is a very complex phenomenon. In optical sense, this flow field is a transparent environment with a complex light refraction index. The light refraction index in each flow field point is the function of air density in that point, which, on the other side, is the function of speed, pressure and air temperature. The relation between air density $\rho(x,y,z)$ and the refraction index $n(x,y,z)$ is called the Gladstone-Dale equation: $n = 1 + K\rho$. The Gladstone-Dale constant K has a value of ρ^{-1} and is different for each gas. The Refractive index for gas, which is a mixture of several components e.g. air, eq. (1) becomes: $n = 1 + \sum K_i \rho_i$. The Gladstone-Dale constant for air at a temperature of 288 K varies between $2.239 \cdot 10^{-4}$ to $2.33 \cdot 10^{-4}$ m³/kg.

According to Snell's law, a light ray, passing through a nonhomogeneous refracted field, is deflected from its original direction and a light path is different from that of an undisturbed ray. If a recording plane is placed in front of the light ray, after disturbing media, three quantities can be measured: the vertical displacement of the disturbed ray, the angular deflection of the disturbed ray with respect to the undisturbed one and the retardation of the deflected ray, i.e. the phase shift between both rays, owing to their different optical path lengths. Optical visualization methods are based on the recording of one of these three quantities (or a combination of them). The shadowgraph is used for the first phenomenon, the Schlieren method is used for the second one and interferometry for the last one.

There are significant differences between these methods, since the shadowgraph is sensitive to the changes of the density second derivative (or the refractive index) second derivative $\partial^2 n / \partial^2 y$, the Schlieren method is sensitive to the changes of the density first derivative $\partial n / \partial y$, and interferometry is capable to measure absolute density n changes. If, using an optical method, the light refraction index $n(x,y,z)$ in flow field is determined, other physical parameters of tested environment, significant for aerodynamic testing, can be indirectly determined as well.

5.5.1 SHADOWGRAPH METHOD

The oldest and the simplest of all optical methods for flow visualization is the shadowgraph. Fig.1 shows a typical setup for shadow methods. A light beam passing through the wind tunnel test section is parallel. A spherical mirror or lens makes the light parallel. The light source should be small to ensure good sharpness of

the obtained image. Observation and recording the deflected beam parts are in the perpendicular plane screen at a distance of l from the test section.

If the test section is large, the recording is impossible without focusing the image onto the film. For this purpose it is preferable to use a second spherical mirror (or lens). The camera lens in that case is placed in the focal plane of the second mirror. The recorded shadowgraph is linearly reduced, but it is identical with that obtained by the arrangement presented in Fig.1.

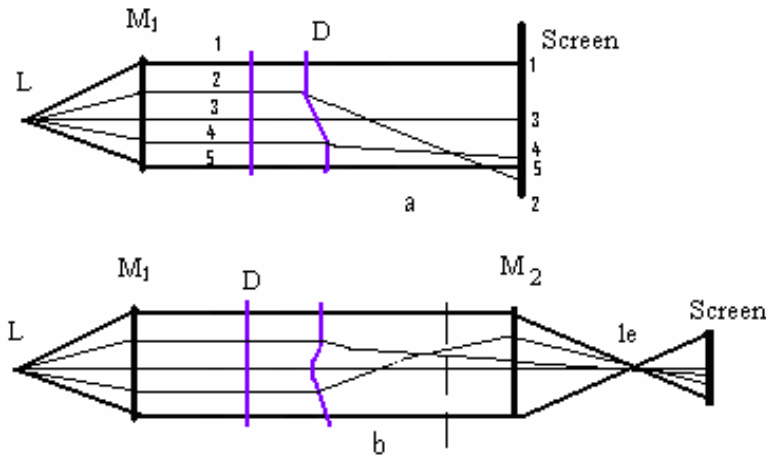


Figure 5.9 . Schematic arrangement of the shadowgraph system, deflection of light rays in a field of the variable $\partial^2 n / \partial^2 y$

To understanding the shadow image, it is useful to analyze the paths of three rays in the section where there are parts with a different amount of $\partial^2 n / \partial^2 y$ (Fig.1). If ray 2 passes through the section with a higher value of $\partial^2 n / \partial^2 y$ then along two other ray, 2 will be deflected to a great extent, so ray 5 on the photographic plate or screen will fall between ray 4 and 2. A darker region appears therefore on the screen between ray 1 and 3 - it represents the shadow of the disturbance through which ray 2 has passed. The uniform illumination of the screen is destroyed.

The investigation of these intensity alterations gives a lot of useful information about the flow field. A shock wave and turbulent motion in a compressible flow can be detected and recorded with a shadowgraph. Fig.5.10 a shows the bow shock wave ahead of a sphere in the wind tunnel T-36 at $M_\infty = 1.86$. The trace of the shock wave in the photo is a band of absolute darkness bounded on the downstream side by an edge of intense brightness. The exact geometrical position of the shock front is the other edge of the dark zone. Diffraction effects are visible on the bright edge of the shadow because the shock wave represents a jump of the refractive index and because of low gas density in the free stream. The air density increases after the shock and the incident ray deviates to the inside edge. It is an analog result to that obtained with a convex lens.

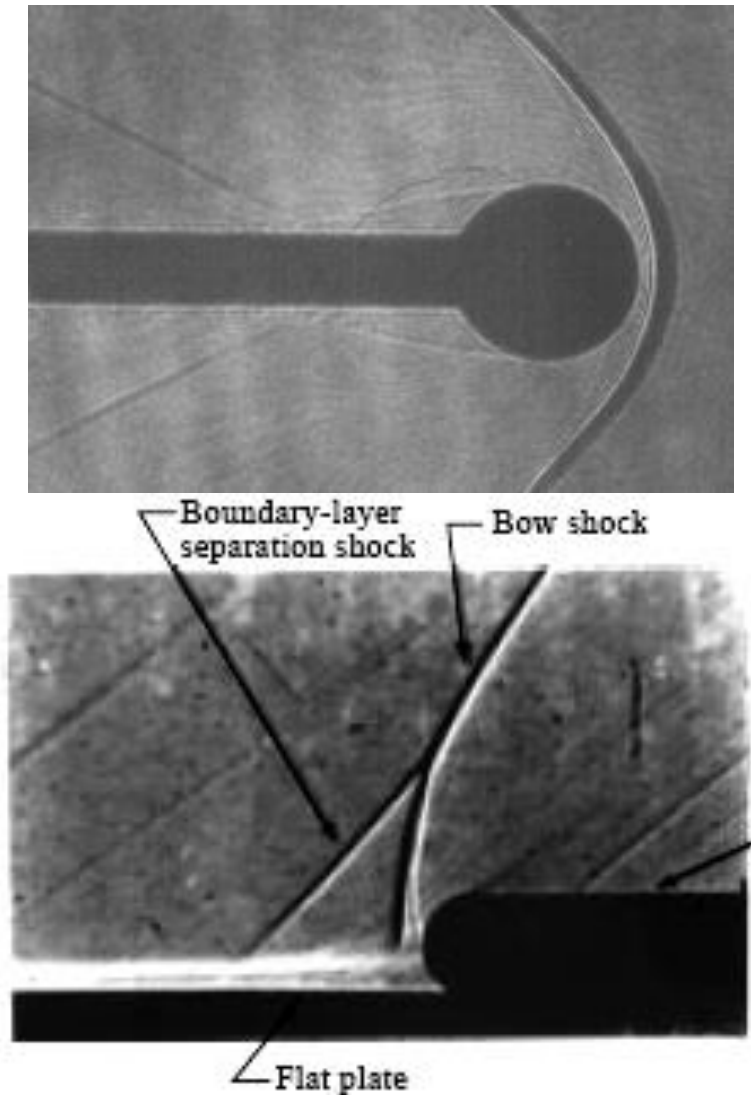


Figure 5.10. Shadowgraph visualization around a sphere (a), and typical shadowgraph images showing the spherical tipped cylinder mounted on the flat plate (b)

Since the density in the disturbance is lower than in the surrounding field, (Prandtl-Meyer expansion fan at the sharp end of the nozzle) the bright band appears at the beginning of the shadow. The same result is obtained when the compressible boundary layers is visualized. Its effect on a light ray can be compared with the effect of a concave lens. Fig.5.10b is a typical shadowgraph showing the flow around the spherical tipped cylinder mounted on the flat plate.

Shadowgraph methods with short duration light pulses can be used for fine visualization of turbulent compressible flows.

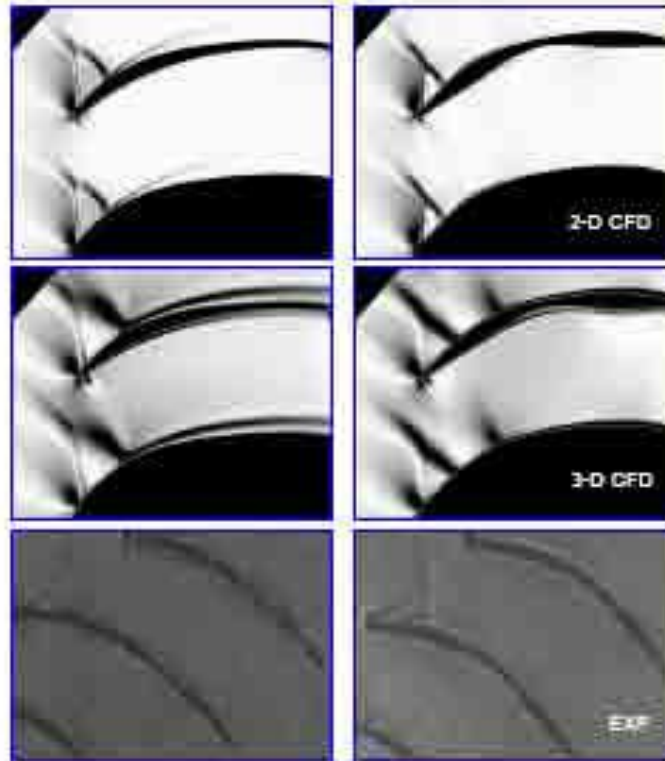


Figure 5.11. Numerical and experimental shadowgraph visualization of the supercritical cascade flow $M_\infty=0.87$

The shadow performances can be illustrated by Fig.3. The blade performances were experimentally confirmed in the Virginia Tech High Speed Cascade Wind Tunnel. The numerical and experimental methods were performed to reveal the associated flow physics, particularly the loss mechanisms. Flow diagnostic techniques such as blade surface pressure measurement, blade surface oil flow visualization, and shadowgraph were used in the experiments to study the pressure/velocity distribution, shock pattern and boundary layer behavior.

5.5.2 SCHLIEREN METHOD

As mentioned before, the Schlieren method is sensitive to the changes of the first derivative of density (or refractive index) and it can record the angular deflection of the disturbed ray with respect to the undisturbed in a transparent medium with local non homogeneities. Today the Schlieren method is the most frequently used in aerodynamic laboratories, since it is relatively simple and very useful.

If a parallel beam of light passes through the air where there is a density gradient normal to the beam direction, the light travels more slowly where the density is greater and the beam is refracted towards the region of greater density. The most simple one is the Schlieren system with parallel light through the wind tunnel test section. In practice there are different systems with lenses or mirrors.

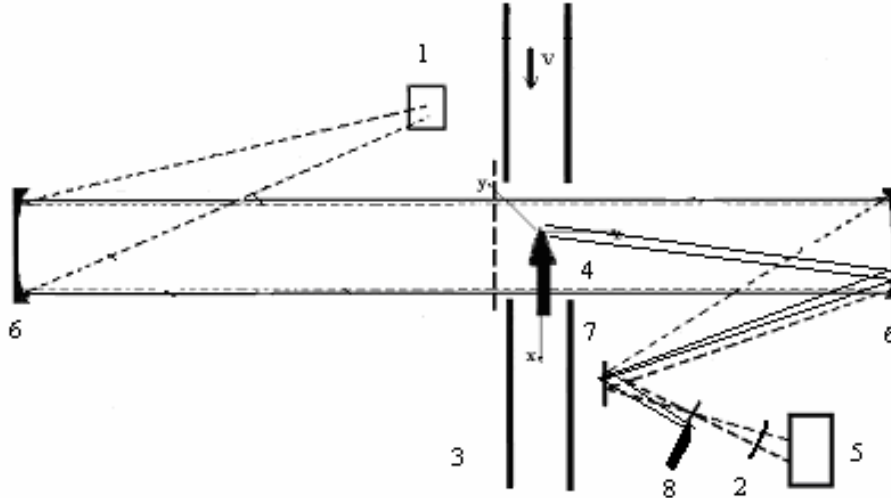


Figure 5.12. Töepler schlieren system

Töepler system as the base of all other modified systems is illustrated in Fig.3. The detailed description of the system is given. Today many different systems are used, e.g.: Schlieren system with finite slit, with lens for projection, double lens system, single mirror system, system with two mirrors, plane concave mirror system and Twin mirror, (asymmetric twin mirror system) ,etc.

The new dimension has been introduced into the schlieren system replacing the knife-edge by a filter consisting of several parallel, transparent, colored strips (most often three colored sheets, red - blue - yellow or blue - green - red). The color filter can be consist of four differently colored strips arranged in a square filter to visualize the grad n in two directions. If the flow is axisymmetric, complementary colors appear for the same event (compression or expansion) above and below the flow axis. The recorded pure colors and color combinations are a measure for the local direction of density gradient in the test section. A contemporary modification of the schlieren system concerns the replacement of the knife-edge by optical elements which influence somehow the phase of the schlieren light beam. Fig.4 shows scheme of töepler Schlieren system.

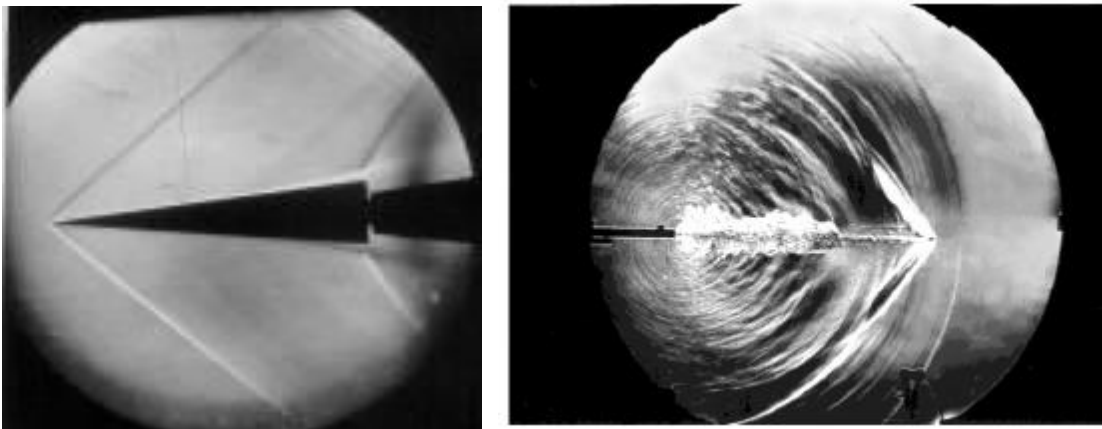


Figure 5.13. Black and white schlieren photos obtained in the T-36 wind tunnel for $M_\infty = 1.56$ (a) and instantaneous image of Bullet and Muzzle Blast from a 22-Caliber Rifle (b)

Fig.5 shows the parts of schlieren systems in the T- 34 hypersonic wind tunnels in the MTI. Figures 6 and 7 illustrate schlieren effects recorded with the schlieren system with the knife edge (black and white schlieren). In order to investigate the interaction between the boundary layer on the injector plate and the jet, a

transverse sonic jet was injected into a supersonic cross flow (Mach 1.7) [16]. Fig.7a. shows a typical result of schlieren flow visualization. The jet expansion led to the barrel shock and the Mach disk shown in Fig.7a.

On the other hand, the injectant jet caused interaction phenomena between the cross flow and the jet itself. In other words, the jet acted on the cross flow as an obstruction. The schematic of the flow field obtained from the schlieren photograph is shown in Fig.7b. Attempts to increase the amount of information extractable from the schlieren photography have led to the use of various opaque filter geometries other than a knifeedge as well as of transparent phase and color filters A combined holographic interferometer and Schlieren device, has been designed, made and tested for the T-38 trisonic wind tunnel.

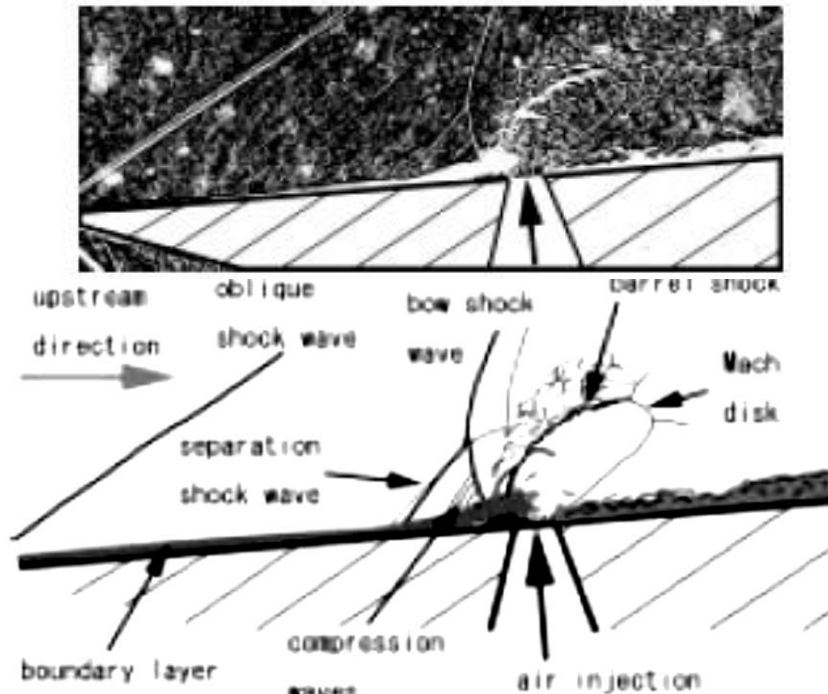


Figure 5.14 Schlieren photograph of the flow field. (Mach 1.7) a) and Schematic of the flow field obtained by the schlieren flow visualization b).

It is a basis for various optical flow visualization experiments. The device can be included in tests either as a schlieren system or as an interferometer. The dimensions of such a system are out of standard (optical field diameter is $\Phi = 900$ mm, uniform, without aberrations). It allows to visualize flows in transonic and supersonic wind tunnel test sections. The detection range of the density gradient is 0,1- 6,52 kg/m⁴, the refractive index 10^{-7} to 10^{-4} and the resolution in full scale is 10^{-7} .

5.5.3 INTERFEROMETRY

In most gas dynamics applications, it is useful to know flow density changes in wind tunnels, shock tubes or supersonic jets. The phase alteration beam passing through a disturbed section of a tested field can be compared with an undisturbed beam. The effects of interference make the basis of interferometry. The application of this principle in visualizing compressible flow fields is as old as the schlieren method.

Classical interferometry

The most used type of interferometers in wind tunnel tests is the Mach-Zehnder interferometer (MZI). Two light beams (test and reference ones) in the MZI are separated by its four plates. This instrument is suitable for quantitative density measurements in large wind tunnels. It requires an extremely high degree of mechanical precision and complexity of construction. Mechanical and optical tolerances are in order of a wavelength or below. This makes the instrument expensive and its cost grows rapidly with increasing the diameter of the desired size of the field of view.

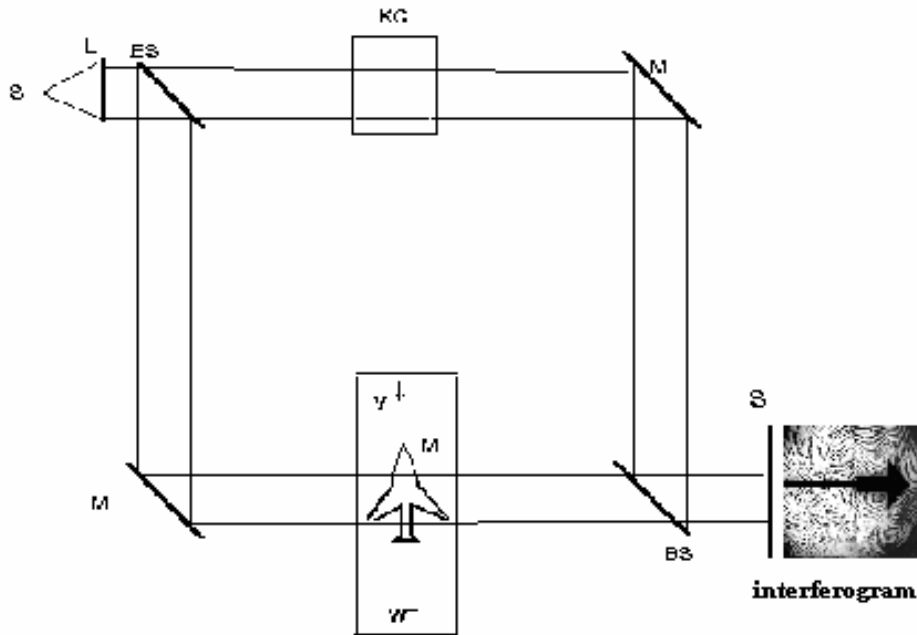


Figure 5.15. Mach Zehnder interferometer

The basic arrangement of the MZI is shown in Fig.5.15. The source light is made parallel with the lens S. The amplitude of the beam is divided into two parts by semireflecting mirrors. The four plates are situated in the corners of a rectangle and are all parallel in the start. The test section with its two glass windows is brought into the path of the test beam. In order to compensate the phase difference in two beams, two identical glass plates are inserted into the path of the reference beams. After being rejoined, corresponding rays of the two light beams can interfere and a certain pattern of interference fringes appears on the screen or photographic plate. An non homogeneity in the test section produces a certain amount of disturbance of the no-flow fringe system. It can be quantitatively related to the density distribution of the flow field

The most important quality requirements for an "ideal" MZI are: homogeneity in the refractive index of the glass of splitter plates, test section, windows, and compensation plate; constant and equal thickness of each pair of splitter plates and windows; exact plane parallelism and surface quality of all mirrors, plates and windows; exact coating of the surface of beam splitters with the prevention of any absorption; a high degree of reflection of full mirrors; exact mounting which prevents all plates from bending, sagging and other mechanical deformations, and protection of the instrument from mechanical vibrations and other disturbances. The basic adjustment is very difficult. It is necessary to align the test beam parallelly to the surface of a two-dimensional test object to avoid light reflection. The last step in adjusting is always bringing the achromatic fringe (zero order) into the field of view. Much patience is required while adjusting the MZI.

The MZI has been applied in practically all cases of gas flow investigations, where density difference becomes noticeable, such as: thermodynamic data, thermal conductivity of gases, dissociation, aerodynamic application, turbulence, wave or sonic booms.

Holographic Interferometry

Holographic interferometry is an optical method that enables complete flow field testing. The method is noncontact (it does not disturb the flow field) and is used for testing different objects and phenomena. The flow density can be measured directly using interferometry. The greatest advantage of holographic interferometry, in relation to the schlieren method, is the fact that it provides complete information stored in a single plate, allowing a postponement selection of specific types of flow visualization.

This method is based on holography, developed in the last forty five years. The holography represents a two stage method which, apart to light amplitudes, records light phases as well. The three-dimensional image recording is performed in the first stage, while its reconstruction is performed in the second stage (Fig.16). Lasers are used as light sources. The light from a reconstructed image from a hologram reaching the observer's eye is the same as the one that would come from an original object. A holographic image has the same depth, parallax and different perspectives as those available in the actual object scene.

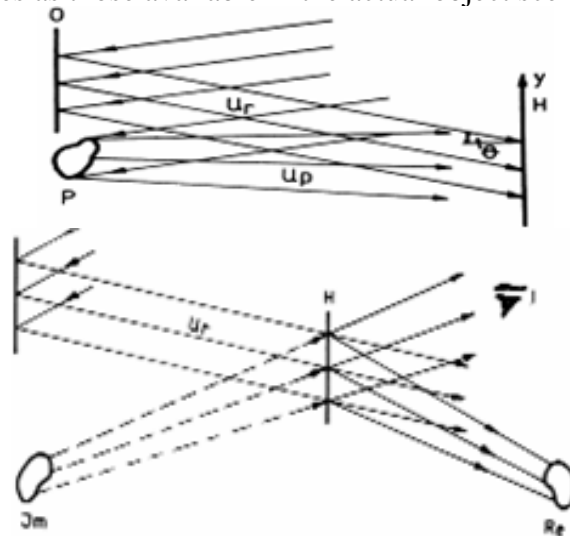


Figure 5. 16. Arrangement for holograms recording a) and reconstruction b)

If the image of one object is recorded two times in different moments, in the process of reconstruction both images (figures) will appear simultaneously and in the same place in space. Since the object waves are mutually coherent (they originate from the same light beam that illuminates the hologram) they interfere and the interference effects can be observed in the reconstructed object image. If no change occurs on the object between the first and the second exposition, then there is no difference in images and there are no interference fringes. If certain difference appears, then the reconstructed image contains the system of interference fringes N that indicate that change.

Quantitative flow testing using holographic interferograms is performed by determining the number of fringes $N(x,y)$ in the field image with respect to a reference point of known density. After that, the index of light refraction $n(x,y)$ and the air density $\rho(x,y)$ can be calculated. For the isentropic flow, there are relations between N , n , ρ , pressure P , temperature T , velocity V , and Mach number M . The physical basics and mathematical interpretation of the holographic interferometry are explained in references. One simple case is the 2D flow

Review of holographic interferograms

The usage of classical methods of the nozzle edge flow field testing comprises the introduction of a probe within the expansion region and holes perforation on nozzle surface. These methods significantly change the flow field and give the erroneous image of processes. Furthermore, it would be necessary to have very dense grating of measuring points, thus rendering these methods very inefficient. In realization of this experiment the holographic interferometer represented in Fig.36 was used. The holographic interferograms were used for numerical calculation of flow field parameters in the vicinity of the nozzle edge where the expansion fan is formed (Fig.19). The fringe number N was read from this hologram. The points in front of the expansion fan have $N=0$, since the last fringe has $N=17$. The theoretical and experimental values of the Mach numbers in the expansion area are in good agreement $M_{exp} = 2.15$, $M_{the} = 2.13$.

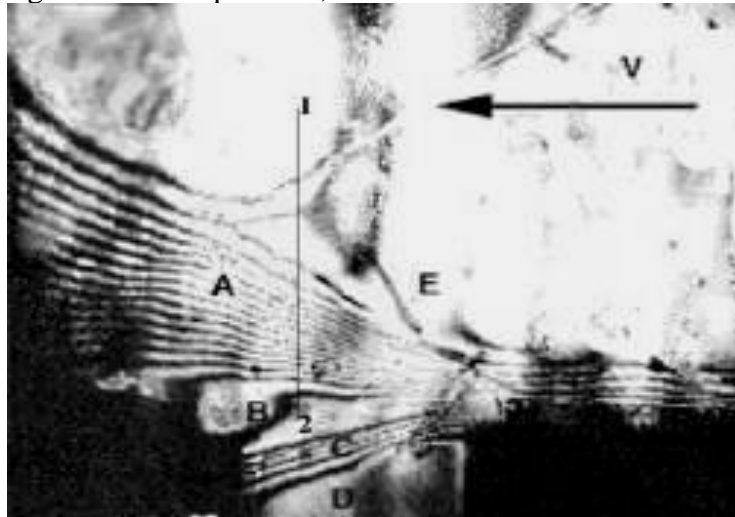


Figure 5.17. Holographic interferometer of supersonic flow in a two-dimensional model of the nozzle edge (Prandtl-Mayer expansion) $M_{\infty} = 1.56$

The photos in Figures 20a and 20b present holographic interferograms of the flow around a sphere for $M_{\infty} = 0.8$ (without shock wave) and 1.06 (bow shock wave is in front of the model). Fig.20b is a combination of holographic interferograms (upper part) and a schlieren photo of the same flow. The interferometric photo clearly shows: the stagnation point, the detached bow wave, the vortex sheet generated past sphere, etc.

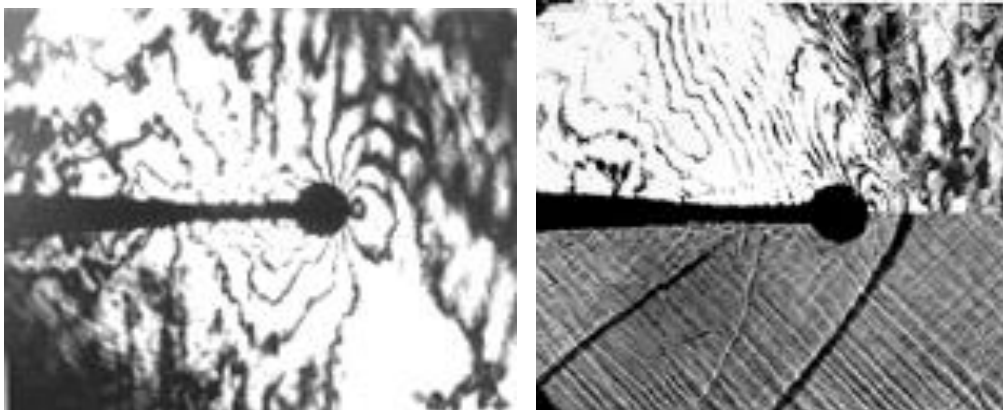


Figure 5.18. Holographic interferogram of the flow around a sphere for $M_{\infty} = 0.82$ (a) and mixed; hologram and schlieren for $M_{\infty} = 1.06$ (b)

Other interferometric methods used for flow visualization world wide

The holographic interferometry, today, is one of very important wind tunnel optical methods for transonic and supersonic flow visualization. In the VTI wind tunnels, the most often used method is the double exposure method. Other centers apply the real time method, the average or sandwich methods, the speckle interferometry, refraction interferometry, differential interferometry, etc. Optical holography is most frequently used, with laser light in the visible spectrum. In standard procedures the interferential effects are recorded on photo or thermosensitive emulsions. Electronic holography uses CCD cameras. In some specific cases acoustic and microwave holography, with electron beams X – rays, or computer holography can be used. Besides holographic interferometry, similar possibilities today have speckle interferometry, moiré interferometry and shearography. Only two methods of them will be mentioned here as methods used for flow visualization, without pretending to be the best choice.

Laser speckle photography is an optical method which can be applied for quantitative measurements of fluid flow density fields in a wide dynamic range. In the conventional method, the density gradient vector map of a density field is reconstructed by the optical Fourier transform of a double exposed laser speckle pattern recorded on a photographic film.

5.6 NON OPTICAL METHODS:

INTRODUCTION:

In all kinds of fluid flow research, the visualization is an important tool in experimental fluid mechanics, which can provide the overall picture of the flow field. Flow visualization has probably existed for as long as fluid flow research itself. Experimental flow visualization techniques are applied for several reasons:

- to get a picture of fluid flow around a scaled model of a real object, without any calculations;
- to develop or verify new and better theories of fluid flow or models.

If the flow could be made visible by some kind of flow visualization technique, it would be possible to observe flow phenomena which are essentially inviscid (e.g., vortex flows, flows distant from surfaces) as well as those phenomena which are dominated by the effects of viscosity (e.g., boundary layer flows, separation). In addition to qualitative observations, under certain conditions it would be possible to make quantitative measurements from flow visualization data as well.

Flow visualization may be divided into surface flow visualization and off-the-surface visualization. Surface flow visualization involves tufts, fluorescent dye, oil or special clay mixtures, which are applied to the surface of a model. Visual inspection of such tufts and coatings as a function of time or after some time, will give valuable information on such things as the state of the boundary layer (laminar or turbulent), transition, regions of separated flow and the like.

It must be remembered in such visualization that what is observed on the surface is not always indicative of what is happening in these free streams.

The second type of visualization involves the use of such tracers as smoke particles, oil droplets or helium-filled soap bubbles. Each of these methods requires appropriate lighting and some device for recording the image such as a still or video camera. If the flow field is illuminated in a plane by appropriate masking of the light source it is possible to examine discrete sections or slices of the flow.

Flow Visualization by Tufts

Very frequently, flow visualization in the vicinity of the model in the subsonic flow is performed using tufts. However, tuft size, distribution on the model's surface and sticking are important for turbulent flow testing and higher quality boundary layer visualization on complex models. If tuft diameter is less than 0.1mm, the problem of recording occurs due to a small amount of reflected light and long exposure time. Tufts can be used for testing the entire flow field in the wind tunnel. A grid with attached or glued tufts as screen can be used to visualize the vortex shedding behind the model or in the interaction regime of different fields. The grid should be placed in the wind tunnel normal to the mean flow direction and the tufts pattern should be observed or photographed from downstream (Fig.13.) numerous advantages in comparison with the ordinary silk tufts. By using fluorescent dyes, the tuft diameter virtually increases as well as the illumination, thus allowing higher quality of recording and using thinner tufts (0.01-0.1 mm). They can be stuck onto the model surface using very small glue quantities, (0.04 mm), thus avoiding boundary layer disturbances. Strong centrifugal forces interfering with flow field act on tufts stuck onto the model surface and their resultant determines tuft orientation.

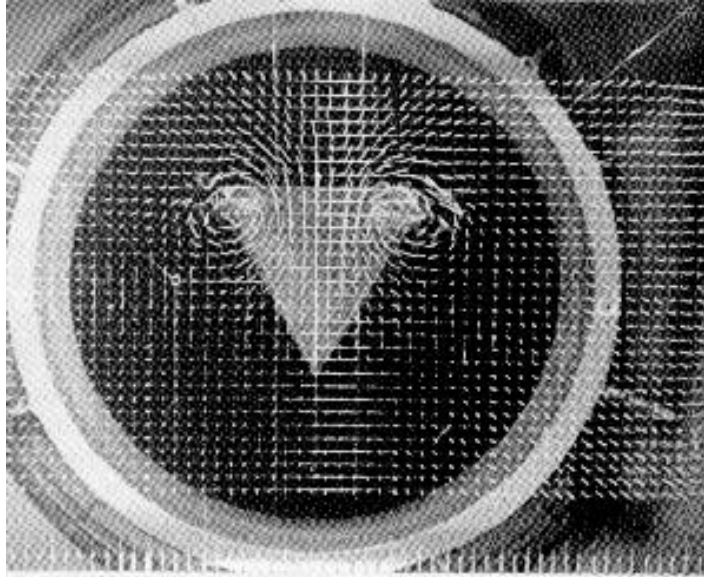


Figure 5.19. Trailing vortices behind delta wing

Aerodynamic forces are proportional to tuft diameter, while centrifugal forces are proportional to the square of the diameter. The problem with small size diameter is overcome by dyeing tufts with fluorescent dyes and using light source with rich ultraviolet part of the spectrum, or special filters transmissible to that part of the spectrum. This increases tuft luminance making it look much thicker and brighter. Hg or Xe lamp with UV filters for $\lambda = 350 \text{ nm}$ are used for steady flow testing. Stroboscopic light sources are most frequently used for unsteady flow. Visualization effect can be recorded by still or TV camera. Fluorescent tufts are also used for flow visualization in water tunnels, as well as in-flight flow testing.



Figure 5.20. Flow visualization with cotton tufts in wind tunnel T-35 for flow with $V = 100 \text{ m/s}$

Figures 14 and 15 demonstrate the results of the experiments in T-35 and T-32 wind tunnels; flow visualization with ordinary cotton and fluorescent silk tufts. Light combat aircraft model has surface painted in opaque black with 840 tufts stuck onto it. Tufts are made of silk 0.05 mm and 20 mm long (Fig.15). Fluorescent spray was used for tuft dyeing. The flow speeds have been between 20 and 40 m/s and angle of attack altered

from -8 to +24°. UV lamp with 100 W has been used as light source. Visualization effects are recorded with still camera Minolta. Black and white Ilford HP film (1600 asa) is used. Exposure time is from 1/60 to 3 s.

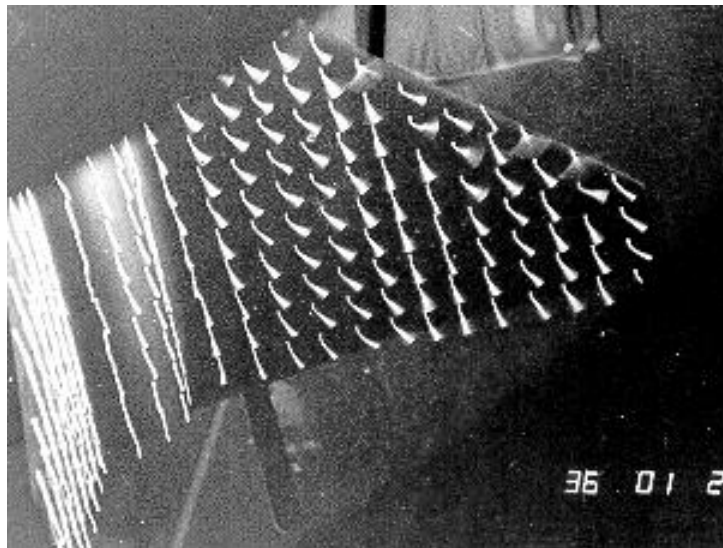
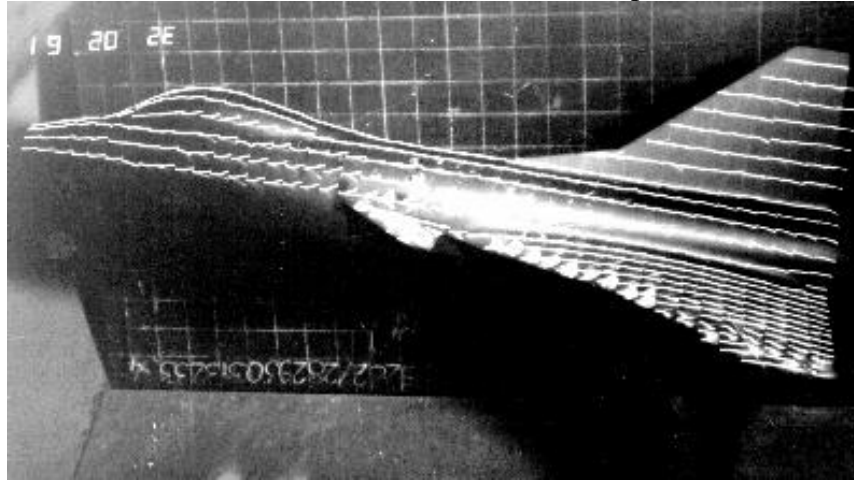


Figure 5.21 Flow visualization with fluorescent tufts in T-32 wind tunnel

In order to overcome the problem of non defined model edges, fluorescent dyes were used for marking. Another method for providing the differentiation of model and the background is to select proper background with different reflexive coefficient relative to model or elevate the film sensitivity to more than 1600 asa.

5.7 SURFACE FLOW VISUALIZATION METHODS

For observation of flow characteristics close to the wall of the model, the body wall can be coated with a certain material which indicates the local wall temperature, surface pressure, or the streamline pattern of the flow adjacent to the wall.

Surface Oil Film

Oil film or dots on the model surface enable obtaining a picture of the flow pattern at the surface of the model placed in the wind tunnel quickly and easily. The special mixture can be prepared from an appropriate oil and fine pigment (Al_2O_3 ; TiO_2 , powder, fluorescent dye, colouring pigments, graphite). The technique allows observation of the lines of separation and reattachment of the flow to the body. Fig.16a shows the

visualization with $\text{TiO}_2 + \text{oil}$ on the surface around two vertical cylinders fixed on the plate in T-35 for $V=50$ m/s and around the sphere used for turbulence test for $M_\infty = 0,2$ (Fig.16b). Fig.17 gives oil flow visualization of the airflow on the end wall of a turbine blade cascade. Boundary layer flow visualization on the laser guided bomb model with an oil film, performed in the T-38 wind tunnel, (a) top of the model with fins and flow on the fin upper surface (b) for $M_\infty= 0.9$ are presented in Fig.18.

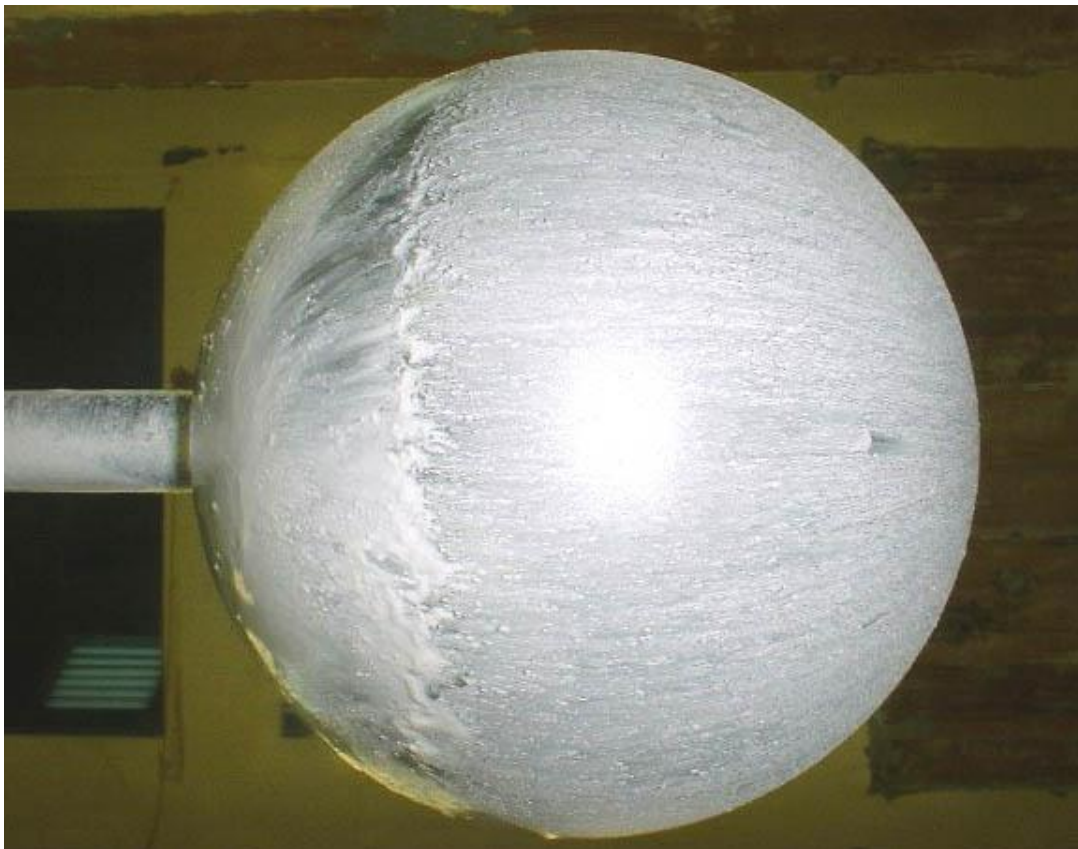
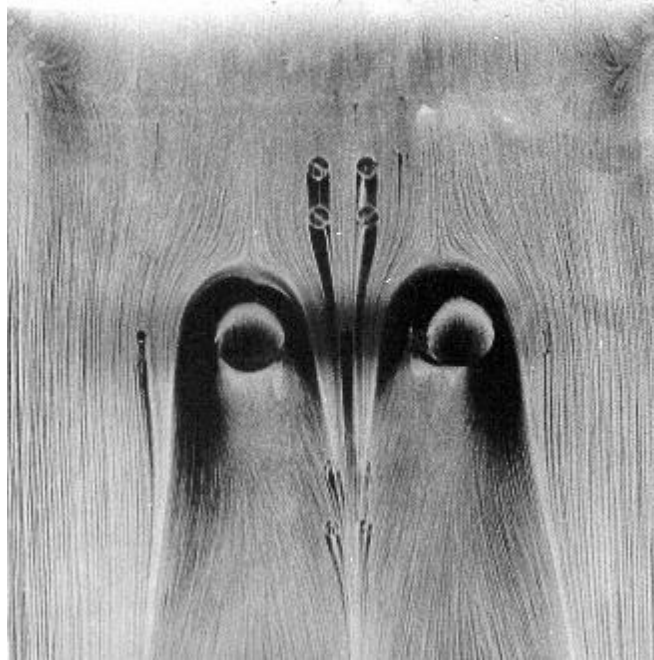


Figure 5.22. Flow visualization around two cylinders fixed on the plate in

the large wind tunnel T-35 for $M_\infty = 0,5$ with oil film (a) and around sphere for $M_\infty = 0,2$ (b),



Figure 5.23. Oil flow visualization, airflow on the end wall of a turbine blade cascade. (Von Karman Institute)

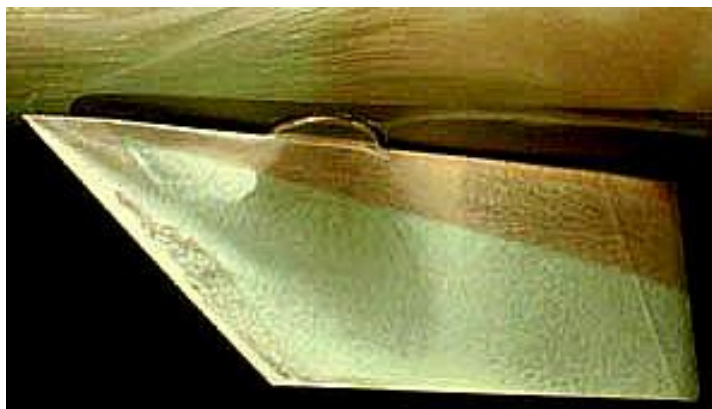
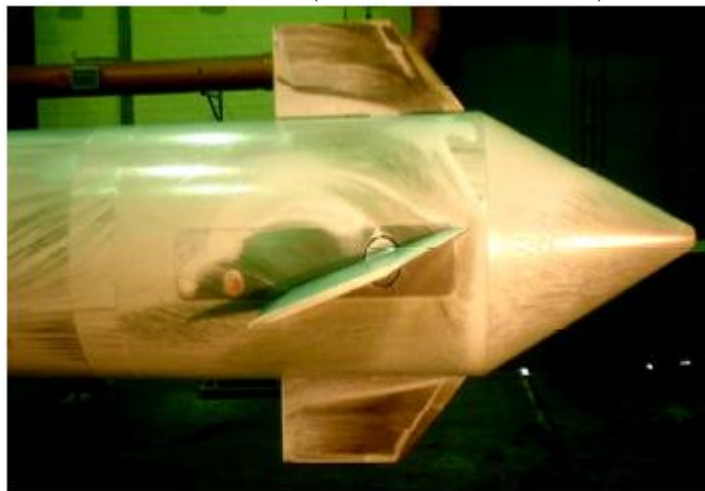


Figure 5.24. Boundary layer flow visualization on the laser guided bomb model with oil film,(a) top of the model with fins and (b) flow on the fin upper surface for $M_\infty = 0.9$

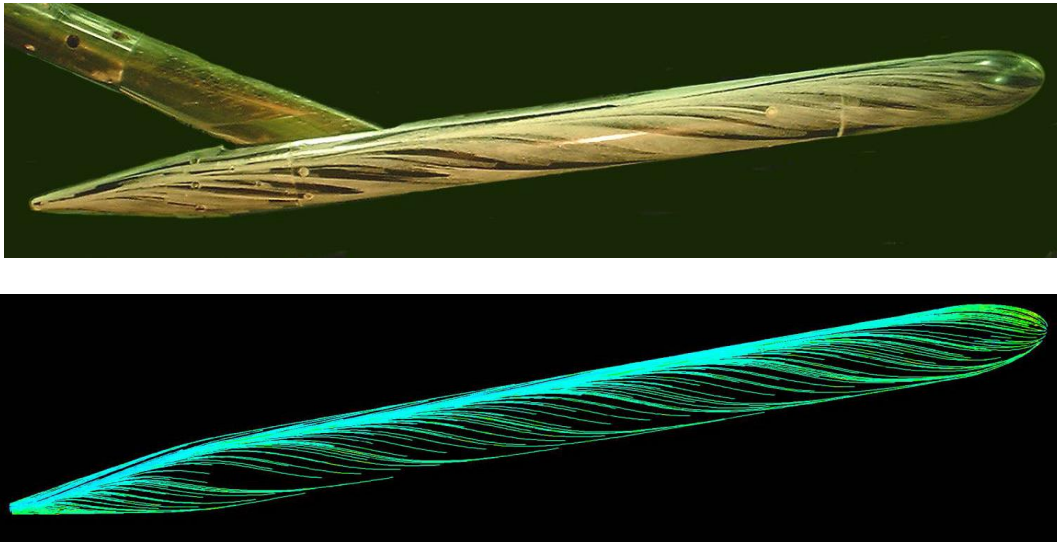


Figure 5.25. Flow pattern on the model obtained by the experiment (a) and by the simulation of the flow for $M_\infty = 0.3$ and $\alpha = 8^\circ$ (side view) (b)

Test of the flow field around the axy-symmetrical body – model of the torpedo without fins and control surfaces, was performed in the trisonic wind tunnel T-38 of VTI, for the speed of undisturbed flow that corresponds to Mach number $M_\infty = 0.3$. Aerodynamic forces and moments were measured by six-component internal strain gage balance. Oil emulsion film with addition of oleic acid and TiO_2 powder was used for flow visualization in the boundary layer (Fig.23)

The goal of the experiment was to make comparison of the aerodynamic coefficients and flow pattern obtained by the experiment and by the simulations of the flow possible. Fluent 6 was used for simulating the flow. Analysis of the shown photographs (Figures 19a and 19b) demonstrates an excellent agreement of flow patterns obtained by the experiment and numerical simulations. Certain differences are visible in the area behind the model support sting and in its immediate vicinity because the sting is not included into the numerical model

5.8 Liquid crystals and temperature sensitive paints

A surface-temperature distribution can be gained by coating a test model with cholestric liquid crystals. If they are illuminated with white light under a certain angle of incidence, liquid crystals reflect only one light wavelength at each viewing angle, depending on small temperature changes in the crystal sheet. Liquid crystals are able to respond to finer changes of temperature in the boundary layer, due to laminar-to-turbulent transitions or indicate the place of shock waves. The colours of liquid crystals are reverse if the temperature changes in the opposite direction. Therefore, liquid crystals are very attractive for boundary-layer studies. Model to be tested should be made of a material with low heat conductivity and coated with black paint as base. Fig.20 demonstrates the application of liquid crystals for hot streams visualization in a little smoke wind tunnel.



Figure 5.26 Flow visualization in the small wind tunnel with liquid crystals

The surface temperature, the local heat transfer rate and coefficient on a body tested in high speed flow facility can be measured by means of temperature sensitive paints. An important difference between liquid crystals and temperature sensitive paints is, that the temperature span over the liquid crystals colour change is much smaller (a few degrees only) than that of paints (several hundred degrees).

5.9 Pressure sensitive paint (PSP)

The spatially continuous pressure and temperature distribution on aerodynamic test surfaces is important for understanding complex flow mechanisms and comparison with predictions of computational-fluid-dynamics models. Conventional pressure measurements are based on pressure taps and electronically scanned transducers. Pressure taps provide pressure information only at discrete points.

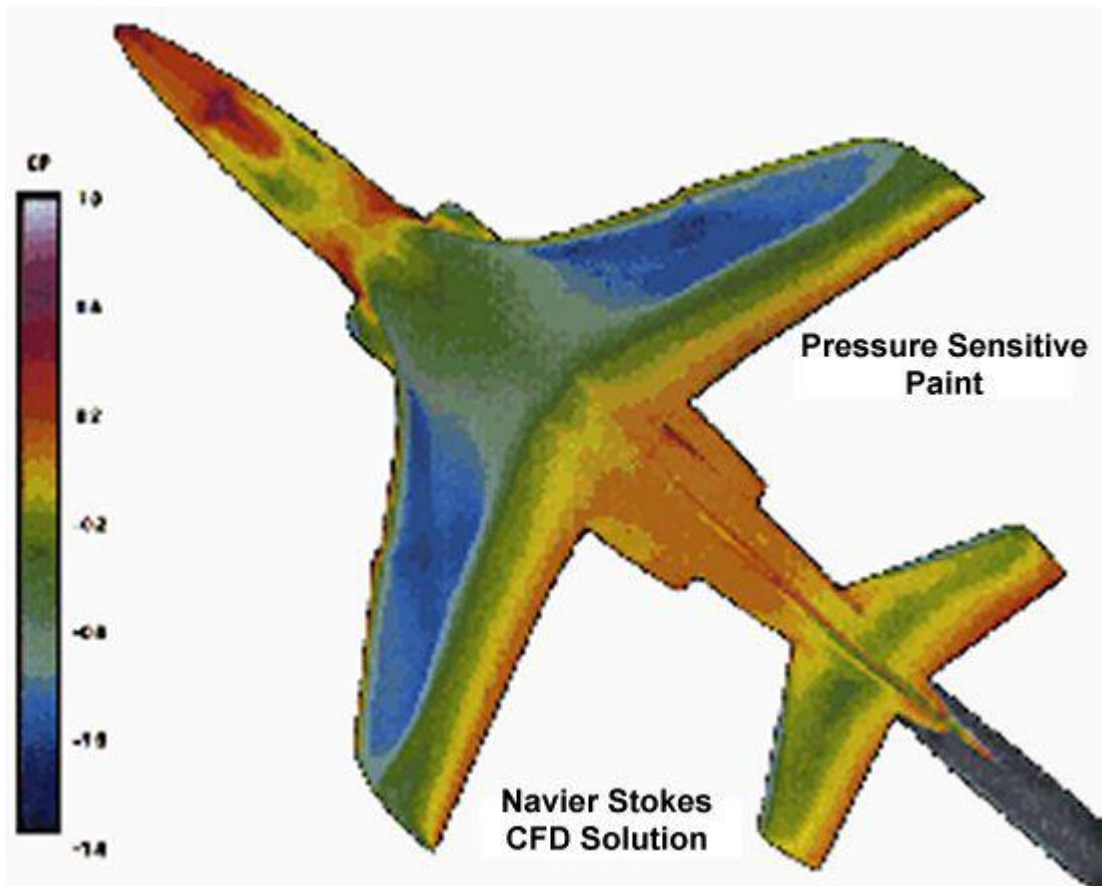


Figure 5.27 A comparison of pressure results between PSP (right side of model) and Computational Fluid Dynamics (left side)

PSP technology has emerged as an alternative for determining static and transient surface-pressure fields for aerodynamic applications and flow visualization. The pressure sensitivity is based on the oxygen (O_2) quenching of luminescent molecules dispersed in a film that is coated onto a test surface. In practice, the PSP/TSP (temperature sensitive paint) coating is illuminated with light of the appropriate energy (colour) to excite the coating-entrapped probe molecules. The resulting luminescence output is inversely proportional to the surface pressure or temperature of the test model.

The resulting luminescence from the model can be imaged using a CCD camera. Pressure is correlated with the ratio of PSP images acquired at a reference condition of the known pressure and temperature (wind-off) and condition (wind on) through a modified form of the Stern-Volmer relationship. Calibration of this intensity ratio (I_{ref} / I), or lifetime (τ) is then correlated with the output of the CCD, providing a convenient tool for generation of a spatially continuous pressure map, allowing the entire test surface to be sampled simultaneously. CCD cameras have a million or more pixels and this technique provides continuous surface pressure measurements with high spatial resolution. The output of the CCD array can be visually represented as a two-dimensional image, with the luminescence corresponding to a grey or false-colour scale. Fig.5.27 represents the illustration for PSP applications.

5.10 Flow Visualization with Special techniques

Third group of visualization methods is based on two principles: introducing a foreign invisible substance into the incompressible flow and visualizing the density variations in the flow by optical methods. The foreign substance in this case is energy transferred to certain portions of the flow to increase the energy

level (spark, electron beam and glow discharge methods) and make artificial density variations. Such portions of the flow have an altered density and can be visualized by the optical methods.

They are applied to visualize the rarefied gases that are for several reasons distinguished from the ordinary compressible flows. The gas flow with extremely high level of kinetic energy becomes luminous in a stagnation point where the kinetic energy is transferred into heat. That heat excites electronic transition in the gas and the flow itself is visible (Fig.5.28).

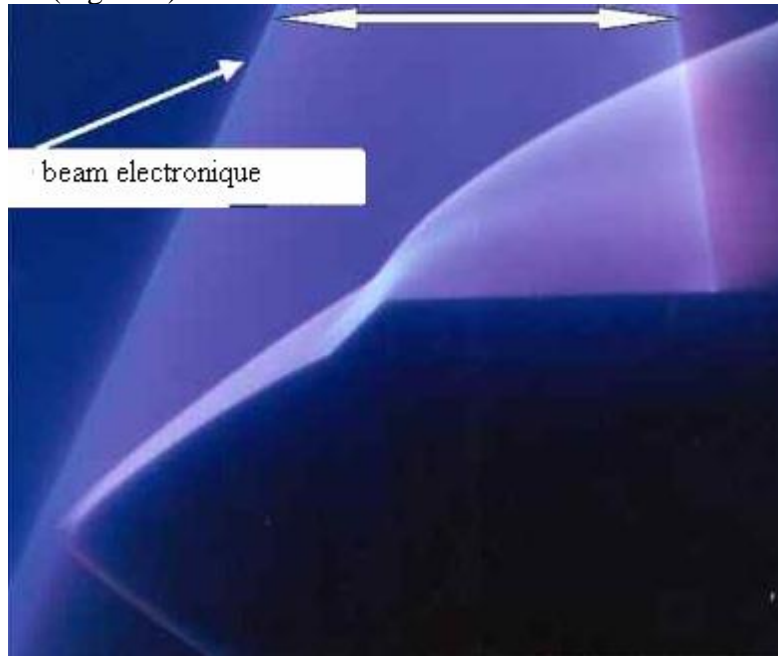


Figure 5.28 Flow visualization by electronic beam in hypersonic wind tunnel for $M = 10$

An intensive hot spot can be obtained by means of a spark discharge across two electrodes into a gas stream or using a giant pulse laser for producing the luminous plasma (Q-switched giant pulse ruby laser of 100 MW). Another way of artificially introducing density changes in a flow is to seed the flow with a foreign gas of different refractivity (benzene vapour, CO₂).

Very often, methods mentioned as special techniques where the double refracting liquids, solutions or suspension of certain macromolecules in a neutral solvent are used for flow visualization. A transparent medium can be birefringent if it consists of optically anisotropic molecules. An incident light wave is separated into two linearly polarized components with the planes of polarization being perpendicular to one another. The birefringence in these solutions can be observed by means of a polariscope. With the isochromates and isoclines recorded on a photograph, a data field from which shear distribution in a two-dimensional flow field can be deduced and flow velocity calculated.

Analogous methods are of interest in the flow visualization technique. The hydraulic analogy has the widest application. For e.g., the formation of gravitational waves of long wavelengths on the free surface of a liquid is analogous to the pattern of pressure waves in an isentropic supersonic flow. The hydraulic analogy has been used to investigate the wave pattern in the supersonic flow around models. Fig.5.29. shows the flow around a model in free surface water tunnel that is analogous with the supersonic flow $M_{\infty} = 4.1$.

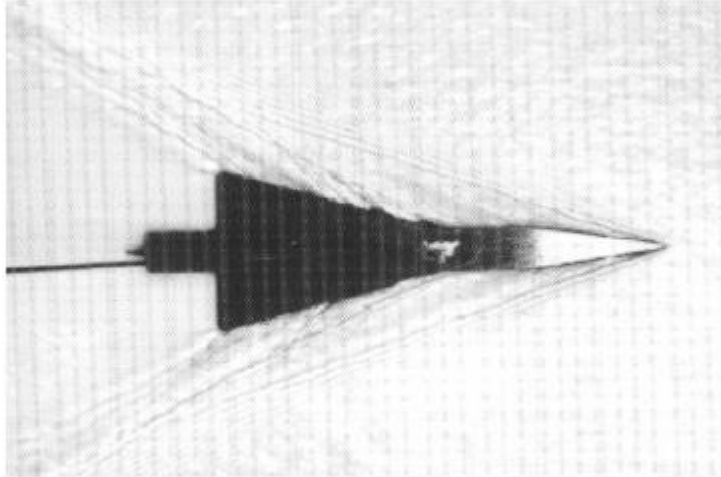


Figure 5.29 2D model using the hydraulic analogy to simulate supersonic flow ($M_\infty = 4.1$)

For the purpose of flow visualization high speed photographic techniques are usually applied in connection with one of the visualizing methods. High speed cameras with exposure time of 10^{-6} to 10^{-9} s in connection with associated illumination systems can record the shock wave motion. If a single shot photograph is used, the synchronization between the unsteady flow pattern and the exposure of the photograph must be made. A high speed cinematographic system is also very suitable for visualizing application.